21126

NATIONAL LIBRARY
OTTAWA

BIBLIOTHÈQUE NATIONALE
OTTAWA

NAME OF AUTHOR: PETER R. TREMAINE

TITLE OF THESIS: DIELECTRIC AND OTHER PROPERTIES OF THE SOLID POLYMORPHS OF PHENOL UNDER PRESSURE, AND THE STATIC DIELECTRIC CONSTANTS OF THE LIQUEFIED FLUOROMETHANES

UNIVERSITY: U. of ALBERTA

DEGREE FOR WHICH THESIS WAS PRESENTED: Ph.D.

YEAR THIS DEGREE GRANTED: 1974

Permission is hereby granted to THE NATIONAL LIBRARY OF CANADA to microfilm this thesis and to lend or sell copies of the film.

The author reserves other publication rights, and neither the thesis nor extensive extracts from it may be printed or otherwise reproduced without the author's written permission.

(Signed) Peter Tremaine

PERMANENT ADDRESS:

94 THORNRIDGE DR
THORNHILL
ONT.

DATED: Nov. 30 1973

NL-91 (10-68)

THE UNIVERSITY OF ALBERTA

DIELECTRIC AND OTHER PROPERTIES OF THE SOLID POLYMORPHS OF PHENOL UNDER PRESSURE, AND THE STATIC DIELECTRIC CONSTANTS OF THE LIQUEFIED FLUOROMETHANES

by

© PETER TREMAINE

A THESIS

SUBMITTED TO THE FACULTY OF GRADUATE STUDIES AND RESEARCH
IN PARTIAL FULFILMENT OF THE REQUIREMENTS FOR THE DEGREE
OF
DOCTOR OF PHILOSOPHY

DEPARTMENT OF CHEMISTRY
EDMONTON, ALBERTA
SPRING 1974

THE UNIVERSITY OF ALBERTA

FACULTY OF GRADUATE STUDIES AND RESEARCH

The undersigned certify that they have read, and recommend to the Faculty of Graduate Studies and Research, for acceptance, a thesis entitled

'DIELECTRIC AND OTHER PROPERTIES OF THE SOLID POLYMORPHS OF PHENOL UNDER PRESSURE, AND THE STATIC DIELECTRIC CONSTANTS OF THE LIQUEFIED FLUOROMETHANES'

submitted by PETER TREMAINE in partial fulfilment of the requirements for the degree of Doctor of Philosophy.

....
Supervisor

R E D McClung
....

....

....

....

....
External Examiner

Date: November 29, 1973

To Karin

ABSTRACT

The transition between phenol I and II has been studied below 0°C. The results show that phenol II cannot be prepared from phenol I below about 1300 bar. At atmospheric pressure, phenol II reverts to phenol I at -48 ± 2°C. The enthalpy change of the II → I transition at one atmosphere is 0.43 ± 0.09 kcal/mole. Quenched samples of phenol II were prepared, and their x-ray powder diffraction pattern at -190°C and atmospheric pressure is reported. This diffraction pattern can be fully indexed using an orthorhombic unit cell whose dimensions are a = 10.59 ± 0.01 Å, b = 16.31 ± 0.02 Å, c = 17.39 ± 0.02 Å. The x-ray powder diffraction pattern for phenol I at -190°C was measured. The orthorhombic unit cell parameters at -190°C are a = 6.00 ± 0.02 Å, b = 8.91 ± 0.03 Å, and c = 14.59 ± 0.03 Å, compared with the previously reported values of a = 6.02 ± 0.02 Å, b = 9.04 ± 0,04 Å, and c = 15.18 ± 0.04 Å at 20°C.

The volume compressions and compressibilities of polycrystalline phenol I and II were measured in a piston-cylinder pressure vessel at 10°C and pressures up to 3 kbar. The expression obtained for the compression of phenol I is

$$\frac{-\Delta V}{V_o} = -2.821 \times 10^{-9} P^2 + 2.375 \times 10^{-5} P$$

and, for phenol II,

$$\frac{-\Delta V}{V_o} = -6.735 \times 10^{-10} P^2 + 1.291 \times 10^{-5} P + 0.07891$$

where P is the pressure in bar. The dielectric constants of phenol I were determined as a function of temperature

and pressure from -10°C to 35°C in a coaxial dielectric cell. The expression for the pressure dependence of the dielectric constant at 50 kHz and 10°C is

$$\varepsilon' = 2.8824 + 4.4278 \times 10^{-5} P - 2.9302 \times 10^{-9} P^2$$

At 10°C, and 2 kbar the 50 kHz dielectric constant of phenol II was found to be 3.10 ± 0.06 from measurements in both coaxial and parallel plate dielectric cells. The density dependence of the molar polarization, $\overline{P}$, of phenol I between 0 and 1500 bar at 10°C was found to follow the relationship $\overline{P}(\text{cm}^3) = 20.30 + 11.75\ V/V_o$. At 10°C and one atmosphere, the electronic and atomic polarizations of phenol I are 26.91 ± 0.30 cm^3 and 5.14 ± 0.40 cm^3, respectively, and the molar polarization of phenol II at 2 kbar and 10°C is 30.75 ± 0.50 cm^3. Neither phase shows signs of dynamic orientational disorder. The properties of a transient double dielectric dispersion which appeared during the I → II transition were studied, and the apparent enthalpies of activation for each dispersion were obtained. The dispersions were attributed to the effect of impurities precipitated during the transition.

The static dielectric constants of carbon tetrafluoride, chloroform, difluoromethane, and methyl fluoride were measured at temperatures ranging from their melting points to their normal boiling points under the saturated vapour pressure of the liquids. The molar polarization of carbon tetrafluoride agrees with that of the gas phase to within experimental error. The deviation of the dielectric constants of the polar fluoromethanes from the values predicted by the Onsager equation cannot be fully due to the non-spherical shape of these molecules. It is postulated that the polarization resulting from the liquid lattice vibrations may account for much, or all, of the deviation for methyl fluoride and difluoromethane, but that a significant parallel alignment of the molecular dipoles is certainly present in fluoroform and may also be present in methyl fluoride and difluoromethane.

Preface

The purpose of this work was to obtain physicochemical information about the polymorphic modifications of molecular crystals under pressure. It was first necessary to establish the apparatus and methods for the measurement of dielectric constants, phase transitions, and compressibilities under pressure. These techniques have been valuable in elucidating the properties of the solid polymorphs of compounds (1,2), most noticeably the ices (2-6). They were deemed to be desirable additions to the spectroscopic and x-ray techniques which are already being used in this laboratory (7-9) and which are particularly suitable for the study of high pressure phases that are metastable at atmospheric pressure below about -120°C (10, 11). The polymorphs of solid phenol were chosen as suitable systems on which to apply the above techniques for reasons which are outlined in Section 1.6 and the results obtained from this work are presented in Chapters 3 to 5. Chapter 6 presents a study of the static dielectric constants of the fluoromethanes in the liquid state, which was carried out at the suggestion of Dr. G. R. Freeman who, in the course of his own research program, became aware that these values had never been determined. The results were treated using extensions of the Onsager equation which are discussed at some length in Section 6.1.

ACKNOWLEDGEMENTS

I would like to express my appreciation to Dr. J. E. Bertie for his guidance and encouragement throughout the course of this work. I would also like to thank the other members of the department, especially those in Dr. Bertie's research group, for their interest and cooperation. It has been a pleasure to work with them. Particular thanks must go to the staff of the departmental electronics and machine shops, for their prompt and competent workmanship in building the apparatus.

The preparation of the fluoromethane samples (Section 6.2) was entirely the work of Dr. Maurice G. Robinson. I would like to thank Dr. Robinson, and also Dr. G. R. Freeman, for bringing the fluoromethane project to my attention and for their help with this work.

I am very grateful to my wife, Karin, for her work on the manuscript, and for her patience and understanding while the work was in progress. I would also like to take this opportunity to express my gratitude to my parents for their continuing advice and encouragement through the years.

The National Research Council of Canada has been most generous in providing financial assistance during the course of this work.

Symbols Used In This Work

In a few cases the same symbol is used to denote more than one quantity but the context of their usage should prevent confusion between any such symbols.

α	distortion polarizability at the frequency in question.
α_e	electronic polarizability.
α_a	atomic polarizability.
$\beta = -1/V_o(\partial V/\partial P)_T$	bulk compressibility.
C_o	the cell constant or geometric capacitance, i.e. the capacitance of an evacuated dielectric cell.
$C^* = C' - jC''$	the complex capacitance of a system. C' and C'' are the real and imaginary components of C^*.
d	density (g/cm^3).
$\varepsilon^* = \varepsilon' - j\varepsilon''$	the complex dielectric constant (complex relative permittivity). ε' (the dielectric constant or permittivity) and ε'' (the dielectric loss) are the real and imaginary components of ε^*. ε is occasionally substituted for ε' when $\varepsilon'' = 0$.
ε_o	the low frequency limit of the dielectric constant.
ε_∞	the high frequency limit of the dielectric constant.
$\bar{\varepsilon}_o$	the permittivity of free space (8.854×10^{-12} farad/m in the rationalized mks system, 1 e.s.u. in the cgs electrostatic system). In the cgs system the permittivity of a material, $\bar{\varepsilon}_o \varepsilon'$, is identical to its dielectric constant, ε'.
f	the frequency in Hz unless otherwise specified.

G	electric conductance.
$G_o = \lim_{\omega \to o} G$	D.C. conductance.
σ	specific electric conductance.
h	Cole-Cole distribution of relaxation time parameter.
$j = \sqrt{-1}$	
M	molecular weight (g).
$n^* = n' - jn''$	the complex refractive index. n' (the refractive index) and n'' (the absorbance) are the real and imaginary components of n^*.
N	Avogadro's number.
P	Pressure minus ambient pressure (bar). The term 'one atmosphere' is often used in the text to denote ambient pressure ($P = 0$).
$\bar{P}$	molar polarization at the frequency in question, $\bar{P} = \frac{(\varepsilon'-1)}{(\varepsilon'+2)} \frac{M}{d}$.
$\bar{P}_e$	electronic polarization.
$\bar{P}_a$	atomic polarization.
pmho	picomho.
pf	picofarads.
μ	dipole moment (in Debyes).
V	volume.
ω	the angular frequency (rad./sec), $\omega = 2\pi f$.

TABLE OF CONTENTS

Page

Abstract.. v

Preface.. viii

Acknowledgements.. ix

Symbols Used in This Work.. x

List of Tables.. xv

List of Figures.. xviii

Chapter I. Introduction 1

1.1 Capacitance Measurements at Audio-Radio Frequencies 1

1.2 Dielectric Constants and Relaxation 7

1.2a The Clausius-Mossotti Equation 8

1.2b Dielectric Relaxation: The Debye and Cole -Cole Equations 11

1.3 Dielectric Effects Resulting from Impurities and Sample Inhomogeneity 18

1.3a D.C. Conductance and Electrode Polarization 18

1.3b Maxwell-Wagner Effects 22

1.4 Solid-Solid Phase Transformations 24

1.4a Order-Disorder Transitions 26

1.4b Hysteresis and the Coexistence of Two Solid Phases 29

1.5 Properties of Phenol 34

1.5a Phenol I 34

1.5b Phenol II 40

1.5c Vitreous Phenol 43

1.6 Objectives of This Work 43

Chapter II. Experimental 46

2.1 Purification of Materials 46

2.2 Temperature Measurement 52

TABLE OF CONTENTS Continued.

Page

2.3 Compressibility Measurements 53

2.4 Instrumentation for the Measurement of Capacitance and Loss 56

2.5 High Pressure Dielectric Cells 59

2.5a The Coaxial High Pressure Dielectric Cell 61

2.5b The Parallel Plate High Pressure Dielectric Cell 66

2.6 Isolation and Temperature of Transformation of Phenol II at One Atmosphere ... 68

2.6a Preparation of Phenol II 68

2.6b Thermal Analysis 71

2.7 Powder X-ray Diffraction Studies 73

Chapter III. The Volume Compression and Compressibilities of Phenol I and II at 10°C 76

3.1 The Volume Compressions Uncorrected for Cylinder Deformation 76

3.2 The Effect of Elastic Deformation of the Compressibility Cell on Compression Results 86

3.3 Analysis of the Experimental Uncertainties in the Determination of the Volume Compressions 98

3.4 The Volume Compression and Compressibilities Corrected for Cylinder Deformation - Results and Discussion 103

Chapter IV. The Phase Diagram of Solid Phenol Below 0°C and Powder X-ray Diffraction Studies of Phenol I and II at -190°C 109

4.1 Methods for the Determination of the Phase Diagram of Phenol 109

4.2 The Phase Diagram of Purified Phenol 111

4.3 The Effect of Impurities on the Phase Diagram 117

4.4 The Temperature and Enthalpy Change of the Phenol II to Phenol I Transformation at One Atmosphere 119

4.5 Powder X-ray Diffraction Results 125

TABLE OF CONTENTS Continued.

Page

Chapter V. The Dielectric Properties of Phenol I and II 137

5.1 Methods for the Determination of the Dielectric Constants of Phenol I and II . 137

5.2 The Dielectric Constants of Phenol I as a Function of Temperature and Pressure .. 140

5.3 The Dielectric Constant and Molar Polarization of Phenol II at 10°C 170

5.4 The Transient Dispersion in Phenol II ... 189

5.5 Corrections to Dielectric Constants Obtained in the Coaxial Cell for Cell Deformation under Pressure 202

5.6 The Electronic Polarization of Phenol ... 206

Chapter VI. The Static Dielectric Constant of the Liquefied Fluoromethanes 211

6.1 The Onsager Equation and Other Related Equations 212

6.2 Purification of Materials 219

6.3 Dielectric Constant Measurements on Liquefied Gases 220

6.4 The Molar Polarization of Carbon Tetrafluoride 224

6.5 The Static Dielectric Constants of Fluoroform, Difluoromethane, and Methyl Fluoride 228

6.6 Conclusion 236

References 237

LIST OF TABLES

Table		Page
1	Some physico-chemical parameters for pure phenol..	37
2	Thermodynamic parameters for the phenol I → II transformation........................	42
3	Ranges of measurement and accuracy of the 1615-A capacitance bridge..................	58
4	Various parameters for the compression runs on phenol..................................	77
5	The linear displacement, L, of the pistons plus support blocks for the compression runs on phenol..................................	79
6	The linear displacement, L, of each phenol sample..	80
7	Expressions for the compression of each phenol sample before correcting for the deformation of the bore of the pressure vessel..	87
8	The expansion of the bore of the compressibility cell under pressure, assuming ideal expansion..	89
9	Various parameters for the compression runs on the alkali halides........................	92
10	The displacement, L, of the pistons plus support blocks for the compression runs on the alkali halides..	93
11	The displacement, L, of each alkali halide sample..	94
12	Expressions for the compression of the alkali halides as a function of internal pressure..	95
13	The compression of the alkali halides and the expansion constant of the compressibility cell..	96
14	Expressions for the volume compressions of phenol I and II at 10°C after correction for cylinder expansion..	99
15	The volume compression of phenol I and II at 10°C..	105
16	The volume compressibilities of phenol I and II at 10°C..	106

Table	Page

17 Transition pressures for solid-solid transformations in phenol.................. 114

18 The enthalpy change of the phenol I → II transformation at one atmosphere........... 124

19 The wavelength and filter material of each radiation source.......................... 126

20 X-ray powder diffraction data for phenol I at room temperature and at -190°C.......... 128

21 X-ray powder diffraction data for phenol II at -190°C and atmospheric pressure......... 132

22 Dielectric constants of phenol I at 50 kHz, uncorrected for the distortion of the pressure vessel, at various temperatures and pressures.............................. 141

23 The dielectric constant of phenol I at 50 kHz as a function of pressure for various temperatures.......................... 150

24 The dielectric constants of phenol I at 10°C and 50 kHz.......................... 151

25 The molar polarization of phenol I at 10°C. 153

26 Dielectric constants at 50 kHz for phenol I adjusted for errors in the cell constants for each sample............................ 158

27 The dielectric constant of phenol I at 50 kHz as a function of temperature for several pressures.......................... 161

28 Isobaric thermal expansivities of phenol I at 10°C.................................. 168

29 The capacitance at 50 kHz of the parallel plate dielectric cell containing samples 4 and 5 as phenol I at 10°C................ 181

30 The dielectric constants of phenol I and II at 10°C, measured in the parallel plate cell, and related data.................... 183

31 The dielectric constant and molar polarization of phenol II at 2 kbar and 10°C...... 186

32 Relaxation parameters obtained from sample 6 at several temperatures and 2 kbar....... 197

33 Relaxation parameters obtained from sample 7 at several temperatures and 2 kbar...... 198

Table | Page

34 The effect of pressure on the cell constant of the coaxial dielectric cell........ 205

35 The refractive index of liquid phenol at 45°C and several wavelengths............... 209

36 The dielectric results for the fluoromethanes in the liquid state............... 225

37 Values of μ_o^2/I for several halomethanes.. 233

38 The discrepancies between the gas phase molar polarizations and those required to fit the methyl halides to the Onsager equation using molecular eccentricities.... 235

LIST OF FIGURES

Figure		Page
1	Different representations of a real capacitor..	3
2	The Debye and Cole-Cole dispersion relationships and a Cole-Cole plot of each.............	13
3	The Cole-Cole plot of a resolved dispersion....	17
4	Dielectric relaxation data for impure hexamethylene tetramine............................	20
5	A plot of the linear displacement of a sample of commercial phenol against pressure at 12°C showing hysteresis in the I → II transformation	32
6	The phenol I lattice...........................	39
7	Schematic diagram of the zone refining apparatus..	47
8	The compressibility cell.......................	54
9	The coaxial high pressure dielectric cell......	62
10	A closeup of the electrode assembly of the coaxial dielectric cell........................	63
11	The electrode assembly of the high pressure parallel plate capacitance cell...............	67
12	The pressure vessel used to prepare quenched samples of the high pressure phases of solids..	69
13	The calorimeter................................	72
14	The compression of phenol plotted against the apparent pressure............................	83
15	Possible errors in the alignment of the displacement gauges............................	102
16	The capacitance vs. pressure plots from which the transition pressures of phenol I and II were obtained..................................	113
17	The phase diagram of phenol....................	115
18	Capacitance vs. pressure plots for pure and impure samples of phenol......................	118
19	The warming curves for quenched phenol II at one atmosphere................................	121
20	The dielectric constants of phenol I at 50 kHz and 10°C as a function of the apparent pressure	147

Figure | Page

21 The dielectric constants of phenol I at 50 kHz after adjusting the cell constants............. 157

22 Dielectric constant isobars for phenol I obtained by different methods.................. 163

23 The apparent dielectric constants of phenol II at 10°C, measured in the coaxial cell at 50 kHz and plotted against the applied pressure....... 172

24 The capacitance at 50 kHz of the parallel plate dielectric cell containing sample 4 at 10°C, plotted against the applied pressure........... 177

25 The capacitance at 50 kHz of the parallel plate dielectric cell containing sample 5 at 10°C, plotted against the applied pressure........... 179

26 The dielectric constant of phenol I at 10°C and 50 kHz, plotted against pressure........... 185

27 The molar polarization of phenol I and II at 10°C as a function of (V/V_0)................... 188

28 Cole-Cole plots showing the decay in the magnitude of the dispersion in a sample of newly formed phenol II......................... 190

29 Cole-Cole plots showing the decay in the magnitude of the dispersion in a sample of newly formed phenol II......................... 192

30 Cole-Cole plots of the transient dispersion in sample 7 at several temperatures............... 194

31 Cole-Cole plots of the transient dispersion in sample 7 at several temperatures............... 195

32 The temperature dependence of the apparent relaxation times for the low and high frequency dispersions.................................. 199

33 The capacitance of the evacuated dielectric cell as a function of temperature.............. 221

34 The dielectric cell for measurements on liquefied gases in its insulated box.............. 223

35 The static dielectric constants of the liquid fluoromethanes................................ 227

Chapter I. Introduction

Part I of this thesis presents a study of several properties of phenol under pressure. The volume compression and compressibility of phenol in phases I and II at 10°C and at pressures up to 3 kbar are discussed in Chapter III. Chapter IV presents the phase diagram of phenol below 0°C at pressures up to 3 kbar, and powder x-ray diffraction data for phenol I and II at 1 atmosphere and -190°C. The dielectric constants of phenol I and II and their variation with temperature and pressure are presented in Chapter V. The experimental methods are described in Chapter II. Since many of these topics and methods require very little introduction, Chapter I is largely confined to the discussion of selected aspects of the measurement (Section 1.1) and analysis (Section 1.2) of dielectric data, including commonly encountered difficulties (Section 1.3), and a general account of phase transitions with emphasis on order-disorder transitions and hysteresis phenomena (Section 1.4). A literature survey of previous studies of the physical properties of phenol (Section 1.5), and a statement of the objectives of this work (Section 1.6) are also included.

1.1 Capacitance Measurements at Audio-Radio Frequencies

This section presents a discussion of the equations by which the real and imaginary dielectric constants of a material may be obtained from measurements of the capacitance and conductance of a capacitor which contains the material in question.

An A.C. circuit containing a real capacitor can be represented by a pure resistance and a pure capacitance in series, as a series equivalent circuit, or in parallel, as a parallel equivalent circuit, since the two situations cannot be distinguished by one measurement. In order to simplify the analysis of these circuits, the impedance is commonly expressed as a complex number (12,13).

In the case of the series equivalent circuit (Figure 1A) the complex impedance, Z^*, is given by:

$Z^* = R_s + jX_s$, where R_s = series resistance [1.1]

X_s = series reactance = $-1/\omega C_s$ for capacitors

$j = \sqrt{-1}$

In the case of the parallel equivalent circuit (Figure 1B), the complex impedance is a complicated function of the resistance, R_p, and the reactance, X_p, and so the reciprocal impedance, Y^*, is used for mathematical convenience. Thus

$Y^* = G + jB$, where Y^* = admittance = $1/Z^*$ [1.2]

G = conductance = $1/R_p$

B = susceptance = $-1/X_p = +\omega C_p$ for capacitors

A. Series Equivalent Circuit

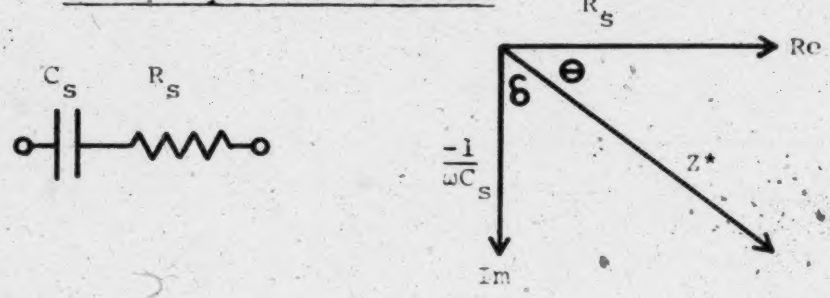
C_s
R_s
R_s
Re
θ
δ
$\frac{-1}{\omega C_s}$
Z^*
Im

B. Parallel Equivalent Circuit

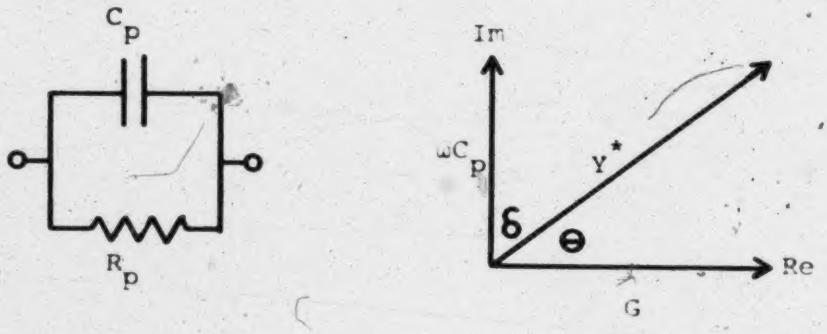
C_p
R_p
Im
ωC_p
Y^*
δ
θ
Re
G

C. Complex Capacitance

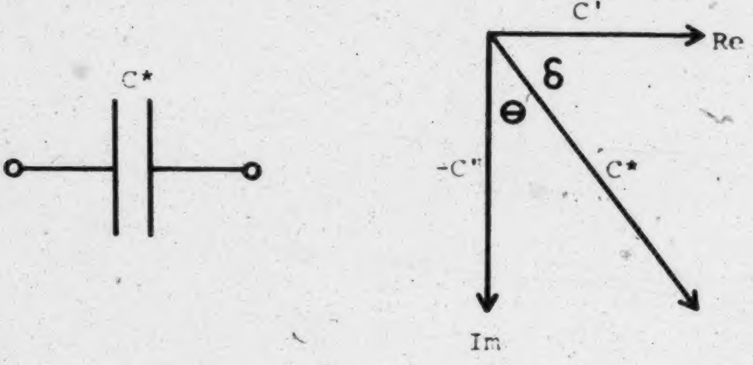
C^*
C'
Re
δ
θ
$-C''$
C^*
Im

Figure 1. Different representations of a real capacitor.

In this work, the terms conductance and susceptance refer only to the parallel equivalent circuit as defined above.

The phase angle, Θ, between series resistance and impedance, or between conductance and admittance is independent of the circuit description and is given by the expressions

$$\Theta = \mathrm{Cos}^{-1}(R_s/|Z^*|) \text{ for the series equivalent circuit,}$$

and

$$\Theta = \mathrm{Cos}^{-1}(G/|Y^*|) \text{ for the parallel equivalent circuit.}$$

The dissipation factor, D, of the A.C. circuit is defined to be the cotangent of Θ and hence it is also independent of the formalism used to describe the circuit. Thus, for the series case

$$D = \cot \Theta = \tan \delta = R_s/X_s$$

where

$$\delta = \pi/2 - \Theta, \qquad [1.3]$$

and

$$D = \cot \Theta = G/B$$

for the parallel case.

In the series equivalent case

$$D = \omega C_s R_s, \qquad [1.4]$$

while in the parallel equivalent case

$$D = G/\omega C_p, \qquad [1.5]$$

From expressions [1.1], [1.2], and [1.5], it may be shown that:

$$C_p = C_s/(1 + D^2) \qquad [1.6]$$

and

$$R_p = R_s(1 + D^2)/D^2.$$

In dielectric theory, in order to avoid the use of an equivalent circuit, it is convenient to express the capacitance itself as a complex quantity as shown in Figure 1C, i.e.

$$C^* = C' - jC''. \qquad [1.7]$$

From either equation [1.1] or [1.2], this yields

$$Z^* = -j/(\omega C^*) = 1/Y^*$$

and hence,

$$Y^* = \omega C'' + j\omega C' = G + j\omega C_p.$$

By equating real and imaginary scalars,

$$C' = C_p \qquad [1.8]$$

$$C'' = G/\omega\ . \qquad [1.9]$$

From equation [1.3],

$$D = C''/C'. \qquad [1.10]$$

The General Radio 1615A transformer ratio arm capacitance bridge (Section 2.4) can be used to measure either D and C_s, or G and C_p at a given frequency. These can be readily converted to C' and C" using equations [1.6], and [1.8] to [1.10]. If calibration of the dielectric cell has shown a lead capacitance to exist, this capacitance may be subtracted directly from the observed value of C_p to yield C_p for the cell itself, since the geometry of most cells puts any lead capacitance in parallel with the capacitor plates of the cell. The value of the lead capacitance is determined by measuring the total capacitance of the leads plus the cell, filled with two samples of known dielectric constant, ε', (see below) of which one is usually air or a vacuum. These measurements give

$$C_p = \varepsilon' C_o + C_L \qquad [1.11]$$

for two values of ε' and C_p, where C_L is the lead capacitance and ε' and C_o are defined below. C_o and C_L are then determined by solving the two resulting linear equations.

The complex dielectric constant of a dielectric material, ε^*, is defined by the relationship (14)

$$\varepsilon^* = \varepsilon' - j\varepsilon'' = C^*/C_o \qquad [1.12]$$

where C_o, the cell constant, is the real capacitance of the empty cell. From equations [1.7], [1.9] and [1.12],

$$\varepsilon' = C'/C_o \qquad \varepsilon'' = C''/C_o = G/(\omega C_o), \qquad [1.13]$$

ε' is referred to as the dielectric constant, or relative permittivity, while ε'' is commonly called the dielectric loss. The conductivity, σ, of a dielectric may be calculated from the conductance and the cell constant by the relationship (15),

$$\sigma(\mu\text{mho/cm}) = 0.08854 \frac{G(\mu\text{mho})}{C_o(\text{pf})} \qquad [1.14]$$

Thus the dielectric loss, ε'', is related to the conductivity through the proportionality $\varepsilon'' \propto \frac{\sigma}{\omega}$.

1.2 Dielectric Constants and Relaxation

For all solids, the dielectric constant, ε', is greater than about 1.5 at frequencies below 10^{10} sec^{-1}. Furthermore, if no molecular dipoles in the solid are reorienting, no dielectric loss will be observed until, at low frequencies, the presence of ionic impurities causes an increase in ε'' with decreasing frequency, i.e. $\varepsilon'' = 0$ except for the effect of impurities. If the crystal does contain reorienting molecular dipoles, dielectric loss will be observed at about the frequency at which the reorientation of the dipoles takes place. These reorientation processes are relaxation rather than resonance phenomena and, as such, their rates decrease with decreasing temperature. The dielectric constant, ε', increases with decreasing frequency through the region in which ε'' is not zero and ε_o and ε_∞ are defined as the limiting values of ε' to low and high frequency, respectively, of the relaxation process. Systems in which these phenomena are observed are said to exhibit dielectric relaxation and/or dielectric dispersion. Since the dielectric loss is a measure of the energy absorbed by the system, dielectric relaxation studies are, in effect, spectroscopic studies of the reorientation processes. Section 1.2a describes how the limiting high frequency dielectric constant, ε_∞, is related to the molecular polarizability through the Clausius-Mossotti equation. The equations which describe the interdependence of ε', ε'', and frequency, are discussed in Section 1.2b, along with practical methods of analyzing dielectric relaxation data. Experimental values of ε_o may be related to the magnitude of the reorienting dipole moment by the Onsager equation and other related equations. These are only pertinent to Chapter 6 of this thesis and are presented in Section 6.1.

1.2a The Clausius-Mossotti Equation

The macroscopic dielectric constant measured to high frequency of any dielectric relaxation processes may be related to the polarizability of the molecules in the material at the frequency in question by the Clausius-Mossotti equation (16). This equation takes the form

$$\frac{\varepsilon' - 1}{\varepsilon' + 2} \cdot \frac{M}{d} = \frac{4}{3}\pi N\alpha \equiv \bar{P} \qquad [1.15]$$

where

N = Avogadro's number

α = molecular polarizability

M = molecular weight

d = density

$\overline{P}$ = molar polarization

The equation assumes the validity of the Lorentz expression (16,17) for the local field acting on a molecule. That is, it assumes that the molecule resides at the centre of a macroscopic spherical cavity in the dielectric and that the field acting on it is due to the charges on the capacitor plates and their adjacent dielectric surfaces plus the polarization charges on the spherical surface of the cavity. Although the cavity is filled with material having the bulk dielectric constant, the Lorentz expression assumes the field resulting from molecules in this region to be zero, an assumption which is only valid for ideal gases and cubic solids (16,17). It should be stressed that the values of $\overline{P}$, ε' and α are all frequency dependent. If ε' is measured to low frequency of all vibrational transitions but to high frequency of any dipolar reorientation ($\varepsilon' = \varepsilon_\infty$), the molar polarization which appears in the Clausius-Mossotti equation is the sum of the atomic and electronic polarizations, $\overline{P}_a + \overline{P}_e$ (18,19).

The Lorenz-Lorentz equation (18) is identical to equation [1.15] except that, from Maxwell's equations*, the square of the refractive index is substituted for ε'. It is useful for calculating the molar polarization which results from electronic transitions only (Section 5.6). The atomic polarization, $\bar{P}_a$, can be determined either from the Lorenz-Lorentz and Clausius-Mossotti equations, or by a Kramers-Kronig transformation (21) of the infrared absorptivity measured over a frequency range that includes all the vibrational transitions.

Although the molar polarization is often assumed to be independent of density (22,23), this assumption may be rendered invalid by changes in the molecular polarizability with either temperature or pressure (24). A more fundamental error arises from the use of the Lorentz expression for the local field, because it assumes that the field arising from neighboring molecules is zero. This assumption is certainly not valid for non cubic solids, real gases, and liquids because the average field is not zero. It is not strictly valid even for ideal gases and cubic solids for which the average field is zero, because the instantaneous field acting on the molecule in question is non-zero due to thermal motion (24). Several corrections to the Clausius-Mossotti equation to allow for the effect of the thermal motion in liquids and gases have been suggested (24-28), but no such general correction can be made for solids and the equation is used in its simplest form, equation [1.15], as a first order approximation.

---

* This substitution is valid only if $\varepsilon'' = 0$ at the frequency in question (20) since strictly $\varepsilon^* = n^{*2}$, where $n^* = n' + jn''$, and hence $\varepsilon' = n'^2 - n''^2$ and $\varepsilon'' = 2n'n''$.

1.2b Dielectric Relaxation: The Debye and Cole-Cole Equations

Dielectric relaxation in solids may be characterized by one or more relaxation times which are related to the frequencies at which the molecules reorient. In many systems, the interdependence of ε', ε'', and frequency is related to the macroscopic relaxation time of the system, τ_o, by the Cole-Cole equation (29),

$$\varepsilon^* - \varepsilon_\infty = (\varepsilon_o - \varepsilon_\infty)/[1 + (j\omega\tau_o)^{1-h}] \qquad [1.16]$$

where ω is the angular frequency of measurement, ε^* is the complex dielectric constant, ε_o and ε_∞ are the limiting static and high frequency real dielectric constants for the process in question, and h describes the range of τ_o values. The values of ε_o and ε_∞ may be related to molecular parameters by the Onsager and Clausius-Mossotti equations, respectively (Sections 6.1 and 1.2a). The relaxation time, τ_o, is that of the macroscopic system and it must be related to the actual molecular reorientation time by an appropriate model. There are a number of suitable theories but τ_o generally lies within 30% of the molecular reorientation time (30). The parameter h indicates the spread of the reorientation times of the system. For the special case when h = 0, the system is characterized by a single relaxation time, τ_o, and equation [1.6] reduces to the Debye equation (31). If $h \neq 0$, the system contains a symmetrical Cole-Cole distribution of relaxation times, of which τ_o is the mean; the larger h, the broader the distribution. Such a situation would arise, for instance, if a single molecular reorientation process were occurring in a number of different environments, distributed symmetrically and continuously about the most probable environment. τ_o is related to the first-order kinetic rate constant, k, by the relationship $\tau_o = 1/k$ and thus may be readily used in the Eyring (32) or Arrhenius (33) equations to calculate thermodynamic activation parameters.

When experimental values of ε' and ε'', measured at a variety of frequencies, are plotted on an Argand diagram, the plot takes the form of a semicircular arc whose centre is depressed below the real axis by an angle $h\pi/2$. Such a plot is called a Cole-Cole plot. Figure 2 shows Cole-Cole

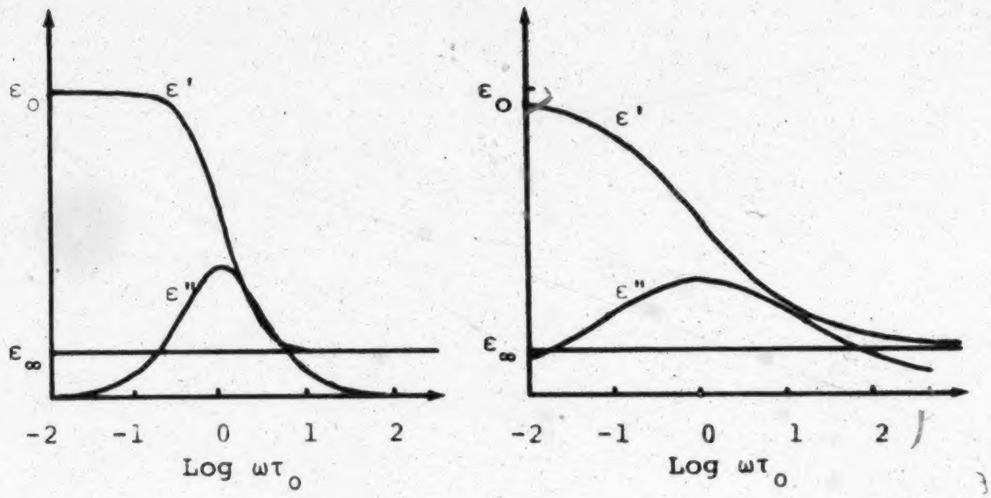

A. Debye Relaxation

B. Cole-Cole Relaxation

C. A Cole-Cole Plot

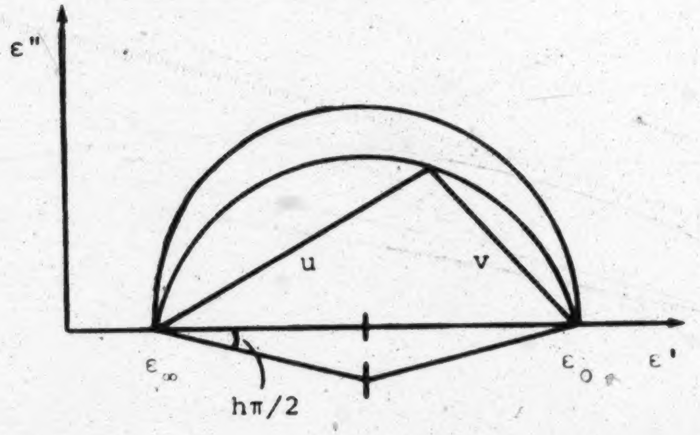

ε''
u
v
ε_∞
$h\pi/2$
ε_o
ε'

Figure 2. The Debye and Cole-Cole dispersion relationships and a Cole-Cole plot of each. The upper and lower semicircles in the Cole-Cole diagram represent plots of the Debye and Cole-Cole relationships respectively.

plots for systems which exhibit Cole-Cole and Debye relaxation and also shows the frequency dependence of ε' and ε'' for the two types of relaxation. ε_o, ε_∞, and h can be determined from a Cole-Cole plot by algebraically bisecting chords drawn between pairs of data points and averaging the points of intersection of all the bisectors to obtain the centre of the semicircle, and then determining the average radius. Because frequency is not one of the variables plotted, τ_o cannot be determined directly from the Cole-Cole plot and other treatments must be used. Three well defined procedures are discussed below.

τ_o may be determined from the relationship (29,34)

$$v/u = (\omega\tau_o)^{1-h} \qquad [1.17]$$

where u and v are the chords defined in Figure 2, by plotting log(v/u) vs. logω and noting the intercept. Obviously h may also be determined from this graph, but it has been found (reference 34 and this work) that the data can always be fitted by assigning h the value determined from the Cole-Cole plot and, if this is done, the τ_o values so obtained are more consistent with those determined by other methods described below.

τ_o may also be calculated from the equation

$$\operatorname{Cosh}^{-1}(\varepsilon''_M/\varepsilon'') = h' \ln(\omega/\omega_M) \qquad [1.18]$$

where ε''_M is the maximum observed imaginary dielectric constant and occurs at frequency $\omega_M (\omega_M = 1/\tau_o)$, and ε'' is the loss at frequency ω. This equation is derived from the Fuoss-Kirkwood relationship (7) which is identical to the Cole-Cole equation at frequencies near that of maximum absorption (8). ε''_M is known from the fitted Cole-Cole plot and a plot of $\text{Cosh}^{-1}(\varepsilon''_M/\varepsilon'')$ against $\ln\omega$ intercepts the $\ln\omega$ axis at $\omega = \omega_M$, i.e. at $1/\tau_o$. h' is an arbitrary constant, similar to but not necessarily equal to h. The $\cosh^{-1}(\varepsilon''_M/\varepsilon'')$ vs. $\ln\omega$ data should always be plotted rather than simply being treated by numerical curve fitting since the relationship may be non linear at points far removed from ω_M (36) and using such points in a curve fit will yield erroneous values for ω_M.

Another method of calculating τ_o has been formulated by Williams (37), who derived the expression

$$\omega^n = \frac{1}{\tau_o{}^n} \left\{ \frac{(\varepsilon_o - \varepsilon')}{\varepsilon''} \sin \frac{n\pi}{2} - \cos \frac{n\pi}{2} \right\} \qquad [1.19]$$

where n = 1-h if the distribution of relaxation times follows the Cole-Cole expression. A value of n is chosen by trial and error such that a plot of ω^n vs. $(\varepsilon_o - \varepsilon')/\varepsilon''$ gives a straight line of slope $(\sin n\pi/2)/\tau_o{}^n$ and intercept $(\cos n\pi/2)/\tau_o{}^n$.

In the case where two distinct reorientation processes are occurring concurrently, the system would best be described by two different relaxation times rather than by a distribution. The locus of two or more simultaneous Debye relaxation processes is given by the expression (38)

$$\varepsilon^* - \varepsilon_\infty = \sum_{i=1}^{n} (\varepsilon_{i-1} - \varepsilon_i)\,(1 + j\,\omega\tau_{oi})^{-1} \qquad [1.20]$$

hence,

$$\varepsilon' = \varepsilon_\infty + \sum_{i=1}^{n} A_i\,(1 + \omega^2\tau_{oi}^2)^{-1} \qquad [1.21]^\dagger$$

and

$$\varepsilon'' = \sum_{i=1}^{n} A_i\omega\tau_{oi}\,(1 + \omega^2\tau_{oi}^2)^{-1} \qquad [1.22]^\dagger$$

where $A_i = \varepsilon_{i-1} - \varepsilon_i$ is the amplitude and τ_{oi} is the relaxation time of the i^{th} dispersion, and n is the number of reorientation processes. A typical Cole-Cole plot of two such dispersions is shown in Figure 3. Obviously the frequencies of maximum dispersion in the observed Cole-Cole plot do not correspond exactly to those of the individual dispersion plots. Resolution into separate Debye dispersions is only possible if a complete set of accurate data is available, as discussed in reference 38, and becomes progressively more difficult as the separation between relaxation times decreases.

---

† These equations are given incorrectly in reference 38.

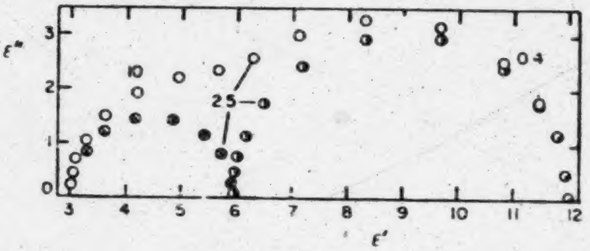

Figure 3. The Cole-Cole plot of a resolved dispersion (taken fron reference 38). Numbers beside points indicate the frequency in kHz. The open points show the dispersion resulting from the superposition of two Debye dispersions (ε_o= 12.00, ε_1=6.00, $\varepsilon_2=\varepsilon_\infty$=3.00, τ_1=2.00x10^{-4} sec, τ_2= 2.00x10^{-5} sec. The other points show the results of resolving the above data into two dispersions using the method presented in reference 38.

1.3 Dielectric Effects Resulting from Impurities and Sample Inhomogeneity

Impurities and inhomogeneities in dielectric samples can cause complicating effects which must be treated before the intrinsic properties of the sample can be determined using the methods discussed in Section 1.2. In this section, those effects which are commonly encountered are discussed and methods of correcting for them are indicated where possible.

1.3a D.C. Conductance and Electrode Polarization

The presence of uniformly dispersed, mobile, charge carrying impurities in a dielectric gives rise to a conductance, G_o, which is essentially independent of frequency and which is called the D.C. conductance (39). Since $\varepsilon"_{app} = G_{app}(\omega)/\omega C_o$ (Section 1.1) where $\varepsilon"_{app}$ and $G_{app}(\omega)$ are the apparent values of $\varepsilon"$ and conductance, and since $G_{app}(\omega) = G_o + G(\omega)$ where $G(\omega)$ is the intrinsic conductance, the term G_o causes a sharp rise in $\varepsilon"_{app}$ with decreasing frequency. G_o can be evaluated if $\varepsilon"_{app}$ can be measured to low frequency of any intrinsic conductance, since $\varepsilon"\omega C_o$ is constant and equal to G_o in regions where the intrinsic conductance is zero.

In practice, G_o is usually determined as the low frequency limit of $\varepsilon''_{app}\omega C_o$. Corrected values of ε'' at any frequency are then given by the equation

$$\varepsilon'' = (G_{app}(\omega) - G_o)/\omega C_o \qquad [1.23]$$

where values of G and C_o are in units of pmho and pf, respectively.

Curves A of Figure 4 show conductance data and a Cole-Cole plot uncorrected for the cell constant (i.e. a plot of C' vs. C") that are seriously perturbed by D.C. conductance. The sample was hexamethylene tetramine hydrate that was prepared (9) from triply distilled water which was not freshly boiled to remove carbon dioxide. The results were obtained during the present work using the parallel plate dielectric cell (Section 2.5b) at -18.4°C and 803 bar. It was not possible to correct this data for the effects of D.C. conductance by rigorous methods because conductance values were not measured at sufficiently low frequencies, and so a value of 1.2×10^7 pmho was arbitrarily assumed for the D.C. conductance. When this D.C. conductance was subtracted from the measured conductance values and the resulting values of C" were plotted against C', curve B of Figure 4 was obtained. The relaxation time, τ_o, obtained from the data in curve B of Figure 4 was $5.35 \pm 0.10 \times 10^{-5}$ sec., which compares with

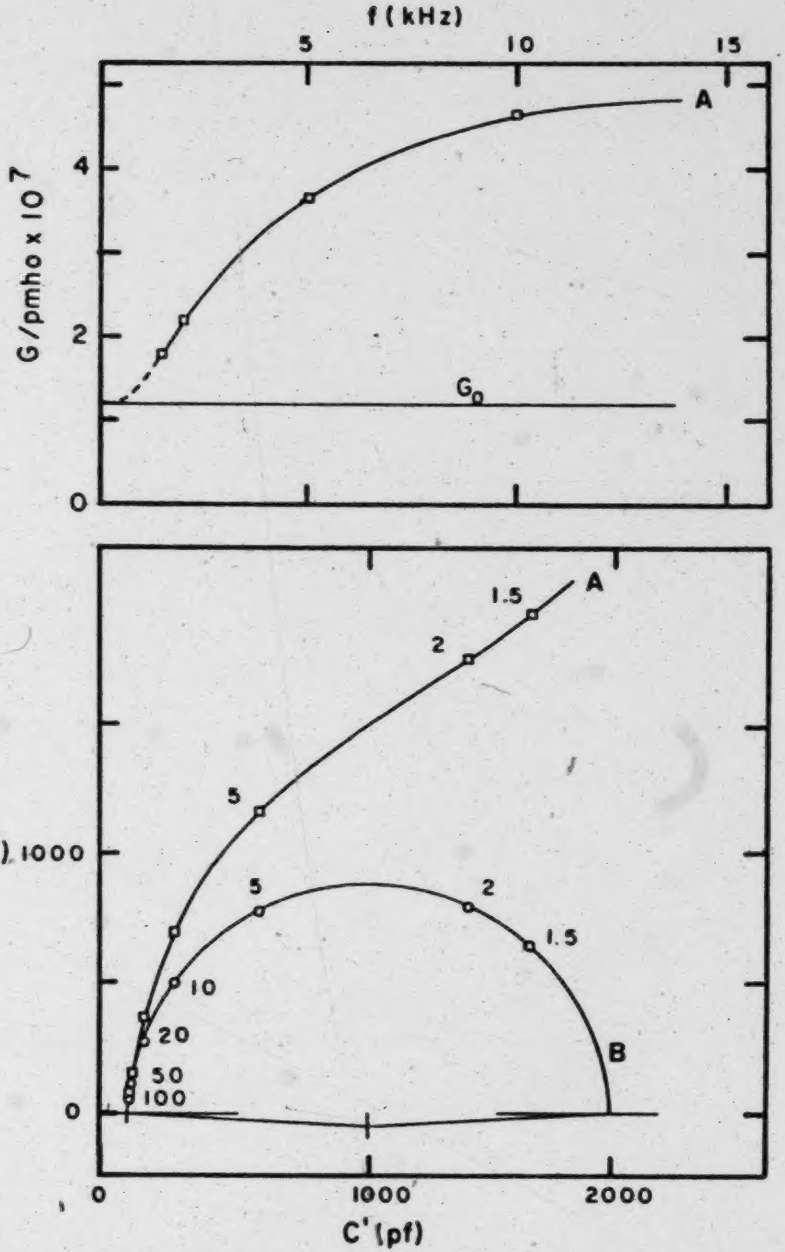

Figure 4. Dielectric relaxation data for impure hexamethylene tetramine hydrate at -18.4°C and 803 bar. In the upper box, curve A represents the measured conductance values, and the line marked G_0 indicates the assumed D.C. conductance. In the lower box, curves A and B are Cole-Cole plots of the capacitance data before and after correcting C" for D.C. conductance. The number beside each point is the frequency in kHz.

the value 6.5 x 10^{-5} sec. at -18.4°C and one atmosphere which can be measured from the graph in Davidson's paper (40). The value of h obtained from curve B of Figure 4 is 0.04 which is consistent with the values of 0.07 at -38°C and 0.23 at -84°C reported by Davidson. While rather crude corrections for D.C. conductance, such as that discussed above, are often useful, it is obviously desirable to obtain reliable conductance measurements to low frequency of the relaxation so that an accurate correction can be made. It should be noted that, for some relaxation mechanisms, the presence of impurities may affect the relaxation time of the system (41).

Although D.C. conductance does not affect ε', an associated phenomenon, the build up of ions at the electrode faces or in regions of the sample, can drastically increase ε' at low frequencies (42,15). This 'electrode polarization', or, more properly, 'space charge polarization', is well defined for liquids and may be readily subtracted (15). In the case of solids, space charge polarization affects both ε' and ε". If the conductance is large enough ($G \gg \omega\varepsilon' C_o$) gross corrections can be made (15) but, if this condition is not met, the equations in question become prohibitively complicated. Since the effect occurs predominantly at electrode surfaces, it may be minimized by increasing the distance between the capacitor plates, or by covering the plates with a layer of inert dielectric with known thickness, dielectric constant, and negligible conductivity so that the resulting Maxwell-Wagner effects (Section 1.3b) can be subtracted (43). In solid samples, both the D.C. conductance and the electrode polarization become increasingly noticeable as the melting point is approached.

1.3b Maxwell-Wagner Effects

If some regions of a nonhomogeneous medium have appreciable conductivity, the medium can be shown to exhibit Debye-like dielectric relaxation (44,45). This 'Maxwell-Wagner' effect depends on the size, shape, and conductivity of the conducting region, but for the simple case of a parallel plate capacitor containing two dielectric layers of thickness d_1 and d_2 arranged parallel to the capacitor plates, the relaxation parameters are given by the following equations (45)

$$\varepsilon_o = \frac{d(\varepsilon_1 d_1 \sigma_2^2 + \varepsilon_2 d_2 \sigma_1^2)}{(\sigma_1 d_2 + \sigma_2 d_1)^2} \qquad [1.24]$$

$$\varepsilon_\infty = d\varepsilon_1\varepsilon_2/(\varepsilon_1 d_2 + \varepsilon_2 d_1) \qquad [1.25]$$

$$\tau = \varepsilon_o(\varepsilon_1 d_2 + \varepsilon_2 d_1)/(\sigma_1 d_2 + \sigma_2 d_1) \qquad [1.26]$$

$$\sigma = d\sigma_1\sigma_2/(\sigma_1 d_2 + \sigma_2 d_1)$$

where ε_i, σ_i and d_i refer to the dielectric constant, D.C. conductivity, and thickness of the i^{th} layer respectively and d is the total thickness of the sample. The remaining quantities refer to bulk properties of the medium. The conductivity or specific conductance, σ, is related to the conductance, G, by equation [1.14].

A many layered 2-component system is described by these same equations where d_i represents the total thickness of each component. Equations describing the effects of other shapes and arrangements are reviewed by Van Beek (45). In general, needle shaped conducting regions cause much larger dispersions than spherical regions. It should also be noted that if two parallel layers are arranged perpendicular to the plates, their contributions to the dielectric constant are simply proportional to their cross sectional areas, and no loss is observed.

Maxwell-Wagner effects may be observed experimentally in a dielectric through which particles of a second material are dispersed, for instance, hydrocarbons contaminated with water, colloidal dispersions, and powder mixtures (46). If the second component is an impurity, measurements to high frequency of the dispersion will yield reasonable values for ε_1, since, from equation [1.25],

$$\varepsilon_\infty \approx \varepsilon_1, \text{ if } d_1 >> d_2.$$

The special case of cracks, or air gaps, in a sample has been considered by Auty and Cole (39). It is clear from equation [1.25] that the dielectric constant may be drastically lowered by even thin cracks parallel to the plates. Chan and Chew (22) have shown that the application of a pressure of 10 bar to a sample of solid cyclohexane yields values of ε which increase with decreasing temperature while previous studies (47), in which pressure was not applied, show ε to fall with decreasing temperature, presumably because cracks formed as the sample contracted.

1.4 Solid-Solid Phase Transformations

Since dielectric measurements provide a valuable technique for investigating the nature of solid-solid phase transformations, a brief discussion of such transformations is in order. Phase transitions which are accompanied by a discontinuous change in the first derivatives of the Gibbs free energy, G, with respect to temperature or pressure are defined as 'first order' transitions (48,49). Such transitions exhibit, therefore, discontinuous changes in volume, entropy, and internal energy. They are commonly studied by applying pressure isothermally to a polycrystalline sample and noting the pressure at which the volume discontinuity occurs (50).

The variation of the transformation pressure with temperature, along with the magnitude of the volume change, can then be treated using the Clapeyron equation (51) to yield the changes in internal energy, enthalpy, and entropy for the transformation at each temperature. The onset of a first order transition is also often indicated by a discontinuous change in the dielectric constant of the solid, mainly because of the effect of the change in density on the dielectric constant (Section 1.2a). Since changes in capacitance can be measured to high precision, observing the variation in dielectric constant with pressure or temperature is a valuable technique for detecting such transformations.

Second and higher order transformations (48) do not show discontinuities in the first derivative of the Gibbs free energy, but derivatives of some higher order do show discontinuities, and it is the order of these derivatives which defines the order of the transformation. For instance, second order transitions show discontinuities in the second derivative of the Gibbs free energy with respect to temperature or pressure. Second and higher order transitions are often called 'lambda' transitions (52) because of the shape of plots of heat capacity against temperature in the region of transition. Many such transitions involve the onset of molecular reorientation and this can readily be observed by dielectric methods if the reorientation process involves a change in the orientation of molecular dipoles.

Two aspects of solid-solid transformations which are of particular relevance to this work are order-disorder transformations and the hysteresis in the isothermal transformation pressures of many transitions. The former warrants discussion because dielectric relaxation techniques yield valuable information about disordered phases and it was partly for this reason that the dielectric apparatus was assembled. The latter is of importance because it is the transformation hysteresis which permits the metastable existence of one phase in the region of stability of another (Section 2.7).

1.4a Order-Disorder Transitions

Ordered crystals are composed of molecules which are situated on regular positions in a crystal lattice and which are oriented in a regular fashion relative to that lattice. Molecules in these crystals thus possess both long range positional and orientational order. There is, however, another class of crystals in which the molecules are on, or nearly on, regular positions in a crystal lattice, but which are oriented in an irregular fashion relative to that lattice. Such crystals are referred to as orientationally disordered crystals (53).

Orientationally disordered crystals may exhibit either dynamic or static disorder, i.e. the orientation of each molecule may or may not change with time. Both dynamically and statically disordered crystals often exhibit broad bands in their vibrational spectra, because the absence of translational symmetry in such crystals causes all possible intermolecular vibrations to be infrared and Raman active (53,54,55). Dynamic disorder results from the rapid rotation of molecules about their lattice sites, as in plastic crystals such as those of the tertiary butyl halides (56), and from the migration of a small number of lattice defects through the crystal, such as occurs in many phases of ice (3). Whenever the mechanism for the molecular reorientation causes a change in the orientation of the molecular dipoles the crystal exhibits dielectric relaxation and the parameters of the reorientation process may be determined by the methods described in Sections 1.1 to 1.3.

If dielectric relaxation is present, ε' to low frequency of the relaxation process, and ε'' near the reorientation frequency, will usually be much greater for a dynamically disordered phase than for an ordered one since, in the ordered phase, if the effects of impurities are ignored, $\varepsilon'' = 0$ and ε' is small. Dielectric methods can thus determine whether a known first order transition involves dynamic disorder. In addition, dielectric techniques are an invaluable tool for detecting first order, order-disorder transitions with small volume changes, and order-disorder transitions of second and higher order, both of which are difficult to observe using volume measurements alone.

The usefulness of the above procedures in investigating the nature of a multiphase system is illustrated by the many studies on the phases of ice (3). The transitions between ice phases I and II, II and V, III and II, and VI and VIII are all first order, order-disorder transitions. This was indicated by the entropy change, calculated from the phase diagram and the transition volume change through the Clapeyron equation (51). The dielectric studies confirmed this result and provided the activation parameters for the reorientation processes in the disordered phases. They also revealed the existence of the ice VII - VIII transition, which cannot be studied by measuring volume because the volume change is very small, and showed that phase VIII is ordered while phase VII is dynamically disordered. Dielectric studies also showed the existence of a higher order transition between ice III (disordered) and ice IX (ordered), both metastable in the region of ice II.

A large number of disorder-order transformations in other molecular crystals were discovered by C. P. Smyth (1) by measuring the dielectric constant of solid samples as a function of temperature at one atmosphere. In favourable cases, such as the t-butyl halides (56), where the change in dielectric constant between the ordered and dynamically disordered phases is large, this is a very useful method for detecting such transitions. However, as discussed elsewhere in this thesis (Sections 1.3b and 5.2), such studies are fraught with the danger of error due to the formation of cracks in the sample as it contracts upon cooling.

1.4b Hysteresis and the Coexistence of Two Solid Phases

When a state function of a given solid phase is measured isothermally as a function of pressure in a piston cylinder pressure vessel, the observed pressure at which a given value of the property occurs while the pressure is being increased is often higher than the pressure observed while the pressure is decreased (e.g. Figure 14 in Section 3.1). Furthermore, when the change from increasing pressure to decreasing pressure, or vice versa, is made, several data points are obtained which are clearly not on a true part of the compression or decompression curves. Such spurious data points can usually be identified (Section 3.1) and, once identified, should be rejected before treating the data. The hysteresis in the observed pressures is caused by friction in the apparatus, friction between the sample and the walls of the pressure vessel and, to some extent, the pressure transmitting properties of the sample.

If the hysteresis of the apparatus can be determined by a blank run and subtracted (Sections 3.1 and 4.2) to yield a set of data containing only the sample hysteresis, the resulting value for the observed pressure at each point represents the pressure at the face of the moving piston and is the maximum or minimum pressure on the sample during compression and decompression, respectively. In this case, once the spurious points have been rejected, a set of data representing the state function of the bulk medium against the average pressure in the cell may be obtained by averaging the pressures at which given values of the state function occur during compression and decompression. If the hysteresis of the apparatus cannot be subtracted (Section 5.2), the above procedure may still be used, on the assumption that the effects due to the apparatus are symmetrical with respect to the direction of the pressure change.

The pressure at which a phase transformation occurs isothermally has also been shown to exhibit hysteresis in many cases. This hysteresis is over and above that due to friction in the apparatus and sample, as determined from measurements on the phase either above or below the transition (50,52,57). To be more specific, the applied pressure must exceed the equilibrium pressure between the two phases by some minimum amount in order to form the high pressure phase and conversely it must be lowered below the equilibrium pressure by a minimum amount in order to reform the low pressure phase. The region about the equilibrium line in which both phases are either stable or metastable with respect to each other and no interconversion can take place (50,58) is called the hysteresis region, or the region of indifference. Figure 5 shows a plot of the linear displacement of a sample of commercial phenol against pressure which illustrates the hysteresis in the I - II transition. The lower curve in Figure 5 shows that although the border of the region of indifference had been passed at a, the transformation was not initiated until point b, after which the pressure fell until it had returned to the hysteresis line at point c. The transition was apparently not complete until point d had been reached, presumably because the mechanical strength of the newly formed phase II prevented pressure from being readily transmitted to the remaining, untransformed phenol I (Section 4.1). The necessity of going beyond the region of indifference to initiate a transformation is apparently purely a nucleation effect analogous to supercooling. The hysteresis phenomenon, i.e. the existence of the region of indifference, is clearly

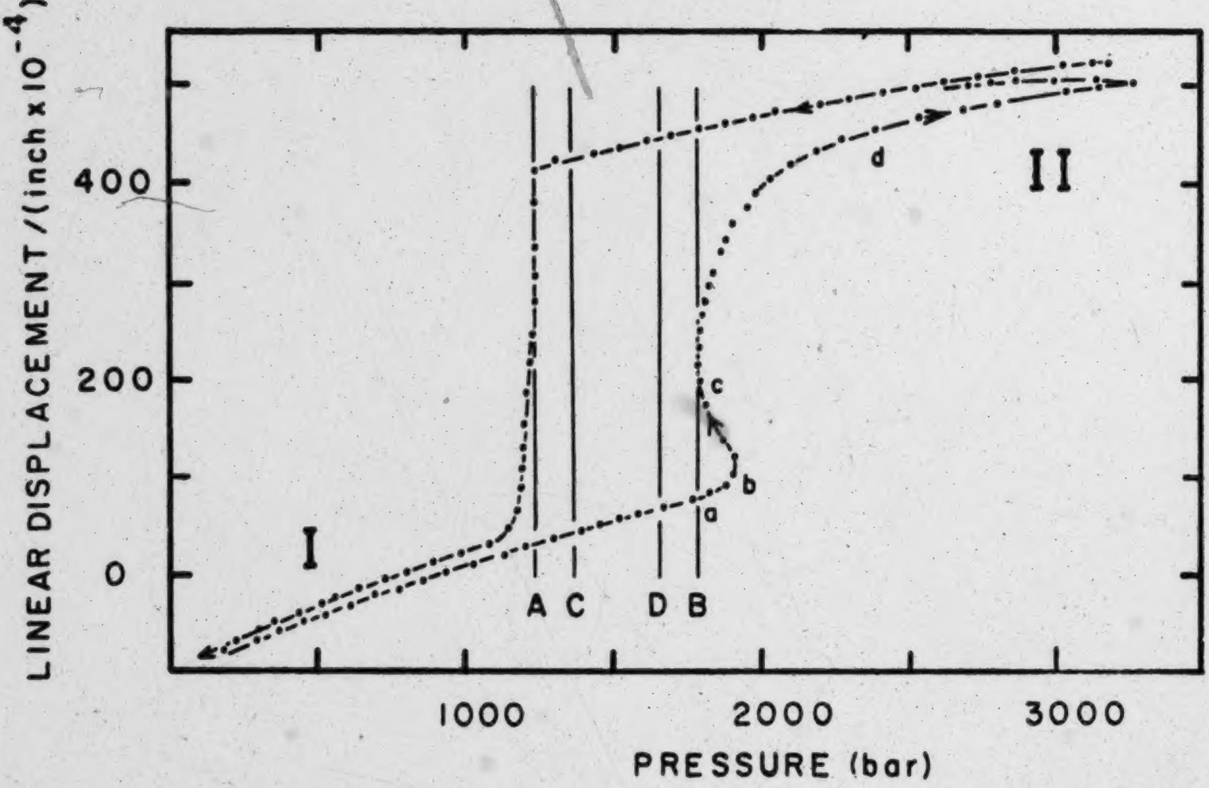

Figure 5. A plot of the linear displacement of a sample of commercial phenol (p. 110) against pressure at 12°C, showing the hysteresis in the I→II transformation. A and B are the borders of the region of indifference, and C and D are the same borders, corrected for the hysteresis in the sample and apparatus. The arrows show the direction of the change in pressure for each curve and I and II denote the regions of stability of phenol I and II.

distinct from supercooling or supersaturation phenomena since, in the latter, the presence of seed nuclei of the stable phase would cause spontaneous crystallization of that phase. An excellent review of the literature is given in reference 52.

There are a number of theoretical treatments of hysteresis (52,57,59,60). Most theories assume the phenomenon to be an equilibrium process and that, before a phase change can occur, the bulk free energy of the unstable phase must be high enough to overcome both the surface free energy at the phase boundary and the free energy arising from the strains which would result if one microcrystal of a given phase, surrounded by a matrix of that phase, were to transform to a second phase of different density. The hysteresis effect has also been attributed (57,61-65) in part, to the existence of a large number of independent microcrystalline domains in the sample, each of which must undergo separate nucleation. This explanation does not apply to all systems since, as Bridgman (66) demonstrated, the nucleation of the new phase is distinct from the propagation process in many systems, such as the one shown in Figure 5. He deduced that in such systems, one nucleus is propagated until the transformation is complete.

It cannot be emphasized too strongly that great care must be taken to ensure that the observed hysteresis is independent of particle shape and size, apparatus, and the pressure transmitting fluid (if present) before hysteresis results are treated quantitatively using an appropriate theory. Since most of the published phase transition data, including that presented in Figure 5 and in Section 4.2 have been obtained under a limited variety of conditions, one cannot unequivocally conclude that the observed hysteresis effects arise solely from conditions of thermodynamic equilibrium. The existence of hysteresis in many solid-solid phase transformations in a variety of apparatuses is a well documented reality, and the models presented in the theories listed above appear plausible. At present, however, the wide range of reliable experimental data necessary to examine the phenomenon in a definitive way is not available.

1.5 Properties of Phenol

1.5a Phenol I

Since the properties of pure phenol have been the subject of controversy since the late nineteenth century, a brief review of the work to date is in order. Much of the uncertainty as to what constitutes pure phenol is reflected in the many reported values of its melting and freezing points, which range from 43°C to 39.7°C (67,68, 69). Perhaps the most reliable value for the liquid-solid equilibrium temperature of pure phenol is that reported by Andon and coworkers (70) who prepared their phenol with extraordinary care and who determined the freezing point of phenol to be 40.90°C using sophisticated apparatus (71). The freezing point method, in general, gives more accurate values for the equilibrium temperature than does the melting point technique (71). Since melting points as high as 43°C (72) and 42.5°C (73) have been reported, it is possible that, although most impurities lower the melting and freezing points (70,74), some commercial products may contain an impurity which causes these values to rise (75). Hence, while studies on samples with abnormal melting or freezing points are highly suspect, a value near 40.9°C does not in itself guarantee purity since the effects of impurities which raise and lower the equilibrium temperature may cancel each other.

Oxidation of phenol, either by hydrogen peroxide (76,77) or by oxygen in the presence of light and water (78), produces catechol, quinol, and quinones. The reddish brown colour of some commercial products is undoubtedly due to the oxidation products (catechol, quinone, and phenoquinone). Contamination with water is common, since phenol is hydrophilic and forms a stable hydrate (74) of composition $C_6H_5OH.1/2\ H_2O$ (79). Timmermans (67) also asserts that contamination with cresols may occur.

Unfortunately, beyond their calorimetric determinations, Andon and coworkers did not measure a wide range of physical properties of their ultrapure phenol. Timmermans (67) on the other hand, has reported results which cover a wide range of physical parameters. His melting point (40.75°C) and boiling point (182.2°C) are in relatively close agreement witn those of Andon et al. (40.90°C and 181.84°C, respectively), and his values for other parameters are consistent with many of those reported by other workers (68,69), all of whom report freezing or melting points between 40.7°C and 40.9°C. In the absence of results on more carefully characterized samples, Timmermans' values must be accepted as being the best available. Values of physical parameters from Timmermans (67) and Andon et al. (70) are listed in Table 1.

Phenol I, the stable phase at atmospheric pressure and room temperature, has a structure consisting of two non-equivalent polymeric chains of hydrogen bonded phenol molecules in each unit cell. The chains are centered on the (1/4, y, 3/4) and 3/4, $\overline{y}$, 1/4) special positions in an orthorhombic unit cell in the space group $P2_122_1$ [non standard setting of $P2_12_12(D_2^3)$] (80,81,82). The cell dimensions at 15°C are (82) a = 6.02 ± 0.02A°, b = 9.04 ± 0.03A°, c = 15.18 ± 0.04A°, with 6 molecules per unit cell. None of the x-ray diffraction studies located the hydrogen atoms in the hydrogen bonds, but the authors deduced (81,

Table 1. Some physico-chemical parameters for pure phenol.[a]

Boiling point/760 mm: 181.84°C (70)

Freezing point: 40.90°C (70)

Freezing point depression: (water) 0.8°C/mole % (74)

(αmethylnaphthalene) 0.85°C/mole % (70)

Density (25°C, solid): $d_{25}(g/cm^3) = 1.132 \pm 0.001$ (70)

Refractive index, n_D^{45}: 1.54027 (67), dn/dt: 0.00050, see also p. 209.

Azeotropic properties of the phenol-water system:

Boiling point/760 mm = 99.52°C

Composition = 90.79% water (99)

[a] Timmermans (68,69) also lists many other physical properties.

82) that the true symmetry was monoclinic $P2_1(C_2^2)$ and that the apparent orthorhombic symmetry resulted from the almost negligible contributions of the hydrogen-bonded hydrogen atoms to the structure factors (82). Presumably the apparent $P2_122_1$ symmetry could also be the result of either orientational disorder in the positions of the hydrogen-bonded hydrogen atoms within the polymeric chains, or disorder with respect to the orientation of the chains themselves. The unit cell is depicted in Figure 6.

Evans (83) has carried out a detailed vibrational analysis of phenol based upon the infrared spectra of the liquid, gaseous, and solid states, and the Raman spectrum of the liquid. Raman spectra of single crystals have also been reported (84,85), as well as the positions of several peaks in the far infrared spectrum (86,87).

In 1932, C. P. Smyth published two papers (73,88) dealing with the dielectric properties of solid phenol over the temperature range 40.5 to -60°C at frequencies from 60 kHz to 0.3 kHz. Smyth's results are interesting in that, while there is no evidence of dielectric relaxation, there is an extremely rapid decrease in the molar polarization of the phenol samples with decreasing temperature. Assuming that the Clausius-Mossotti equation (Section 1.3) is valid, this implies a strongly temperature-dependent atomic or electronic polarizibility of the molecules in the phenol I lattice. The data

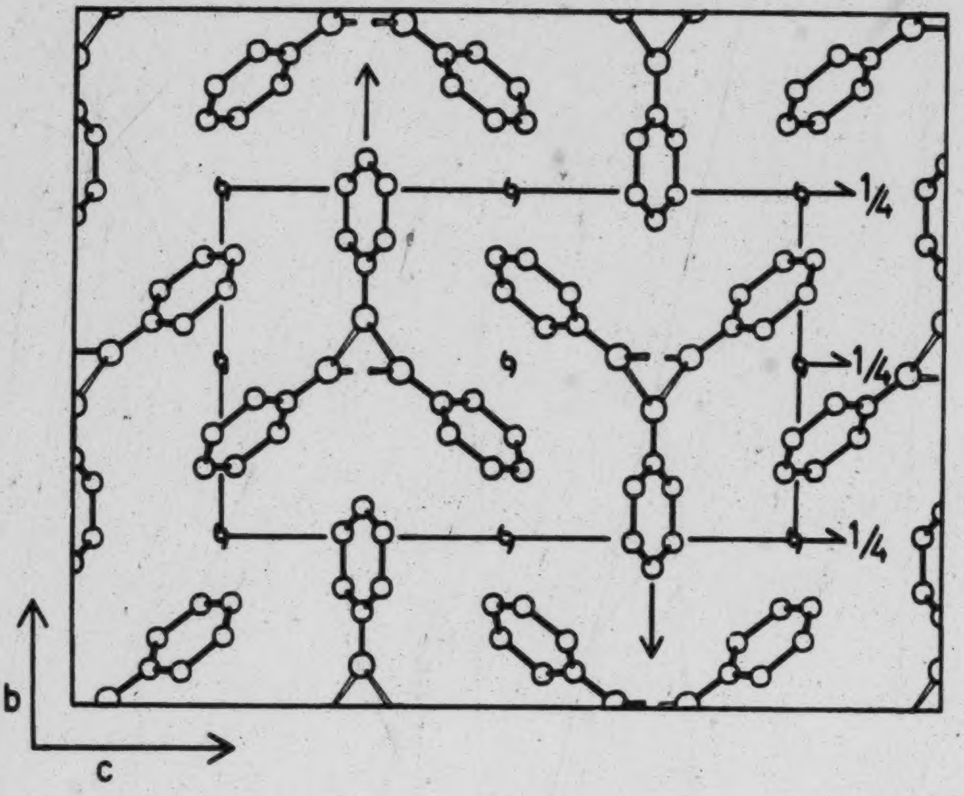

Figure 6. The phenol I lattice, viewed down the a axis. The inner rectangle represents the unit cell. Symmetry elements are shown using the notation found in reference 82. Hydrogen bonds are indicated by the hollow lines.

presented in Smyth's papers indicate that his results were affected by significant space charge polarization, and, furthermore, the high melting point of one sample (73) suggests the presence of significant impurities in that sample. Auty and Cole (39) and Chan and Chew (22) have shown that the formation of cracks upon cooling solid samples can cause an apparent decrease in polarization with temperature, similar to that observed by Smyth for phenol, when the opposite is, in fact, the case. Russian workers have reported results (89) which are essentially the same as those of Smyth and which are suspect for the same reasons.

1.5b Phenol II

The I - II transition in solid phenol was first studied by Tammann (58), who showed that the indifference, or hysteresis, region of the transition was so large that phenol II could be recovered at one atmosphere and -80°C. Although Tammann's sample purity and quantitative results were later shown to be suspect (90), his results indicated qualitatively that phenol II could not be prepared at pressures less than 2 kbar, the transition pressure at his triple point. This result is consistent with the failure of more recent workers to observe a phase change on cooling phenol at atmospheric pressure on a cooling stage to

-50°C (91) and -160°C (92). To further substantiate this observation, cooling a KBr disk of phenol to -180°C (93) produced no significant change in the infrared spectrum.

Bridgman (90) has studied the phase diagram of phenol above 0°C to 12 kbar and determined the thermodynamic parameters for the liquid - I, liquid - II, and I - II phase transformations. The I - II parameters, corrected for an error in Bridgman's pressure calibration (94,95), are listed in Table 2, and show phenol II to have a smaller entropy and enthalpy than phenol I. Bridgman also determined the approximate difference between the volume compressibilities of phases I and II at the triple point, but he did not measure the absolute compressibility of each phase. He later extended his studies to about 50 kbar at 25°C and 150°C but detected no further polymorphic transformations (96).

Pushin (97) observed a solid-solid phase transformation at 64.4°C upon cooling phenol at a constant pressure of 2200 kg/cm^2. This value for the I - II transformation can only be correct if Bridgman's triple point pressure and temperature are too low.

The infrared spectrum of phenol II at high pressure in a diamond cell has been reported (86) by Brasch et al. and the spectrum shows significant differences from that of phase I. Essentially, the frequency assigned to the OH

Table 2. Thermodynamic parameters for the phenol I - II transformation as determined by Bridgman (90) and corrected for his error in pressure calibration (94,95). $\Delta V = V_I - V_{II}$, etc.

Pressure (bar)	Temp. (°C)	ΔV cm^3/g	$\frac{dT}{dp}$	$\Delta\bar{H}$ kcal/mole	$\Delta\bar{E}$ kcal/mole	$\Delta\bar{S}$ e.u.
1315	0.0	0.0593	0.0851	0.428	0.253	1.567
1551	20.0	0.0580	''	0.449	0.247	1.532
1786	40.0	0.0568	''	0.470	0.242	1.501
2021	60.0	0.0556	''	0.490	0.236	1.471

stretching mode shifts from 3200 cm^{-1} (phenol I) to 3400 cm^{-1} (phenol II) as compared with a vapour phase value of 3661 cm^{-1} (83). There were also a number of different features in the far infrared spectrum. Since the authors did not present their spectra and limited their analysis to the comment that the hydrogen bond appears weaker in phenol II than in phenol I, apparently only the gross features of these spectra were detected. These appear to be the only studies of phenol II reported in the literature.

1.5c Vitreous Phenol

Defrain and Trong Linh (98) reported that a vitreous phase of phenol forms when phenol vapour is condensed on a plate at -140°C. The phase can be characterized by its diffuse x-ray diffraction pattern, and cannot be formed by freezing supercooled liquid phenol. Vitreous phenol reverts to phase I above -140°C at a rate which is dependent on the sample temperature.

1.6 Objectives of This Work

As stated in the preface, one of the initial aims of this work was to set up operational equipment for the measurement of dielectric constants, compressibilities of solids under pressure, and phase transitions. The phases of solid phenol were chosen for study because, although a number of studies had been carried out on both phases, particularly phenol I, reliable values of the dielectric constants and compressibilities of each phase and of the transition pressures below 0°C had not been determined. The relatively low pressures required for the I-II transition and the fact that, since phenol is a solid at room temperature, no liquid seals were required in the pressure vessels also made this an attractive system to study. The historical importance of phenol as one of the first solid polymorphs to be observed (58) and the existence of some infrared data for the second phase (86) were also factors in the selection.

The objectives of this study were to prepare and characterize metastable phenol II at one atmosphere and to measure the dielectric constants of phenol I and II as a function of frequency and pressure, both to obtain values for their molar polarizations, and to determine whether dielectric relaxation is present in either phase. The compression measurements were necessary to obtain the densities of phenol I and II as functions of pressure for the molar polarization calculations, and they also provided compressibility data for each phase. The powder x-ray diffraction work was primarily aimed at characterizing phenol II, and the phase diagram was examined both to define the region of stability of metastable phenol II, and to investigate the failure of earlier workers (Section 1.5b) to obtain phenol II by cooling phase I.

Chapter II. Experimental

2.1 Purification of Materials

Analar analytical reagent phenol from freshly opened bottles was used for the compressibility and phase diagram determinations. Titration against standardized base showed this product to be 99±1% pure. One compressibility sample and all of the samples used to determine the phase diagram were further purified by directional freezing in clean, sealed, evacuated glass tubes followed by zone refining. The dielectric studies used freshly opened Mallinckrodt analytical reagent phenol, also purified by directional freezing and zone refining.

The zone refining tubes were constructed as shown in Figure 7 with an i.d. of either 0.5 or 1.5 cm. The bulb on the end of the tubes was filled in a nitrogen purged dry box with enough powdered phenol to fill about 80% of the cylindrical portion of the tube, after which the tube was sealed under vacuum, and the sample melted into the cylindrical region of the tube. Portions of the tube not in contact with sample were wrapped with heating tape to avoid sublimation. The tube was then placed in the zone refining apparatus, which was contained in a dark refrigerator at 10°C. The zone refining was accomplished by pulling the tubes, in a vertical position, up through a

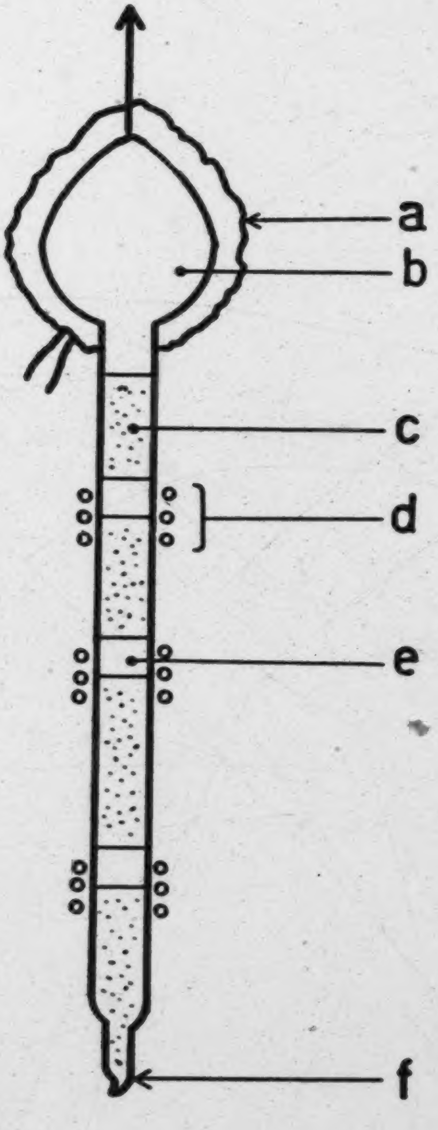

Figure 7. Schematic diagram of the zone refining apparatus: a, heating tape to prevent sublimation; b, glass bulb; c, solid sample; d, heater (a coil of resistance wire); e, a melted zone; f, the sealed tip through which the tube was filled. The arrow indicates the direction of travel of the tube past the stationary heaters.

bank of three heaters at a rate of 0.5 in/hr. The length of the zones was determined by the shape and temperature of the heaters.

Long zone lengths favour rapid initial purification but a relatively low ultimate separation, while short zones have the opposite effect (100). Hence, the procedure adopted here was to use directional freezing, followed by 3 zones of length L/4, and then at least 10 zones of length L/10, where L is the length of the sample. Since commercial phenol may contain impurities which raise the melting point (Section 1.5) in addition to those which are known to lower it (70,74), the lower melting 40%, (at the bottom of the tube), and the high melting 20% (at the top of the tube) were discarded. The desired region of the sample tube was broken away from the remainder in the dry box. The sample was then sublimed out of its portion of tubing under vacuum at room temperature in the dark, before being returned to the dry box to either be used immediately, or to be loaded into a sealed flask to be stored under a dry nitrogen atmosphere at -10°C in the dark. Samples stored for as long as 3 weeks in this fashion showed no change in conductivity.

Under zone refining, the lowest melting zone length of each sample became beige-pink (Analar) or bluish (Mallinckrodt) in colour. Since the sample was zone refined under vacuum and in the dark it is unlikely to have decomposed during the zone refining, and therefore this evidence suggests that existing impurities were indeed separated from the bulk sample. Further evidence of the existence of impurities in the low melting fraction is given in Section 4.3.

Karl Fischer titrations of two purified samples and the commercial products showed the water content to be less than 0.02% by weight in all cases. Titration of a sample doped with 0.2% water verified the reported (101) reliability of this technique. Presumably the low water content in the commercial samples, in spite of the hygroscopic nature of phenol (Section 1.5a), occurred because any water which may have been present sublimed off as the azeotrope during storage in the dry box before use, hence the negative Karl Fischer results.

The refractive index, n_D, of one purified sample and both commercial products was measured at 45.6°C, to an estimated accuracy of ±0.0001, using a Bausch and Lomb Abbe 3L refractometer, carefully calibrated with the factory supplied glass refractive index standard. The refractometer was enclosed in a glove bag and purged with dry nitrogen. The samples were melted on the warm prisms of the instrument immediately before the readings were taken, and the temperature was measured using a calibrated thermocouple placed in the liquid overflow channels immediately beside the prisms. Values of n_D for Mallinckrodt, Analar, and purified phenol were 1.5406, 1.5404, and 1.5401, respectively. These compare with Timmermans' value of 1.5400 at 45.6°C (67).

The 10 kHz conductivities of purified and commercial samples of phenol were measured using about 5 g of sample in the parallel plate dielectric cell (Section 2.5b) at 25°C. The specific conductivities were calculated from the values of capacitance and dissipation factor, using the relationship (Section 1.1):

$$\sigma(\mu\text{mho/cm}) = 8.85 \times 10^{-5} \omega(\text{kHz})\ D\ \varepsilon'$$

Results of 3.5×10^{-5} μmho/cm and 4500×10^{-5} μmho/cm were obtained for the Analar and Mallinckrodt products respectively, while the specific conductivities of purified samples were less than 1.5×10^{-5} μmho/cm, no matter from which of the two sources the starting material was taken.

The refractive index and conductivity data suggest that, while the Analar product appears relatively pure, the Mallinckrodt phenol is contaminated by a conducting impurity, probably the phosphoric acid preservative (0.15%) used in this product. The zone refining procedure appears to effect significant purification of both products.

The freezing points of several pure and commercial samples were determined in an evacuated apparatus which consisted of a tube containing about 3 ml of sample into which a calibrated thermocouple, surrounded by a thin glass capillary, protruded. The apparatus was immersed in a beaker of warm water which was gradually cooled until the freezing of the sample produced a discontinuity in the cooling curve, which was taken to indicate the freezing point. The samples were seeded by dropping a clean cold ball bearing into the melt with the aid of a magnet (71). Results of 40.9±0.1°C were obtained for each sample, including, surprisingly, a beige-pink sample taken from the low melting end of a zone refining tube. Excessive sublimation to upper parts of the cell was observed during the course of each run. This probably removed most of the water from the samples and possibly other impurities as well, and for this reason, results obtained using this apparatus are rather suspect. Doubtless the use of an adiabatic calorimeter and an atmosphere of inert gas as opposed to a vacuum would have minimized sublimation, however construction of a new calorimeter was not considered to be justified since other evidence of sample purity was available.

The water used in calibrating the pressure gauges was distilled once from permanganate, twice from glass, then boiled to remove carbon dioxide. Anachemia reagent grade sodium chloride and Shawinigan reagent grade potassium bromide (Section 3.2) were each taken from freshly opened bottles, dried in an oven at 400°C for 24 hours, then further dried at room temperature under high vacuum for an additional 24 hours before use. Highly purified acetonitrile (Section 4.4) was supplied by Dr. B. Kratochvil (102). All operations on non-aqueous samples were carried out in the dry box.

2.2 Temperature Measurement

Temperature was measured using copper-constantan thermocouples of various gauges in conjunction with a Honeywell model 2733 slide wire potentiometer and a well stirred ice-water reference bath. The thermocouples were calibrated at several different constant temperatures (-80°C to 80°C) against a Hewlett Packard 2801A quartz thermometer which had, in turn, been calibrated against an N.B.S. platinum resistance thermometer. Deviations of the emf observed at each temperature from that listed in the reference tables (103) were fitted to a linear relationship with the observed emf using a least squares technique.

i.e. $\Delta E = aE(\text{observed}) + b = E(\text{reference table}) - E(\text{observed})$

The observed emf could be converted to its corresponding 'reference table' value, and the temperature then taken from the table using this value. The accuracy of the calibration is within ±0.1°C between 80°C and -80°C and is believed to be ±0.3°C at -160°C. The calibration of each thermocouple was checked periodically and in no case did the calibration change by more than 0.05°C.

2.3 Compressibility Measurements

Pressure was generated by a 20 ton press which was of standard design except that, to reduce friction, the oil seal in the ram was a Buna-N O ring instead of the usual leather skirt. The sample was contained in the simple piston-cylinder cell, one inch internal diameter and five inch outer diameter, shown in Figure 8. The pistons were made from Vascomax 350, and the cylinder from Vascomax 300 18% nickel maraging steels and were heat treated to about 50 Rockwell C. Sample extrusion was prevented by two brass, triangular cross-sectioned, back-up rings which sealed the clearance between pistons and cylinder.

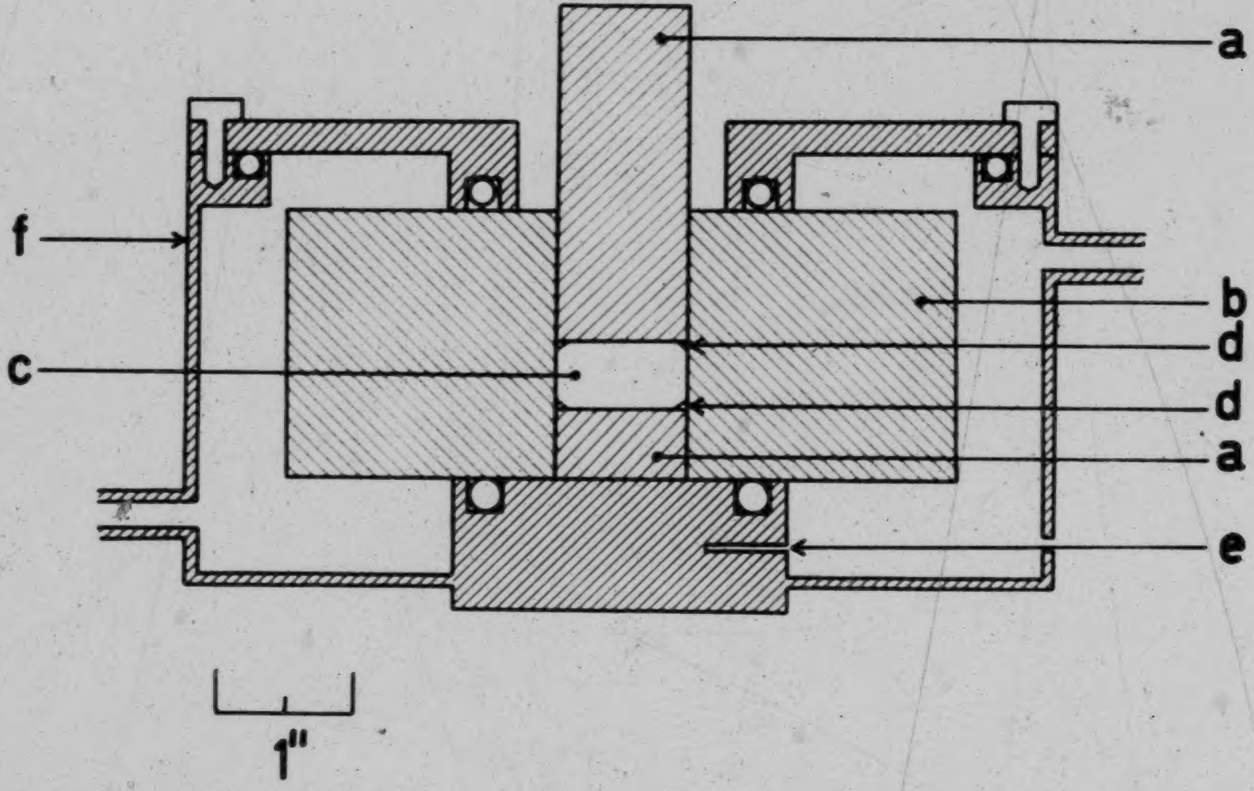

Figure 8. The compressibility cell: a, piston; b, cylinder; c, sample; d, brass back-up rings; e, thermocouple well; f, thermostat jacket.

The pressure in the cell was determined from the radius ratio of the high-pressure cylinder to the ram cylinder, and the oil pressure in the ram. The oil pressure was measured on a factory calibrated, 14 inch diameter Heise, 500 bar bourdon gauge which was carefully zeroed before and re-checked at the end of each run. The effects of friction were minimized by averaging all results over those obtained when increasing the pressure and those obtained when decreasing the pressure (Section 1.4b). The pressure calibration was checked by measuring the ice I-III equilibrium pressure at -28°C. The results agreed with the value of 2106 bar obtained by Kell and Whalley (104) to within 4 bar, i.e. to within 0.2%. This agreement is of the order of accuracy expected for the gauge itself.

The volume changes were determined from measurements of the distance between the plattens of the press. Two Starret linear displacement gauges, #656-617, smallest division 10^{-4} inch, were accurately set at opposite corners of the top platten, equidistant from the centre by means of magnetic bases. The values of linear displacement used were averages of the readings from the two gauges.

Temperature control was achieved by circulating methanol from a Neslab LT9 low temperature thermostat bath through the jacket surrounding the cell (Figure 8). The thermocouple was placed in the supporting block immediately below the piston. The sample temperature so measured is believed accurate to ±0.5°C and, more important, was constant to ±0.1°C for the duration of each run.

Phenol samples were weighed into the pressure vessel in a dry box. The assembled cell was then placed in the press and the sample taken through the I-II transition several times to achieve further purification (Section 3.2). The total linear compression, ΔL, of the sample plus pistons and support blocks was then measured for both increasing and decreasing pressures, by changing the distance between the plattens of the press by fixed increments of about 3×10^{-4} in. Readings were taken three minutes after each increment and the platten distance was changed immediately after each reading. The compression of the pistons and support blocks alone was determined before or after each sample run by performing identical runs in which no sample or back-up rings were used.

2.4 Instrumentation for the Measurement of Capacitance and Loss

All capacitance measurements in this work were carried out on a General Radio 1615-A transformer ratio arm bridge used in conjunction with a GR 1310B oscillator and a Rhode Schwartz type UBM null detector. The Rhode Schwartz null detector was found to be slightly more sensitive, and has a wider continuous frequency range than the GR 1232A null detector which was used in the preliminary measurements. A Hewlett Packard 5221B six figure electronic counter was used to measure the frequency. All connections from the capacitance cell or standards to the bridge were made with coaxial cable and GR 874 connections.

The bridge capacitance controls were calibrated (105) at regular intervals using a GR 1404B 100 pf reference standard capacitor. The accuracy of this calibration was checked in the range of most experiments (1 to 10 pf) with the aid of a GR 1422CD precision variable capacitor. Capacitance readings taken from the bridge agreed with those of the factory calibrated variable capacitor to within 0.003 pf. The factory calibration of the dissipation and conductance controls was assumed not to change and the values of C" calculated during experiments from both D and G were consistent with one another to ±1%. The accuracy of all the frequency measurements was at least ±0.1% as calculated from the manufacturers specifications and the number of figures used.

The ranges of measurements of the various bridge controls, taken from the manual supplied with the bridge (105) are shown in Table 3. Since the maximum applied voltage may not exceed f(kHz) x 30 volts, the low voltage limits sensitivity below about 500 Hz. Also, at low frequency, the dissipation of many samples (e.g. ice I below about -40°C) may exceed the range of the bridge.

Table 3. Ranges of measurement and accuracy of the 1615-A capacitance bridge.

Ranges of measurement	Accuracy
Capacitance, 10 aF to 1.11110 μF(10^{-17} to 10^{-6} farad) in 6 ranges, direct-reading, 6-figure resolution; least count 10^{-17} F (10 aF).	At 1 kHz, ±(0.01% + 0.00003 pF). At higher frequencies and with high capacitance, additional error is [$\pm 3 \times 10^{-5}\% + 2 \times 10^{-3}\% \ (C_{\mu F}) \pm 3 \times 10^{-7}$ pF] $\times f^2_{kHz}$. At lower frequencies and with low capacitance, accuracy may be limited by bridge sensitivity. Comparison, accuracy, unknown to external standard, 1 ppm.
Dissipation Factor, D, At 1 kHz, 0.000001 to 1, 4-figure resolution; least count, 0.000001; range varies directly with frequency.	±[0.1% of measured value + 1×10^{-5} ($1 + f_{kHz} + 5\, f_{kHz}\, C_{\mu f}$)]
Conductance, G, 10^{-6} $\mu\mho$ to 100 $\mu\mho$, 2 ranges +, 2 ranges-, 4-figure resolution, least count 10^{-6} $\mu\mho$ independent of frequency; range varies with C range.	±[1% of measured value + 1×10^{-5} $\mu\mho$ + $6 \times 10^{-2}\ f_{kHz}\ C_{\mu F} \times (1 + f_{kHz} + 5\, f_{kHz}\, C_{\mu F})$ $\mu\mho$]

Capacitance readings taken for a dielectric cell or capacitance standard were constant to ±0.03% below 20 kHz, but readings at higher frequencies drifted rapidly with increasing frequency until at 100 kHz the capacitance differred by about 0.8% from its 1 kHz value. This effect was presumably due to stray inductances in the cables or the bridge itself and was roughly corrected by using the cell constant measured at each frequency to calculate the dielectric constant at that frequency.

Some problems with ground loops between the bridge, null detector, and oscillator were encountered when these components were rack mounted (105). The problem was eliminated by insulating the oscillator and null detector from the rack. Ground loops are indicated when a capacitance reading in excess of 0.00003 pf is required to balance the bridge with the calibration switch on.

2.5 High Pressure Dielectric Cells

The principal experimental difficulty in obtaining dielectric data for a solid under pressure lies in constructing a cell in which the cell constant can be accurately determined and in which hydrostatic pressure can be maintained and cracks and gaps in the sample can be avoided. In principle, electrodes could be fixed to the surfaces of an accurately machined sample and pressure could then be applied using an appropriate pressure transmitting fluid. This is impractical for samples which are air sensitive or unstable at room temperature and it is usually necessary to subject such samples to pressure that is, to a greater or lesser extent, non hydrostatic (4).

Two piston-cylinder high-pressure dielectric cells were constructed for this work. The first used fixed coaxial electrodes which provided an accurately known cell constant, but required a relatively large amount of shear to convert the uniaxial pressure applied by the piston to hydrostatic pressure. In the second cell, plates were set into the two piston faces so that the entire assembly functioned as a parallel plate dielectric cell. Since the electrodes moved as the sample compressed, the cell constant was much less accurately known, but the shear required to achieve hydrostatic pressure was relatively small. The parallel plate cell was preferable for dielectric relaxation studies, since pressure gradients often produce a range of relaxation times (4), while the coaxial cell was preferable for absolute measurement of dielectric constants.

The pressure in each cell was determined from the radius ratio of the high pressure cylinder to the ram cylinder of the press, and the oil pressure in the ram. The press and pressure gauges described in Section 2.3

were also used in this work. Furthermore the pressure calibration described in Section 2.3, which confirmed the accuracy of the gauges and the measured value of 2.625 in for the diameter of the ram cylinder, was considered adequate for the dielectric cells and no further pressure calibration was carried out.

2.5a The Coaxial High Pressure Dielectric Cell

The design of the three terminal coaxial cell is very similar to that used by Whalley et al. (4) and by Gough and Davidson (41). The cell is illustrated in Figure 9 and an enlarged diagram of the electrode assembly is shown in Figure 10. It consisted of an electrode, a, which was glued with epoxy resin to its support b, and which protruded into the centre of a conventional piston-cylinder pressure vessel. The cylinder of the pressure vessel served as the high potential electrode while the central electrode and its support, which were insulated from one another by the epoxy joint, served as the low potential electrode and guard ring, respectively.

The central electrode was connected to the bridge low terminal by an insulated rod, c, which screwed tightly into place and was shielded as shown in Figure 10. Electrical contact between the high terminal and the cylinder was achieved by clamping a coaxial cable, d,

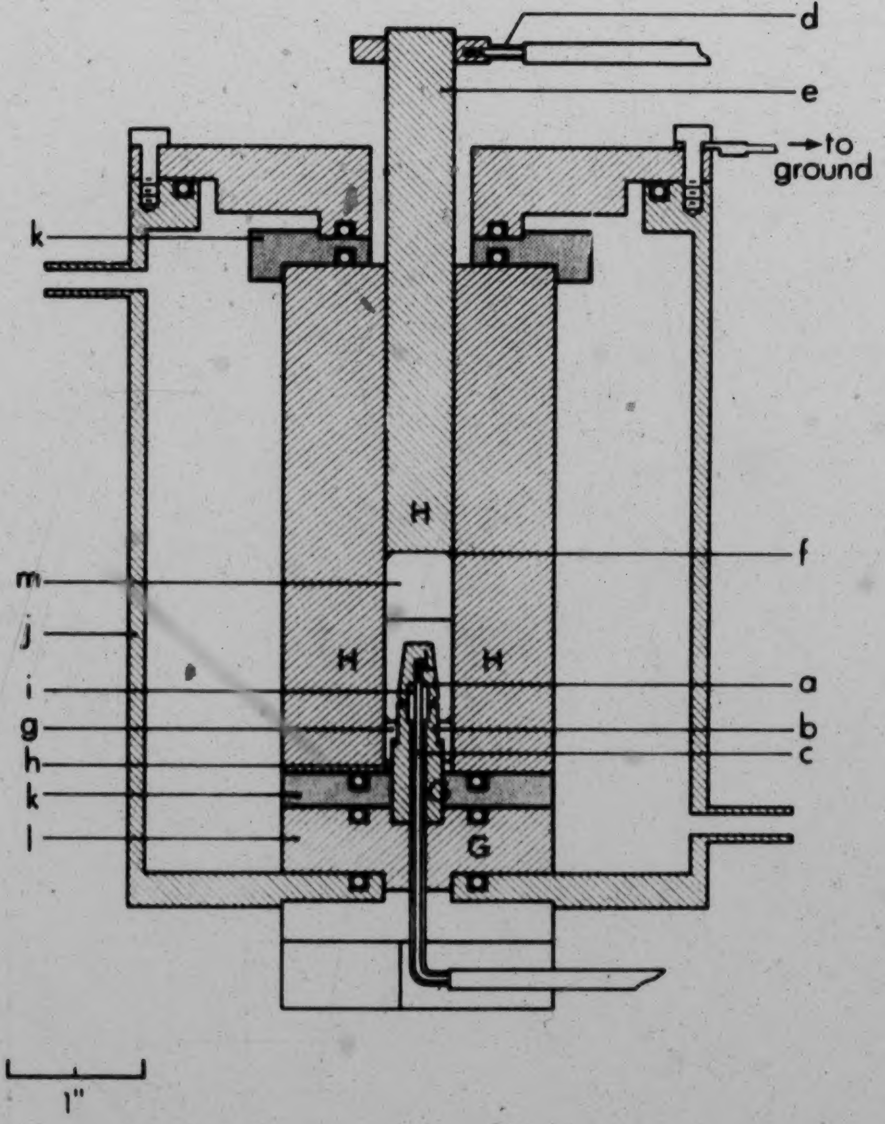

Figure 9. The coaxial high pressure dielectric cell. The meaning of the letters is described in the text. The symbols G,H, and L indicate the guard, high, and low terminal potentials, respectively. This pressure vessel forms a partially guarded, 3-terminal dielectric cell with negligible lead capacitance.

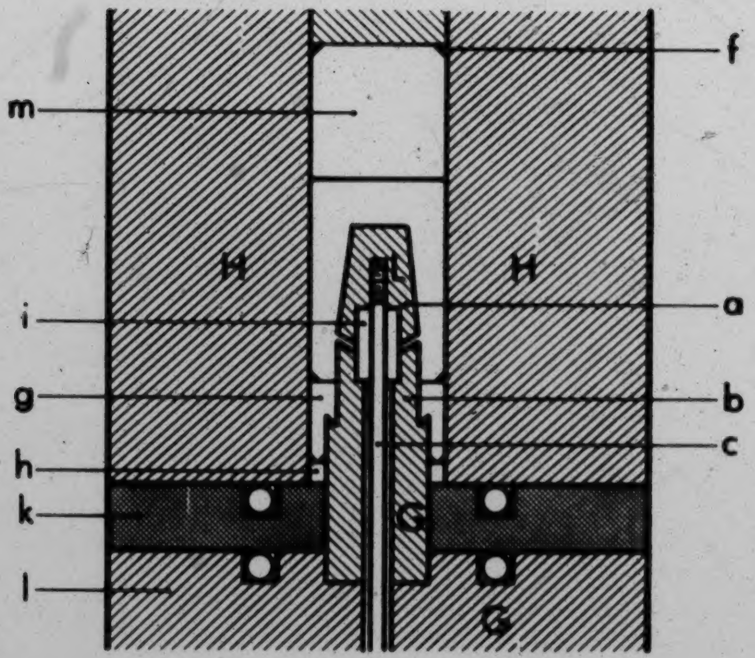

Figure 10. A closeup of the electrode assembly of the coaxial dielectric cell. The taper on the inner electrode is designed to minimize cracks in the sample and to provide a broad base for structural support. Very high pressure gradients exist in this type of cell for all but the most plastic samples.

tightly around the piston, e, as shown in Figure 9. A triangular-section, brass sealing ring, f, provided good electrical contact between the piston and cylinder, and a thin layer of indium seated between the clamp and the piston insured good contact there.

The central electrode was held in position by Teflon and bakelite cylinders, g and h, situated as shown in Figure 10. Brass back-up rings were positioned as shown to seal the vessel. The seal between the central electrode and its support depended on Bridgman's unsupported area principal (106). A thin Teflon cylinder, i, added rigidity to the electrode assembly. All the steel components were machined from Vascomax 350 18% Ni maraging steel and heat treated to 54 Rockwell C.

Temperature control was obtained by circulating coolant through the thermostat jacket, j, which was electrically insulated from the cylinder by bakelite disks, k, positioned as shown, and sealed with O-rings in the appropriate locations. Since this jacket formed part of the electrical shielding around the cell, it was essential to use a non-polar coolant to avoid conductance between the high terminal and ground. Kerosene was found to be a very suitable coolant at temperatures above -20°C, while at lower temperatures a mixture of Skelley C (petroleum ether) and kerosene was used. Temperature was monitored using a calibrated thermocouple set in a copper block which was clamped securely to the cylinder, although a thermocouple well in the side of the cylinder would have been preferable.

Calibration runs using Baker and Eastman spectrograde carbon tetrachloride and cyclohexane from freshly opened bottles, and air, whose dielectric constants were taken from reference 107, showed the cell constant to be about 1 pf and the lead capacitance to be less than the scatter between runs, 0.005 pf. Thereafter, the cell constant was determined from the dielectric constant of air at atmospheric pressure, assuming neglegible lead capacitance. During calibration runs care was taken to seat the central electrode support, b, firmly against its base, l, since erroneous readings result from a 'floating' guard. The cell constant was found not to vary with the position of the piston so long as a 1/2" gap was left between the piston face and the top of the low electrode. To insure that this condition was met, and to reduce friction, a 1/2" Teflon plug, m, was inserted on top of the sample. The cell constant changed by less than 0.05% over a temperature range of +10°C to +35°C and was assumed to be independent of temperature for all subsequent work.

2.5b The Parallel Plate High Pressure Dielectric Cell

The parallel plate dielectric cell was very similar in design to the compressibility cell (Section 2.3) except that the pistons were made as shown in Figure 11a. The assembly thus formed a guarded, 3-terminal, parallel plate dielectric cell, about 1 1/8 inch internal diameter and 5 inch external diameter. The plates of the dielectric cell were insulated from the pistons by bakelite cups and sample extrusion was prevented by thin brass backup rings, positioned as shown. The temperature was controlled, as discussed in Section 2.3, by circulating coolant through a thermostat jacket, set at the guard potential and sealed with O-rings at appropriate locations to prevent coolant from contacting the pistons. The temperature could be kept constant to within ±0.2°C at -40°C and to better than this at higher temperatures. Two thermocouples were placed at opposite ends and sides of the pressure cylinder in holes drilled in the cylinder. Because they gave different readings from each other, the temperature can only be considered known to ±0.1°C at 10°C and to ±0.5°C at -40°C.

The electrode arrangement shown in Figure 11a relies simply on a tight fit between the capacitor plates and the bakelite cups to prevent sample extrusion there. In the phase diagram studies (Section 4.1), the slight extrusion which occurred using this assembly did not affect the

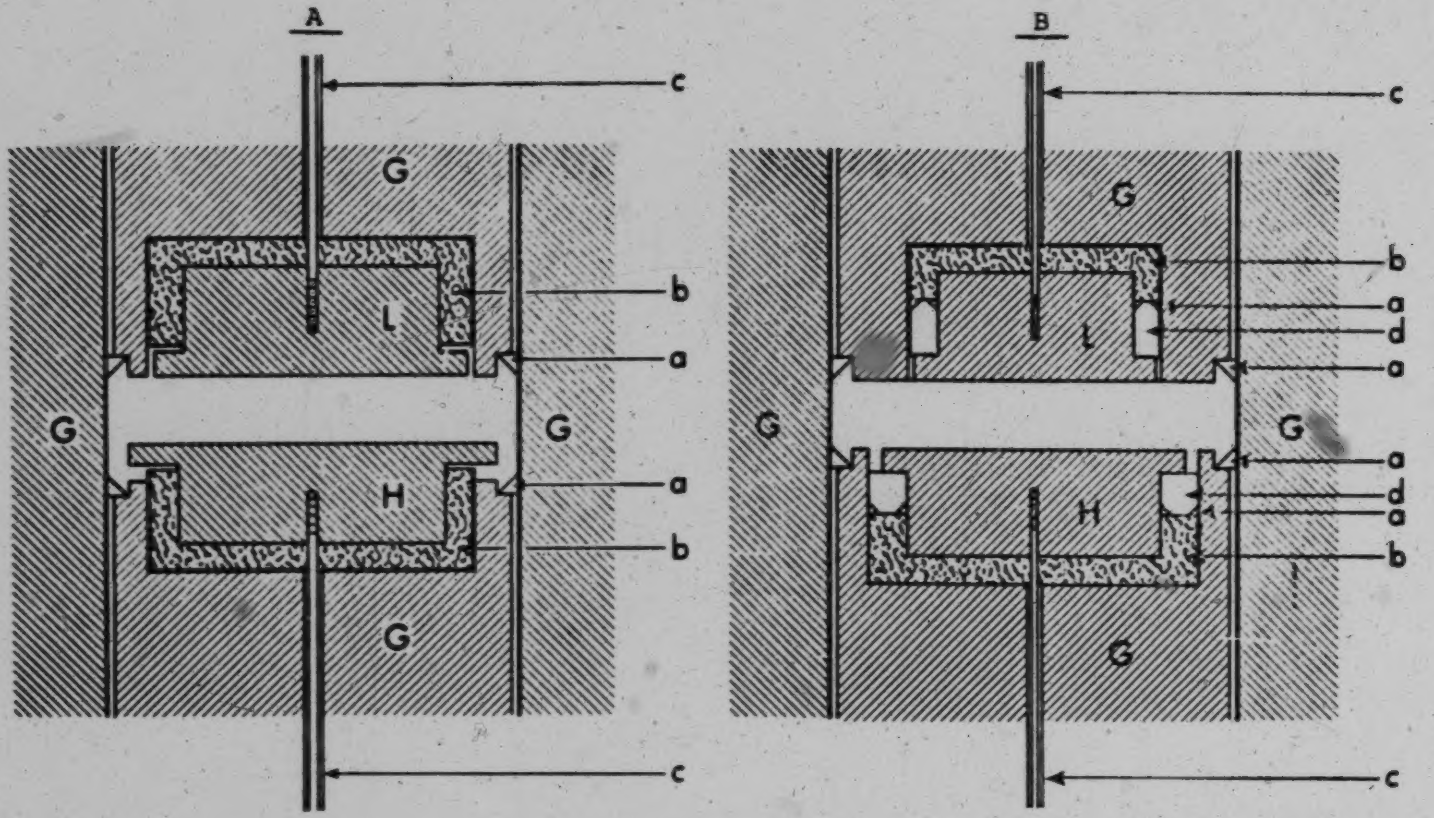
A
B
c
c
c
c
G
G
G
G
G
G
G
G
L
H
L
H
a
a
a
a
a
a
a
a
b
b
b
b
d
d

Figure 11. The electrode assembly of the high pressure parallel plate capacitance cell: a, brass backup rings; b, Bakelite insulation; c, insulated leads to high and low terminals; d, Teflon cylinder. Figure A refers to the cell used in the phase diagram studies. Figure [illegible] shows the modified cell used in subsequent work.

results since it was not necessary to know the dielectric constant of either phase. To obtain dielectric constants using this apparatus (Section 5.3), it is essential that no sample extrudes and, for such work, the electrode assembly was redesigned, as shown in Figure 11b. In this second design, Teflon rings, slightly oversize, were positioned above and below the lower and upper bakelite cups, respectively, which were shortened to accommodate them. Since the Teflon rings were oversize, they bore the brunt of the pressure exerted by the plates and so formed a seal of the Bridgman 'unsupported area' type (106). Thin brass backup rings prevented extrusion of the Teflon. The other modifications in the high potential electrode assembly shown in Figure 11b were designed to reduce the 'dead space' in the cell (Section 5.3). All the steel components, except the cylinder were machined from Vascomax 350 18% Ni maraging steel, and were heat treated to 54 Rockwell C. The cylinder was machined from Vascomax 300 maraging steel and similarly heat treated.

2.6 Isolation and Temperature of Transformation of Phenol II at One Atmosphere

2.6a Preparation of Phenol II

The apparatus used to prepare high pressure phases is shown in Figure 12. The pistons, cylinder and support

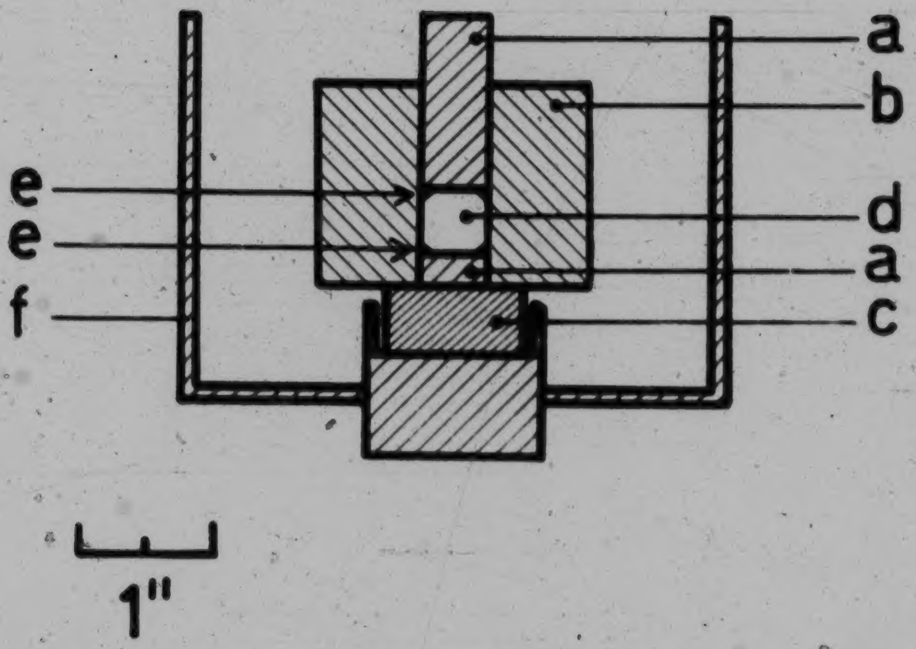

Figure 12. The pressure vessel used to prepare quenched samples of the high pressure phases of solids: a, pistons; b, cylinder; c, support block; d, sample; e, brass back-up rings; f, stainless steel external can. All parts except e and f were machined from Vascomax 350 nickel maraging steel and hardened.

block were machined from Vascomax 350 18% nickel maraging steel, and were heat treated to 54 Rochwell C. Pressure was generated and measured as described in Section 2.3. Sample extrusion was prevented by the triangular sectioned brass rings. The sample was taken well past the phase I - II transition at room temperature (Table 2) to a pressure of 5 - 10 kbar. This pressure was maintained while the temperature of the cell was lowered to -195°C by pouring liquid nitrogen into the surrounding can. When the cell had cooled, the pressure was released, the support block c removed, and the sample was extracted into the cup previously occupied by block c by again applying pressure to the upper piston. The walls of the cylinder around and below the sample had a 2° taper to facilitate extraction.

All operations on the extracted, metastable phase II were carried out on a platform just above a large pool of rapidly boiling liquid nitrogen which served the dual purpose of maintaining the temperature and ensuring a dry nitrogen atmosphere (108). The samples were characterized either by their x-ray powder photographs, or by Tammann's density test (58), which consists of immersing a portion of the sample in a 1:2 mixture of chloroform and petroleum ether at -80°C to see if the sample sinks (phenol II) or floats (phenol I). Samples were stored under liquid nitrogen (109).

2.6b Thermal Analysis

The calorimeter, shown in Figure 13, consisted of a copper cup, whose walls and bottom were about 0.015 in. and 0.030 in. in thickness, respectively, suspended in a massive stainless steel can by a calibrated copper - constantan thermocouple. The massive can was well insulated with styrofoam and its dimensions may be taken from Figure 13.

Samples were placed in the cup with the temperature of cup and can no warmer than -90°C, well below the temperature of transformation of the sample. The top of the can was then bolted in place, the styrofoam cap placed on top of it, and the entire apparatus placed in a close fitting beaker which was then immersed in a constant temperature bath set near room temperature. Heat leaks between the cup and can permitted the temperature of the cup to follow the warming curve of the can except when heat was generated or consumed in the cup. The temperature of the cup was determined as a function of time by monitoring the voltage given by the attached thermocouple with a Hewlett Packard 3420A differential voltmeter.

Runs were carried out on two samples of phenol II, each zone refined and sublimed, and also on two samples of pure acetonitrile supplied by Dr. B. Kratochvil (102). In

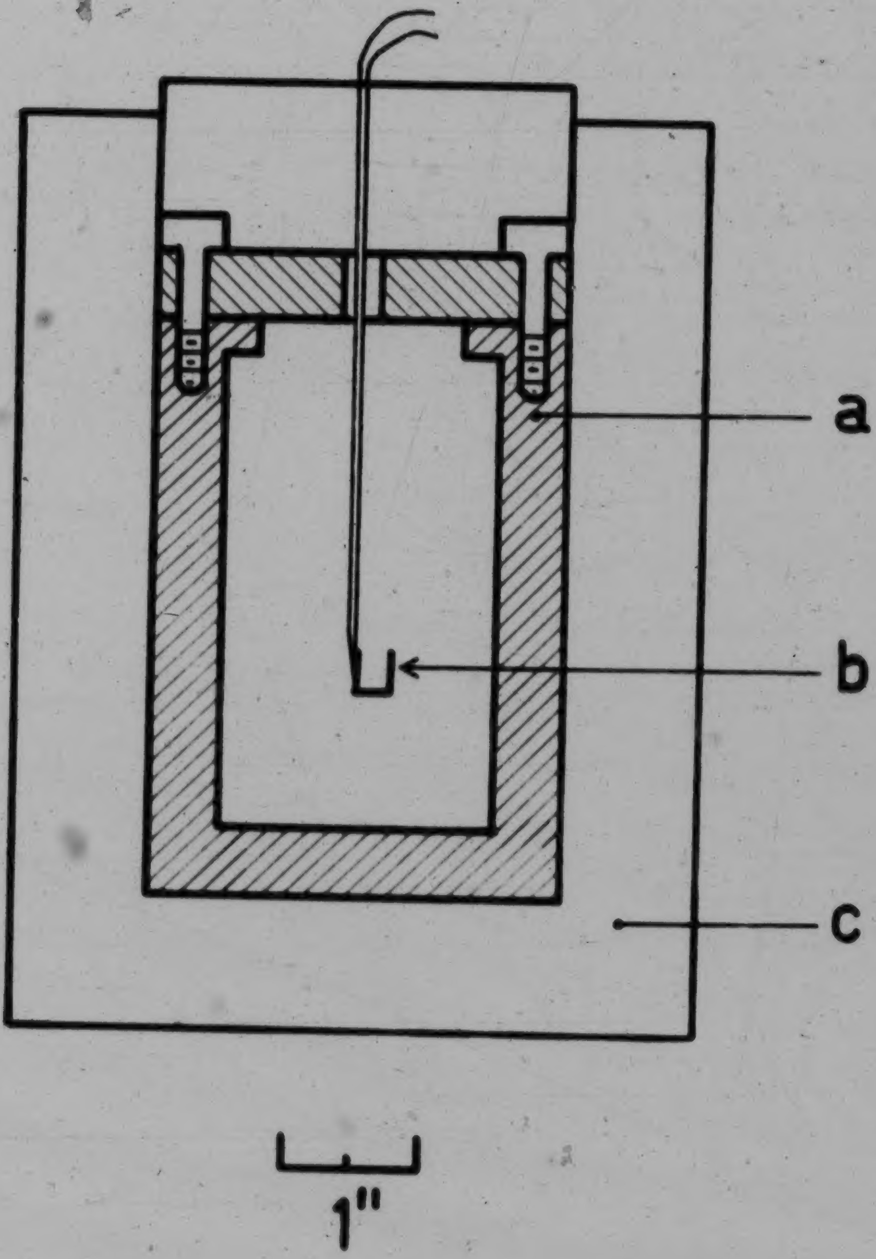

Figure 13. The calorimeter: a, massive stainless steel can; b, copper cup suspended by a thin thermocouple; c, styrofoam insulation.

one run on each compound a cup whose volume was 0.201 cm^3 was used, and in the other run tne cup had a volume of 0.627 cm^3. Each cup was between 65% and 85% full of tightly packed sample.

2.7 Powder X-ray Diffraction Studies

Phenol II samples were prepared for powder diffraction studies by grinding quenched phenol II with a small stainless steel mortar and pestle at liquid nitrogen temperatures. This was accomplished by placing the mortar on a steel table which was surrounded by rapidly boiling liquid nitrogen, as discussed in Section 2.6. The powdered sample was then loaded into a thin walled quartz capillary, about 1 cm long and 0.5 mm in diameter which was held in a vertical position by a brass block, drilled to accommodate the capillary, and which also rested on the steel table. The powdered sample was transferred to the capillary using a long spatula and was tamped firmly in place with a finely drawn glass rod. Tne spatula and glass rod were frequently immersed in the liquid nitrogen to ensure that tney were cold.

The capillary was transferred from the cold nitrogen can to the x-ray apparatus in a small stainless steel crucible containing liquid nitrogen, using long tweezers whose tips were padded with styrofoam to avoid breaking the capillary. The tube was then fitted into place on a cold teflon mount which was affixed to the goniometer head of a Jarrell Ash precession camera. In this position the sample was cooled by a stream of freshly boiled nitrogen gas, surrounded by a coaxial envelope of warm, dry nitrogen to avoid the condensation of ice on the tube (110,111).

The temperature of the samples was determined using a very fine, calibrated iron constantan thermocouple which protruded through the back of the teflon mount into the capillary to within 5 mm of the x-ray beam. During the course of a run the temperature was constant to ±5°C over the temperature range -20°C to the usual temperature, -190°C.

Kα radiation from an Enraf - Nonius Diffractis 601 generator, with copper, cobalt and molybdenum sources was used with appropriate filters (112) (Table 19) to obtain the powder photographs. The precession camera was used as a flat plate camera with the film set perpendicular to the x-ray beam, which struck the sample tube at right angles. The sample to film distance was calibrated by recording the powder photograph of sodium chloride at 25°C (113). The sample tubes were carefully aligned so that they remained in the same part of the x-ray beam during rotation about the dial axis of the camera, and they were slowly rotated during the exposure to average out small residual errors in this alignment. The relative intensities of lines on the powder photographs were measured from two photographs with different exposure times using a Joyce MK. III C double beam recording microdensitometer. Film shrinkage was determined by momentarily exposing two pinholes in the back of the film plate. The difference in the distance between the resulting spots on the developed film and the pinholes themselves indicated the degree of shrinkage.

Chapter III. The Volume Compressions and Compressibilities of Phenol I and II at 10°C.

The volume compressions and compressibilities of phenol I and II have not been previously reported (Section 1.5). They are essential for calculating the molar polarization of each phase (Section 1.2a) and are also interesting in their own right (Section 3.4). This chapter describes the methods and the results of a study to determine the volume compressions and compressibilities of phenol I and II at 10°C.

3.1 The Volume Compressions Uncorrected for Cylinder Deformation

The experimental techniques for measuring the compression are outlined in Section 2.3. Briefly, the average reading of the two displacement gauges, L (in ten thousanths of an inch), was determined as a function of the oil pressure under the hydraulic ram of the press. For each sample, L was measured for the cell pistons plus support blocks plus the sample in the cell and for the pistons plus support blocks alone. Three such runs were carried out, using two samples of Analar commercial phenol and one zone refined sample (Section 2.1). Values of various parameters pertaining to each sample are listed in Table 4. The results were processed as described below, and are as consistent as could be expected considering the

Table 4. Various parameters for the compression runs on phenol.

	Sample Weight (g)	Purification	Temp. (°C)
Run #1	6.4842	commercial	10.1°C
Run #2	7.0408	commercial	9.7°C
Run #3	3.9206	zone refined	10.2°C

The diameter of the hydraulic ram of the press was 2.625 in. and that of the bore of the pressure vessel was 0.9998 in.

possible experimental errors. Little improvement was expected from further runs or further purification.

The values of L for the empty cell were fitted to quadratic functions, $L = ap^2 + bp + c$, separately for increasing and decreasing oil pressure, p. The coefficients obtained for each run are listed in Table 5 along with the standard and maximum deviations, the pressure range, and the number of data points used in each fit. The terms 'up' and 'down' in Table 5 refer to the compression and decompression curves, respectively. These expressions for L were then used to subtract the displacements of the pistons plus support blocks from the total displacement of the sample plus pistons and support blocks for both pressure increments and pressure decrements. This treatment yielded a set of values for the displacement of the sample alone as a function of increasing and decreasing oil pressures. These values of the sample displacement, L, were then fitted to quadratic functions in increasing and decreasing oil pressure, and the resulting coefficients are listed in Table 6. It is important to realize that the term 'displacement', as used here and in Table 5, indicates the average reading of the displacement gauges and is not necessarily zero at $p = 0$. The deviations of the measured points from the fitted curves listed in Tables 5 and 6 were all less than the maximum values shown in the tables, and were random, so there is little point

Table 5. The linear displacement, L, of the pistons plus support blocks for the compression runs on phenol. [a]

		a	b	c	L(x 10^4/in) std. dev.	L(x 10^4/in) maximum dev.	highest & lowest oil pressures (bar)	no. of data points
Run #1	down	-1.9021×10^{-4}	3.9231×10^{-1}	3.0865×10^{1}	0.7	0.8	460.8,38.6	39
	up	-3.8023×10^{-5}	3.0701×10^{-1}	3.2710×10^{1}	0.8	1.3	470.4,54.8	37
Run #2	down	-2.1402×10^{-4}	3.9801×10^{-1}	6.9430×10^{1}	0.7	1.6	453.7,42.9	35
	up	-5.4797×10^{-5}	3.1258×10^{-1}	6.5910×10^{1}	0.5	1.2	459.2,62.5	33
Run #3	down	-1.5884×10^{-4}	3.2789×10^{-1}	-2.5023×10^{1}	0.5	1.2	431.0,60.3	38
	up	-2.8222×10^{-5}	2.5754×10^{-1}	-2.6005×10^{1}	0.6	1.0	459.6,58.3	40

[a] $L = ap^2 + bp + c$, where p is the oil pressure in bar.

Table 6. The linear displacement, L, of each phenol sample. [a]

		a	b	c	L(x 10^4/in)		highest & lowest oil	no. of
Run #1					std. dev.	maximum dev.	pressures (bar)	data points
phenol I	down	-6.9455×10^{-4}	7.7663×10^{-1}	1.2136×10^{1}	0.4	0.8	151.0,36.4	12
	up	-2.9072×10^{-4}	6.6681×10^{-1}	1.0910×10^{1}	0.5	0.9	241.4,56.8	20
phenol II	down	-3.1810×10^{-4}	5.6263×10^{-1}	3.3574×10^{2}	1.2	2.1	455.8,208.3	54
	up	-9.1912×10^{-5}	3.6450×10^{-1}	3.6531×10^{2}	0.5	1.1	480.5,261.0	27
Run #2								
phenol I	down	-6.8155×10^{-4}	8.3741×10^{-1}	-4.4662×10^{1}	0.3	0.9	135.3,33.9	13
	up	-4.0776×10^{-4}	7.3494×10^{-1}	-4.7346×10^{1}	0.7	1.2	247.0,85.7	17
phenol II	down	-2.3315×10^{-4}	5.1306×10^{-1}	3.2669×10^{2}	0.5	1.0	428.2,182.1	24
	up	-3.1400×10^{-6}	3.2583×10^{-1}	3.5176×10^{2}	0.9	1.8	478.2,279.7	27

(Table continued on next page)

Table 6 continued

Run #3		a	b	c	L(x 10^4/in)		highest & lowest oil pressures (bar)	no. of data points
					std. dev.	maximum dev.		
phenol I	down	$-6.0110\text{x}10^{-4}$	$4.8365\text{x}10^{-1}$	$-6.5466\text{x}10^{-1}$	0.3	0.5	168.8,38.3	14
	up	$-3.4857\text{x}10^{-4}$	$4.6388\text{x}10^{-1}$	$-2.4204\text{x}10^{0}$	0.3	0.6	207.6,67.1	15
phenol II	down	$-2.2215\text{x}10^{-4}$	$3.4187\text{x}10^{-1}$	$1.9828\text{x}10^{2}$	0.4	0.8	428.4,199.8	24
	up	$-1.8078\text{x}10^{-4}$	$1.7995\text{x}10^{-1}$	$2.1560\text{x}10^{2}$	0.3	0.5	466.6,267.9	21

[a] $L = ap^2 + bp + c$ where p is the oil pressure in bar.

in tabulating the original data points in this thesis.

To illustrate the results obtained by these procedures, the linear displacements of sample 2 are plotted in Figure 14 as a function of the apparent pressure in the cell. The volume compression, $-\Delta V/V_o$, is also indicated in the figure. Neither $-\Delta V/V_o$ nor the pressure have been corrected for the expansion of the cell bore under pressure. To obtain maximum reproducibility, the displacement was determined for increasing and decreasing pressure within one phase before taking the sample through the transition and commencing measurements on the next phase. The procedure followed is given by the alphabetical order of the letters in Figure 14. The points on the curves cd, ef, gh, and ij were fitted by the least squares procedure to quadratic equations in pressure. The solid lines represent the calculated fits, all of which had a standard deviation of less than 10^{-4} inches, essentially the limit in accuracy imposed by the gauges. In Run 1, the points on both curves ab and ef were used to calculate the expression for the displacement of phenol II with decreasing pressure, and the standard deviation for this fit therefore (Table 6) includes the reproducibility error. In later runs, the pressure was released directly from point a to point b, after which the sample was left at point b for the length of time which would have been required to proceed from a to b using the pressure decrements. This

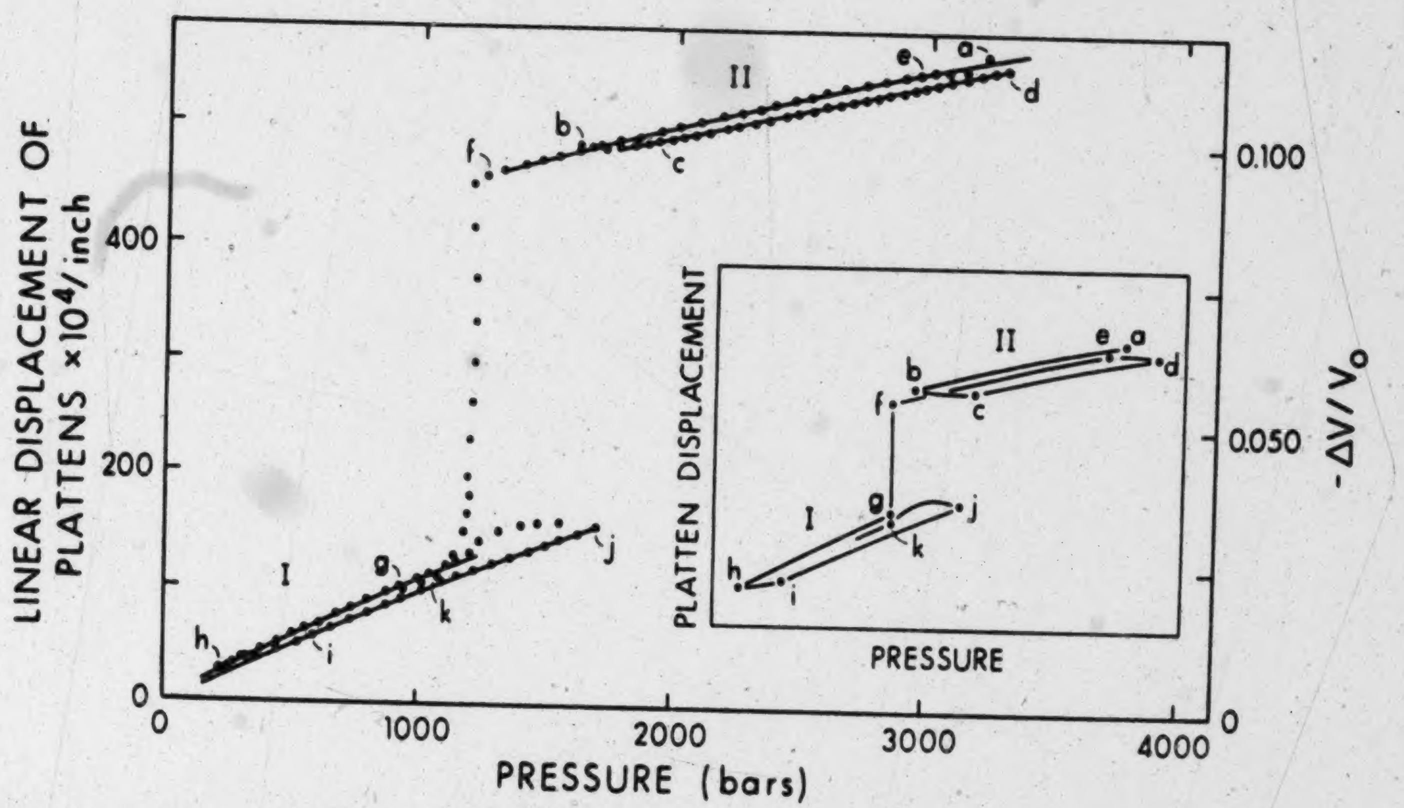

Figure 14. The compression of phenol plotted against the apparent pressure, both uncorrected for expansion of the bore of the cell. The circles indicate the data points and the lines cd, ef, gh, and ij indicate the curves fitted to the data. Phenol I and II were studied in the regions marked by I and II. The alphabetical order of the letters in the main diagram and in the inset schematic indicates the order in which the measurements were made.

change in procedure did not appear to affect the results. Because points between a and b were not determined using this new procedure, the standard deviations of the other curve fits in Table 6 do not include the reproducibility error. This error is given for phases II and I, respectively, by the vertical distances from b to line ef and from k to line gh in Fig. 14. The magnitude of these errors is 3×10^{-4} in. and was essentially the same for all samples and for the compressions of the empty cells. It is, thus, not due to extrusion of the sample, but is probably the result of slight plastic deformation of the pistons or the support blocks.

On changing from increasing to decreasing pressure, or vice-versa, the sample was allowed to sit for several hours to ensure stabilization of any elastic effects in the sample or apparatus. In spite of this precaution, points on the lines bc, de, hi, and jg were obviously not on the true compression or decompression curves and were rejected if they lay more than 10^{-4} inches away from the curve calculated without using the point in question. In practice, each quadratic expression was derived from at least 12 consecutive points. Except for the expression for decreasing pressure on phenol II in Run 1, which includes the reproducibility error, the standard deviation of every curve fit was considerably less than 1×10^{-4} inches, the precision to which the gauges were read. This suggests that no significant error has been introduced by fitting the displacement data to quadratic curves in pressure.

Because of friction along the cylinder walls, the observed pressure (the pressure at the face of the moving piston) is the maximum or minimum pressure in the cell for increasing or decreasing pressures respectively, while, L, the sample displacement, is a function of the net compression of the sample. These frictional effects were eliminated by using the expressions for sample displacement listed in Table 6 to average the pressures at which given values of the displacement occurred on the compression and decompression curves. The resulting values of sample displacement and averaged pressure were fitted to another quadratic equation in oil pressure. Multiplication of the pressure terms of this equation by the square of the ratio of the diameter of the hydraulic ram to that of the bore of the pressure vessel (Table 4) converted the oil pressure to the internal pressure of the cell, and gave an expression which related the sample displacement to the average internal pressure, P.

The displacement gauges were not adjusted to give a displacement reading of zero at ambient pressure. The sample displacement when the average internal pressure is zero, L_o, was calculated from the expression for the displacement of phase I, and subtraction of L_o from the expressions for L gave ΔL, the linear compression of each phase. The expression for ΔL was then converted to an expression for $-\Delta V/V_o$, where V_o represents the volume of phenol I at one bar and ΔV is the difference between V_o and the volume of the phase in question at the given pressure. V_o was obtained from the weight of each sample, assuming the density of phenol, 1.132 g/cm^3, at 25°C (70) is unchanged at 10°C. The resulting expression for converting ΔL to $(-\Delta V/V_c)_o$, the volume compression of a sample uncorrected for bore expansion, is

$$(-\Delta V/V_o)_o = \Delta L \times \pi b^2 \times 16.38706 \times 10^{-4} \times (\text{density/sample weight})$$

where b is the bore radius of the pressure vessel in inches. The expressions obtained for each sample are listed in Table 7. The results in Table 7 were corrected for the deformation of the bore of the compressibility cell using the methods outlined in the following section.

3.2 The Effect of Elastic Deformation of the Compressibility Cell on Compression Results.

In each of the pressure vessels described in sections 2.3 and 2.5, the diameter of the bore may be expected to undergo elastic deformation under hydrostatic pressure. The expression for this expansion of the bore is (114):

Table 7. Expressions for the compression of each phenol sample before correcting for the deformation of the bore of the pressure vessel.

Run #1	phenol I	$(-\Delta V/V_o)_o = -2.2763 \times 10^{-9}\ P^2 + 2.3491 \times 10^{-5}\ P$
	phenol II	$(-\Delta V/V_o)_o = -8.5482 \times 10^{-10}\ P^2 + 1.4598 \times 10^{-5}\ P + 0.076617$
Run #2	phenol I	$(-\Delta V/V_o)_o = -2.3113 \times 10^{-9}\ P^2 + 2.3521 \times 10^{-5}\ P$
	phenol II	$(-\Delta V/V_o)_o = -4.3335 \times 10^{-10}\ P^2 + 1.2338 \times 10^{-5}\ P + 0.079861$
Run #3	phenol I	$(-\Delta V/V_o)_o = -3.9118 \times 10^{-9}\ P^2 + 2.5760 \times 10^{-5}\ P$
	phenol II	$(-\Delta V/V_o)_o = -7.5248 \times 10^{-10}\ P^2 + 1.3203 \times 10^{-5}\ P + 0.080251$

$$\Delta b = 14.5038\,\frac{Pbf}{E}\left[\frac{c^2 + b^2}{c^2 - b^2} + \nu\right] \qquad [3.1]$$

where: b and c are the inner and outer radii of the cylinder respectively, at $P = 0$;

P is the internal pressure in bar minus the external pressure in bar,

E is Young's modulus in p.s.i.,

ν is Poisson's ratio,

$\Delta b = b(\text{at pressure } P) - b(\text{at } P = 0)$.

The factor f, the expansion constant, is an empirical parameter which indicates the degree of ideal expansion which is actually observed. If the ratio of sample length to inner diameter is very small $f = 0$, and as this ratio approaches infinity, f approaches 1. Relative values of the bore diameter after undergoing ideal expansion are given by the expression $(b + \Delta b)/b$, calculated from Equation [3.1] with $f = 1$, and are listed in Table 8 for the compressibility cell (Section 2.3) as a function of the apparent and true internal pressures. The difference between the apparent and true pressures is less than 0.4% below 3 kbar if the expansion is ideal. These values are identical to those calculated for the two dielectric cells (Section 2.5), since the relative dimension of b and c in all three cells are very similar.

The compression of a sample, $-\Delta V/V_0$, may be cor-

Table 8. The expansion of the bore of the compressibility cell under pressure assuming ideal expansion. [a]

True internal pressure (bar)	Apparent internal pressure (bar)	Relative Bore Diameter $\frac{b + \Delta b}{b}$
0	0	1.00000
1000	1001.3	1.00066
2000	2005.3	1.00133
3000	3012.0	1.00199
4000	4021.3	1.00266

[a] The following values were used for the parameters in equation [3.1]: $b = 0.500$ in., $c = 2.500$ in., $\nu = 0.26$(118), $E = 29.1 \times 10^6$ p.s.i. (118), $f = 1$.

rected for the expansion of the bore in the following manner. When the internal radius of the bore increases by Δb, the change in the volume of a sample of length L, caused by a piston displacement ΔL, with ΔL defined as positive for decreasing sample volume, is given by the expression,

$$\Delta V = \pi\{(L - \Delta L)(b + \Delta b)^2 - Lb^2\}.$$

For $b >> \Delta b$,

$$\Delta V = -\pi b^2 \Delta L + 2\pi b \Delta b (L - \Delta L). \qquad [3.2]$$

The uncorrected compression, $(-\Delta V/V_o)_o$, was calculated in Section 3.1 from the expression

$$(-\Delta V/V_o)_o = \pi b^2 \Delta L/V_o,$$

on the assumption that $\Delta b = 0$. Equation [3.2] may therefore be rewritten

$$-\Delta V/V_o = (-\Delta V/V_o)_o - (2\Delta b/b)[1-(-\Delta V/V_o)_o] \qquad [3.3]$$

Furthermore, if equation [3.1] is abbreviated to $\Delta b = f\ P\ b\ G$, then

$$-\Delta V/V_o = (-\Delta V/V_o)_o - 2\ f\ P\ G\ [1-(-\Delta V/V_o)_o] \qquad [3.4]$$

where $G = (14.5038/E)[(c^2 + b^2)/(c^2 - b^2) + \nu]$ [3.5]

In order to determine the degree of expansion of the bore of the compressibility cell, the volume compressions of carefully dried sodium chloride and potassium bromide were measured using the techniques described in Section 2.3. Table 9 lists the sample parameters for each run, while Tables 10 and 11 list the results in the form of the quadratic curve fits for the displacement of the pistons plus support blocks, and for the samples themselves, determined as functions of the oil pressure under the hydraulic ram of the press by the procedures outlined in Section 3.1. The terms 'up' and 'down' in Tables 10 and 11 denote data obtained from pressure increments and decrements respectively. The expressions for sample displacement listed in Table 11 were used to eliminate frictional effects by averaging the pressures at which given values of displacement occurred. The resulting data were fitted to another quadratic equation in pressure, then converted to $-\Delta V/V_o$ using the sample weight, bore diameter, and density, as discussed in Section 3.1. The expressions for $-\Delta V/V_o$, uncorrected for deformation of the pressure vessel, are listed, as a function of the internal pressure in Table 12 along with Slater's published results (115,116).

Table 13 lists values for the compression of the alkali halides at several pressures as determined in this work. The deviations of these results from Slater's values are also listed, along with the deviations which

Table 9. Various parameters for the compression runs on the alkali halides.

	Sample weight (g)	Temperature	density (g/cm^3)
Sodium chloride	11.3796	30.9°C	2.165 (119)
Potassium bromide	16.6546	29.1°C	2.750 (119)

The diameter of the hydraulic ram of the press was 2.625 in. and that of the bore of the pressure vessel was 0.9997 in.

Table 10. The displacement, L, of the pistons plus support blocks for the compression runs on the alkali halides. [a]

		a	b	c	L(x 10^4/in) std. dev.	L(x 10^4/in) maximum dev.	highest & lowest oil pressures (bar)	no. of data points
sodium chloride	down	-2.0440×10^{-4}	4.0893×10^{-1}	2.6130×10^{1}	0.6	1.3	456.7,45.3	42
	up	-6.2140×10^{-5}	3.2803×10^{-1}	$+2.6374 \times 10^{1}$	0.5	1.1	464.3,55.5	42
Potassium bromide	down	-1.5884×10^{-4}	3.2789×10^{-1}	-2.5023×10^{1}	0.5	1.2	431.0,60.3	38
	up	-2.8222×10^{-5}	2.5754×10^{-1}	-2.6005×10^{1}	0.6	1.1	459.6,58.3	41

[a] $L = ap^2 + bp + c$ where p represents the oil pressure applied to the hydraulic ram.

Table 11. The displacement, L, of each alkali halide sample. [a]

					$L(x\ 10^4/in)$			
		a	b	c	std. dev.	maximum dev.	highest & lowest oil pressures (bar)	no. of data points
Sodium chloride	down	$-8.0623x10^{-5}$	$1.5511x10^{-1}$	$-2.9143x10^{1}$	0.6	1.1	443.8,43.5	40
	up	$2.7586x10^{-5}$	$1.0559x10^{-1}$	$-3.2817x10^{1}$	0.4	1.2	460.2,47.4	42
Potassium bromide	down	$-2.5804x10^{-5}$	$2.3362x10^{-1}$	$3.5932x10^{1}$	0.4	0.9	439.2,61.1	39
	up	$-3.0102x10^{-5}$	$2.3498x10^{-1}$	$3.1874x10^{1}$	0.4	0.9	469.7,61.6	42

[a] $L = ap^2 + bp + c$ where p represents the oil pressure applied to the hydraulic ram.

Table 12. Expressions for the compression of the alkali halides as a function of internal pressure.

NaCl	This work,[a]	$-\Delta V/V_o = -1.578 \times 10^{-10}P^2 + 4.812 \times 10^{-6}P$
	Slater (115),	$-\Delta V/V_o = -4.60 \times 10^{-11}P^2 + 4.20 \times 10^{-6}P$
KBr	This work,[a]	$-\Delta V/V_o = -1.2508 \times 10^{-10}P^2 + 7.218 \times 10^{-6}P$
	Slater (115)	$-\Delta V/V_o = -1.065 \times 10^{-10}P^2 + 6.70 \times 10^{-6}P$

[a] Uncorrected for bore expansion under pressure.

Table 13. The compression of the alkali halides and the expansion constant of the compressibility cell.

	P(bar)	$-(\Delta V/V_o)$ (Slater[a])	$-(\Delta V/V_o)$ (this work[b])	Observed deviation from Slater's values	Calculated deviation assuming ideal expansion	f
NaCl	0	0	0	0	0	-
L = 0.409 in.	1000	0.00415	0.00465	0.00050	0.00132	0.38
	2000	0.00822	0.00898	0.00076	0.00263	0.29
	3000	0.01219	0.01300	0.00081	0.00393	0.20
KBr						
L = 0.471 in.	0	0	0	0	0	0
	1000	0.00657	0.00709	0.00050	0.00139	0.38
	2000	0.01297	0.01394	0.00097	0.00262	0.37
	3000	0.01914	0.02053	0.00139	0.00390	0.36

[a] Reference 115

[b] Uncorrected for the expansion of the pressure vessel bore.

one would expect from ideal expansion, calculated using the values of the bore expansion given in Table 8. The expansion constant, f, was given by the ratio of the observed and ideal deviations.

The values of f obtained from potassium bromide are very nearly independent of pressure, while the values obtained from sodium chloride are the same as those from potassium bromide at 1 kbar (f = 0.38) but drop sharply at higher pressures. Intuitively, f should be constant over this small pressure range and, since sodium chloride is less malleable than potassium bromide (117), the decrease in f observed for sodium chloride was assumed to result from non-hydrostatic pressure in the cell. It was concluded that f was equal to 0.38 for the range or pressures and sample thicknesses listed in Table 13.

The equations describing the compression of phenol I and II, (Table 7) were corrected as follows. The effect of the expansion of the bore of the compressibility cell on the pressure was calculated from equation [3.1] using the cell parameters listed in Table 8 with f = 0.38. Since the apparent and true pressures at 3 kbar were found to differ by only 4 bar, the effect of cylinder deformation on the pressure was ignored. If such a correction were necessary, it would best be made on the averaged data points, before curve fitting. Since $(-\Delta V/V_o)_o = AP^2 + BP + C$, as listed in Table 7, then equation [3.5] may be rewritten

$$-\Delta V/V_o = 2\ A\ f\ G\ P^3 + (A + 2\ B\ f\ G)P^2 + (B + 2(C-1)f\ G)P + C.$$

It can be shown numerically that, for phenol at pressures below 3 kbar, the term $2\ A\ f\ G\ P^3$ is negligibly small. Corrected values of $-\Delta V/V_o$ were thus calculated from the expressions listed in Table 7, using the approximation

$$-\Delta V/V_o \approx (A + 2\ f\ G\ B)P^2 + (B + 2(C-1)f\ G)\ P + C \qquad [3.6]$$

The final corrected values for the compression of phenol, calculated using equation [3.6] with $f = 0.38$, are listed in Table 14.

3.3 Analysis of the Experimental Uncertainties in the Determination of the Volume Compressions

This section presents an estimate of the magnitude of the experimental errors in the corrected compression results which are listed in Table 14. This analysis is necessary in order to assess the reliability of the compression results and is also intended to indicate steps which can be taken to improve the precision of future measurements.

The values for the compression of the pistons and support blocks which are listed in Table 5 for Runs 1 and 2 on phenol were obtained before and after the measurements on Sample 2, using the same pistons and blocks. They

Table 14. Expressions for the volume compressions of phenol I and II at 10°C after correction for cylinder expansion.[a]

Run #1,	phenol I	$-\Delta V/V_o = -2.2645 \times 10^{-9}\ P^2 + 2.2986 \times 10^{-5}\ P$
	phenol II	$-\Delta V/V_o = -8.4745 \times 10^{-10}\ P^2 + 1.4130 \times 10^{-5}\ P + 0.076617$
Run #2	phenol I	$-\Delta V/V_o = -2.2994 \times 10^{-9}\ P^2 + 2.3016 \times 10^{-5}\ P$
	phenol II	$-\Delta V/V_o = -4.2712 \times 10^{-10}\ P^2 + 1.1874 \times 10^{-5}\ P + 0.07986$
Run #3	phenol I	$-\Delta V/V_o = -3.8988 \times 10^{-9}\ P^2 + 2.5255 \times 10^{-5}\ P$
	phenol II	$-\Delta V/V_o = -7.4582 \times 10^{-10}\ P^2 + 1.2739 \times 10^{-5}\ P + 0.080251$

[a] $f = 0.38$

agree to within ± 1 x 10^{-4} in. at an oil pressure of 480 bar (3300 bar internal pressure), the maximum pressure used in this work. This result shows that the compression of the pistons and blocks is reproducible to ± 0.5 x 10^{-4} in. over the 1500 bar pressure range used to determine the compression of each phase of phenol. The cumulative standard deviation of all the least squares fits used in analyzing the sample displacements was less than 1.5 x 10^{-4} in. within either phase, and the net reproducibility error, as defined in Section 3.1 was less than 2 x 10^{-4} in. for measurements taken within each phase. Hence there is an inherent uncertainty of no more than 4 x 10^{-4} in. in the sample displacements within the 1500 bar range over which measurements on each phase were obtained. This uncertainty corresponds to error limits of ± 2.5%, ± 2.5%, and ± 3.5% for the values of $-\Delta V/V_o$ obtained for phase I of samples 1, 2 and 3 respectively, and to error limits of ± 0.8%, ± 0.8% and ± 1.2% for the values of $-\Delta V/V_o$ for phase II of these samples. The standard deviations of the curve fits of the pressure-averaged data were negligible (0.1 x 10^{-4} in.).

The displacement gauges, which were mounted on the top platten of the press, were estimated to lie no more than 2° out of perpendicular alignment. Such an error would give use to an uncertainty of 0.1% in the displacement readings. The centre point in the bottom platten of the press was determined from the accurately marked centre of the top platten by lowering the top platten until the plattens almost touched. The points of contact of the displacement gauges were carefully set equidistant from this centre point and diametrically opposed to one another. The overall error in the positioning of the gauges is estimated to be ± 0.125 in. and the distance between gauges was 12.8 in. Figure 15 depicts a pair of displacement gauges mounted perpendicular to the top platten of the press. If d_1 and d_2 represent the displacements of the two gauges, the apparent displacement, d', calculated assuming an accurately centred piston, is given by $d' = (d_1 + d_2)/2$. If the midpoint between the gauges is offset from the true centre of the piston by Δx, and x is the distance between gauges, then from simple geometry the true displacement, d, is given by the expression

$$d = d_2(1/2 - \Delta x/x) + d_1(1/2 + \Delta x/x)$$

Obviously if the piston does not rock during compression, $d_1 = d_2$ and no error is introduced by misaligning the gauges, however, in the limiting case where one gauge does not move (i.e. $d_2 = 0$), the relative error is given by

$$\frac{d - d'}{d} \approx \frac{d - d'}{d} = \frac{2\Delta x}{x}\left(\frac{d_1 - d_2}{d_1 + d_2}\right) = \frac{2\Delta x}{x} \qquad [3.7]$$

Unfortunately, in the runs described here, one dial gauge

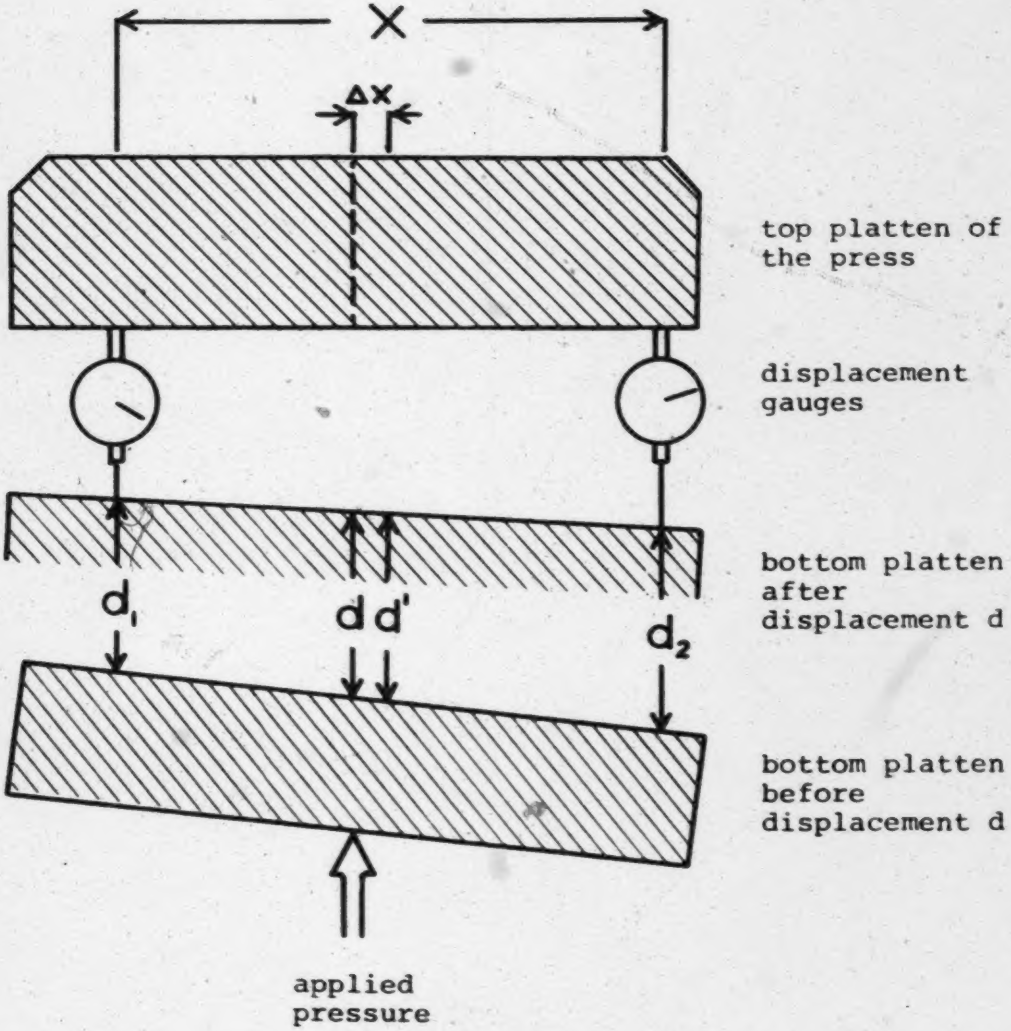
X
ΔX
top platten of the press
displacement gauges
d_1
d
d'
d_2
bottom platten after displacement d
bottom platten before displacement d
applied pressure

Figure 15. Possible errors in the alignment of the displacement gauges. The meaning of the symbols is discussed in the text.

did show a considerably larger displacement than did the other so that this source of error must be considered, and for $\Delta x = 0.125$ in. and $x = 12.8$ in., an inherent error of up to ± 2% in the experimental value of $-\Delta V/V_o$ at any pressure resulted from possible misalignment of the displacement gauges. The total uncertainty in the compression of phenol I is thus ± 4.5%, ± 4.5% and ± 5.5% for samples 1, 2, and 3 respectively, while for phenol II, the error limits are ± 2.8%, ± 2.8%, and ± 3.2% respectively.

Vaidya and Kennedy (120) have obtained compression values with an accuracy of 1 - 2% at pressures as high as 45 kbar using apparatus similar to that used here, but with the displacement gauges held rigidly in place by a metal yoke which fits over the top of the moving piston so that the gauges are aligned reproducibly each time. This arrangement also eliminates the need to measure the compression of the spacer blocks and is recommended for future work.

3.4 The Volume Compression and Compressibilities Corrected for Cylinder Deformation - Results and Discussion

The expressions for the volume compression of each sample of phenol, after correction for cylinder deformation (Section 3.2), are listed in Table 14. The compressibility of each phase, $\beta = -(V_o^{-1})(\partial V/\partial P)_T$, was obtained by differentiating the expression for $-\Delta V/V_o$ with respect to P. Values of the compressions and compressibilities of each sample at several pressures are listed in Tables 15 and 16. After averaging the results from the three runs, the equation representing the compression of phenol I is:

$$-\Delta V/V_o = -2.821 \times 10^{-9} P^2 + 2.375 \times 10^{-5} P \qquad [3.8]$$

and, for phenol II,

$$-\Delta V/V_o = -6.735 \times 10^{-10} P^2 + 1.291 \times 10^{-5} P + 0.07891 \qquad [3.9]$$

where P is the pressure in bar and the temperature is 10°C. Values of compressions and compressibilities of phenol determined from these averaged equations are also given in Tables 15 and 16. The scatter of the results from the individual runs about the mean lies within the estimated experimental uncertainties (Section 3.3).

Bridgman's values for the volume change at the I-II transition (Table 2) can be compared with those calculated from the compression data obtained in this work. Bridgman (90) reported the I-II equilibrium point at 10°C as 1446 kg cm^{-2} which converts directly to 1418 bar. After the correction to his pressure scale (94,95) is applied, this becomes 1433 bar. From equations [3.8] and [3.9], phases I and II differ in volume at the equilibrium line

Table 15. The volume compression of phenol I and II at 10°C

	Pressure (bar)	$-\Delta V/V_o$ Run #1	Run #2	Run #3	Average	Std. dev.
Phenol I	0	0	0	0	0	0
	500	0.0109	0.0109	0.0116	0.0112	0.0004
	1000	0.0207	0.0207	0.0214	0.0209	0.0004
	1500	0.0294	0.0294	0.0291	0.0293	0.0002
Phenol II	1500	0.0959	0.0967	0.0977	0.0968	0.0009
	2000	0.1015	0.1019	0.1027	0.1020	0.0006
	2500	0.1066	0.1069	0.1074	0.1070	0.0004
	3000	0.1114	0.1116	0.1118	0.1116	0.0002

Table 16. The volume compressibilities of phenol I and II at 10°C

		$\beta \times 10^5$ bar				
	Pressure (bar)	Run #1	Run #2	Run #2	Average	Std. dev.
Phenol I	0	2.30	2.30	2.53	2.38	0.13
	500	2.07	2.07	2.14	2.09	0.04
	1000	1.85	1.84	1.75	1.81	0.06
	1500	1.62	1.61	1.36	1.53	0.15
Phenol II	1500	1.16	1.06	1.05	1.09	0.06
	2000	1.07	1.02	0.98	1.02	0.05
	2500	0.99	0.97	0.90	0.95	0.05
	3000	0.90	0.93	0.83	0.89	0.05

by 6.78% of the volume at 1 bar with a maximum deviation of 0.10%, compared to Bridgman's value of 6.64%. The agreement is within the estimated limits of experimental error presented in Section 3.3. Bridgman also reported that the compressibility of phase II was less than that of phase I by about 5 x 10^{-6} bar^{-1} at the triple point. The value obtained in this work is 4.6 x 10^{-6} bar^{-1} at 10°C and 1433 bar, with a deviation of about 1 x 10^{-6} bar^{-1} for individual runs.

The compressibility of a crystal is approximately proportional to the particle radius divided by the average inter-particle force constant. The actual relationship depends on the crystal structure, and Born and Huang (121) have given a specific relationship for the alkali halide structures. The actual relationships for phenol are not known, but it may be useful to take the relationship between the compressibility and an average inter-molecular force constant to deduce the relative strengths of these averaged force constants of phenol I and II. The average molecular radius is proportional to the cube-root of the molar volume and so the average force constant of each phase may be calculated from the compression and compressibility data. The compressibilities of phenol I and II at 1433 bar are calculated from the data given above to be 15.7 ± 1.5 and 11.0 ± 0.6 x 10^{-6} bar^{-1} respectively, yielding a ratio of about 1.4 ± 0.18. Thus, at 1433 bar and 10°C, the average inter-molecular force constant for phenol II is about 40% greater than for phenol I. Accepting, for the purpose of estimation, a large extrapolation of the compressibility data for phenol II, we can compare the force constants of phenol I and II at one atmosphere and find a ratio of 1.8 ± 0.2 and hence, a difference in the force constants of about 80%. This latter value may be more pertinent for comparison with the spectroscopic results on quenched samples at about 100°K, although, of course, tremendous extrapolations are involved.

Since infrared data (86) suggest that the hydrogen bond in phenol II is weaker than that of phenol I, the stronger force constants in phase II must result from some other interaction. Unfortunately the far infrared data currently available (86) are not extensive enough or well enough assigned to give any reliable information on the relative magnitudes of the average intermolecular force constants of phenol I and II. It seems probable, that the difference in compressibilities of phases I and II arises largely from stronger van der Waals forces which presumably exist in phenol II because of its more dense structure.

Chapter IV. The Phase Diagram of Solid Phenol Below 0°C and Powder X-ray Diffraction Studies of Phases I and II at -190°C

The study of a high pressure phase is greatly facilitated if the phase is metastable at one atmosphere and low temperatures since infrared and x-ray diffraction data may then be obtained without using high pressure apparatus. This chapter presents the results of measurements designed to determine the regions of stability of both phases of solid phenol. The phase diagrams of pure and impure phenol below 0°C are reported in Sections 4.1 to 4.3. The warming curve of metastable phenol II, discussed in Section 4.4, was obtained both to determine the approximate heat of the transformation from metastable phenol II to phenol I, and to verify the transition temperature at ambient pressure which was predicted by extrapolating the II → I transition line in the phase diagram to zero bar. The x-ray powder diffraction pattern of the metastable phase was obtained primarily to characterize the phase and is reported in Section 4.5 along with some powder diffraction results for phenol I.

4.1 Methods for the Determination of the Phase Diagram of Phenol

As discussed in Section 1.4, nonhydrostatic pressure in a piston-cylinder pressure vessel results largely from friction between the cylinder wall and the sample. Furthermore, if a sample is taken through a phase transition from a malleable to a non-malleable phase, the rigid phase prevents pressure from being readily transmitted to the remainder of the malleable phase, and a poorly defined phase transition results. Such an effect was found for the phenol I - II transformation at 10°C, as shown in Figure 5 (page 32) and would presumably be more pronounced at lower temperatures. Lubrication of the cylinder walls with either graphite or indium (120,122) or, preferably, the use of a pressure transmitting fluid (90) are techniques which are often used to minimize this problem. An alternative method is to detect phase transformations by plotting the capacitance or resistance of samples which have a large diameter relative to their thickness as a function of pressure.

In this work, the phase transition was detected by plotting the cell capacitance of the parallel plate dielectric cell (Section 2.5b) at the arbitrary frequency of 10 kHz against pressure at several different temperatures. Since the samples were about 1 mm thick, pressure gradients due to friction should have been minimal. The temperature of the cell could be kept constant to ±0.2°C at -40°C, and to better than this at higher temperatures. Because the two thermocouples gave slightly different readings, the temperature can only be considered known to ±0.1°C at 10°C and ±0.5°C at -40°C.

In a typical set of runs, the sample was taken through the I - II transition several times, then left overnight at 2.5 kbar and room temperature. Before commencing a run at a given temperature, the sample was again taken through the transition to achieve further purification (see Section 4.3). The cell capacitance was then determined as a function of increasing and decreasing pressure by changing the pressure by fixed increments at six minute intervals, and reading the capacitance five minutes after each pressure change. This procedure was adopted as being more practical than waiting for all readings to stabilize before changing the pressure since, at 10°C, this would have required 15 or more minutes per point in the region of the transition. This procedure of taking readings at fixed time intervals, rather than waiting for the system to achieve equilibrium, appears to be a common practice (104). At -10°C and -28°C, readings taken at 27 bar pressure increments were shown to yield essentially the same results as readings taken at 13 bar pressure increments and, hence, 27 bar increments were used below -10°C, while 13 bar increments were used at higher temperatures.

4.2 The Phase Diagram of Purified Phenol

Typical plots of the capacitance of the parallel plate cell against pressure are shown in Figure 16. The pressure at which the transition was clearly occurring was chosen by drawing a straight line through the points leading up to the transition and a second line through the points clearly forming part of the transition, then choosing the point of intersection of the two lines as the desired pressure.

The I → II and II → I transition pressures, as determined by this procedure, are listed in Table 17 for each of the three samples in the order in which they were measured, and are shown in Figure 17. The smooth curves drawn through these points in Figure 17 were taken to indicate the I → II and II → I transition lines, that is the borders of the region of indifference in this apparatus. The effect of the hysteresis within the apparatus itself was estimated from the blank compression runs (Sections 2.3 and 3.1) and was subtracted to yield the corrected transition lines, shown by the broken lines in Figure 17. Bridgman's values for the transition lines (90) (Section 1.5a), which were obtained at temperatures above 0°C, are also shown. The hysteresis of the apparatus does not entirely account for the fact that our region of indifference is larger than Bridgman's, but the remaining discrepancy can be attributed to the method used to determine the pressures at which transformations began. The extrapolation technique used here estimates the pressure at which a

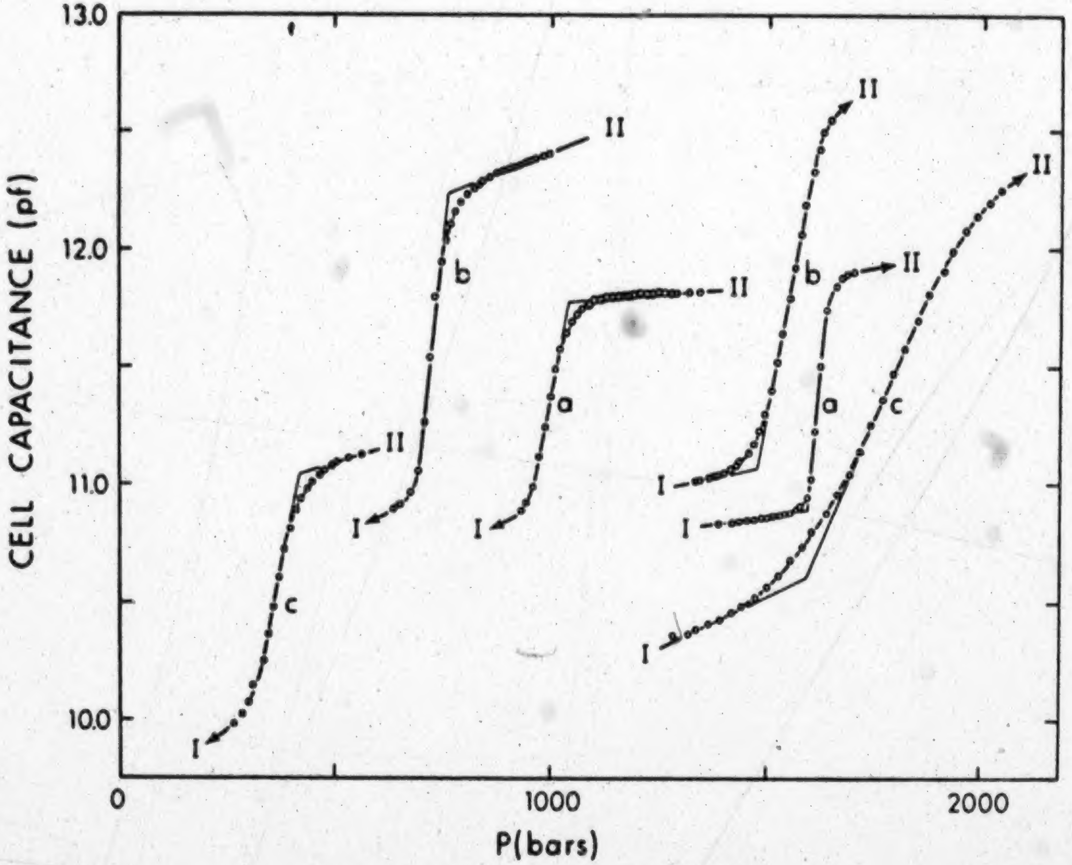

Figure 16. The capacitance vs. pressure plots from which the transition pressures of phenol I and II were obtained. Curves a and b were obtained using sample 3 at 1.9°C and -14.2°C, respectively. Curve c was obtained from sample 2 at -33.4°C. The arrowheads show the direction of pressure change.

Table 17. Transition pressures for solid-solid transformations in phenol.[a]

		Transition Pressures		Equilibrium Pressures		
	T(°C)	$P_{I \rightarrow II}$	$P_{II \rightarrow I}$	P_{eq} (this work)	P_{eq} (Bridgman)[b]	deviation
Sample 1	11.5	1632	1216	1424	1450	-26
	1.6	1595	1059	1327	1333	- 6
	-18.4	1452	768	1110	1099	11
Sample 2	-37.4	1995	293			
	-33.4	1590	397			
	-28.2	1545	465	1005	984	21
	-10.3	1485	947	1216	1194	22
	-19.9	1529	684	1107	1081	26
Sample 3	-34.4	1636	372			
	-14.2	1470	753	1111	1148	-37
	1.9	1587	1031	1309	1337	-29
	-38.2	1763	275			

[a] All pressures are in the units bar.

[b] Calculated using Bridgman's equilibrium line, corrected for pressure calibration, and extrapolated below 0°C.

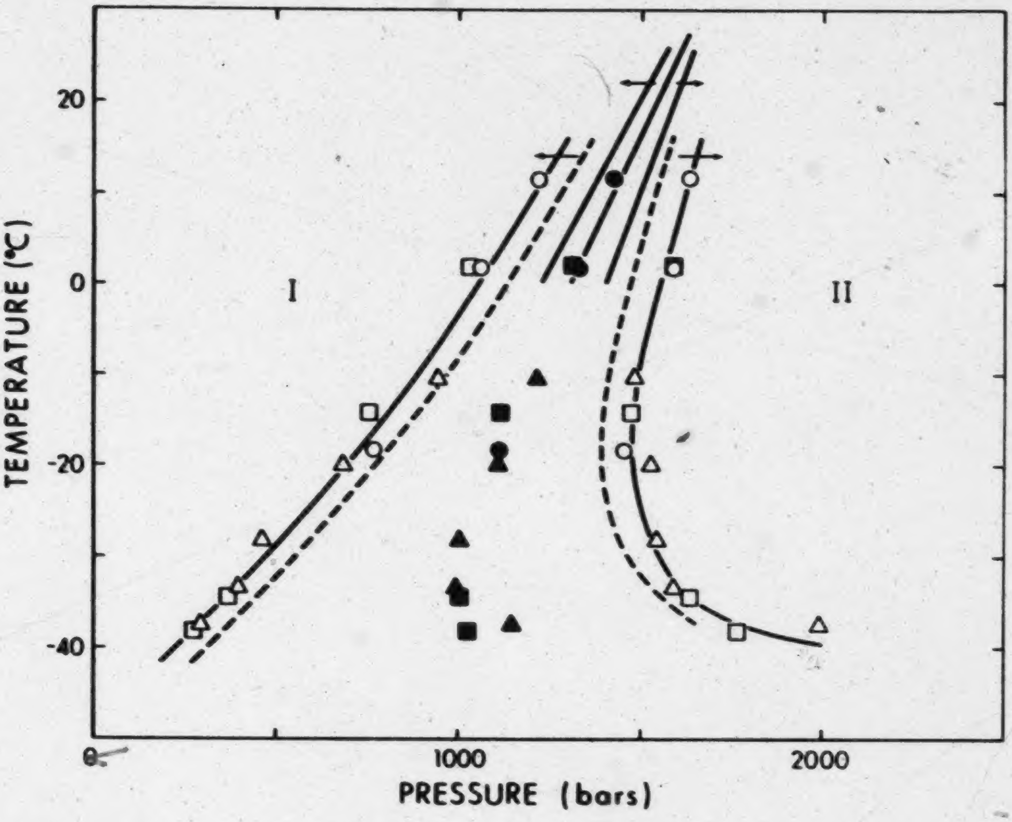

Figure 17. The phase diagram of phenol. I and II indicate the regions of stability of phenol I and II. The symbols represent the transition pressures: ○, sample 1; △ , sample 2; □ , sample 3. The equilibrium pressures are indicated by the corresponding solid symbols. The transition lines are marked by arrows which indicate the direction of the phase changes. The outer pair of transition lines, and the accompanying dashed lines, were obtained from this work, before and after correcting for the hysteresis in the apparatus. The short pair of transition lines were obtained by Bridgman. They bracket his corrected equilibrium line.

transformation occurs rapidly in this apparatus but, because of the slow early growth of the new phase (65), this is not the earliest pressure at which the new phase forms. This effect, which increases with decreasing temperature, is clearly evident in Figure 16 and must reflect the sluggishness of the transition at low temperatures since the size of the pressure increments did not affect the results (Section 4.1). With reference to Figure 17, as the temperature is lowered below about -30°C, the I → II transition becomes increasingly sluggish and the pressure required to make it proceed at a reasonable rate increases drastically, while the II → I transition is not so affected.

The averages of the I → II and II → I transition pressures at each temperature are listed in Table 17 and are represented in Figure 17 by the solid symbols. Following Bridgman's practice (90), these points were considered to represent the I - II equilibrium pressures. The results for 2.0°C and 11.5°C suggest that Bridgman's values for the equilibrium line (Table 2), which have been corrected for an error in his pressure calibration (94,95), are about 15 bar too high, an effect which, because of the results presented in Section 4.3, is almost certainly due to the impurities which Bridgman reported were in his sample. The experimental uncertainties in the transition pressures obtained in this work below 0°C permit only the observation that Bridgman's corrected expression for the equilibrium line, $P_{eq} = 1315 + 11.75\ T(°C)$, where P_{eq} is the equilibrium pressure in bar, fits the data between 12°C and -30°C to a standard deviation of 20 bar (Table 17). Points taken below -30°C deviate considerably from Bridgman's expression and this presumably reflects a relatively abrupt increase in the apparent I → II transition pressure, similar to that observed (123) for the ice transitions, rather than a discontinuity in the true equilibrium line.

Although Bridgman's extrapolated equilibrium line reaches one atmosphere at about -112°C, it is clear from Figure 17 that phenol II cannot be formed from phase I at pressures lower than 1300 bar. This is consistent with the results of earlier workers who have failed to produce phenol II by cooling phenol I at atmospheric pressure (Section 1.5b). Quenched phenol II is metastable at one atmosphere, and reverts back to phase I at -48°C ± 2°C, judging from the extrapolation of the I → II transformation after correction for hysteresis (the dashed line in Figure 17).

4.3 The Effect of Impurities on the Phase Diagram

To investigate the effectiveness of the purification procedures used in this work, the pressures of transformation were determined at 10°C for a sample taken from the low melting, impure tail of the zone refiner. The capacitance vs. pressure curves for this run are shown in Figure 18. The first I → II transformation occurred at 1824 bar, as

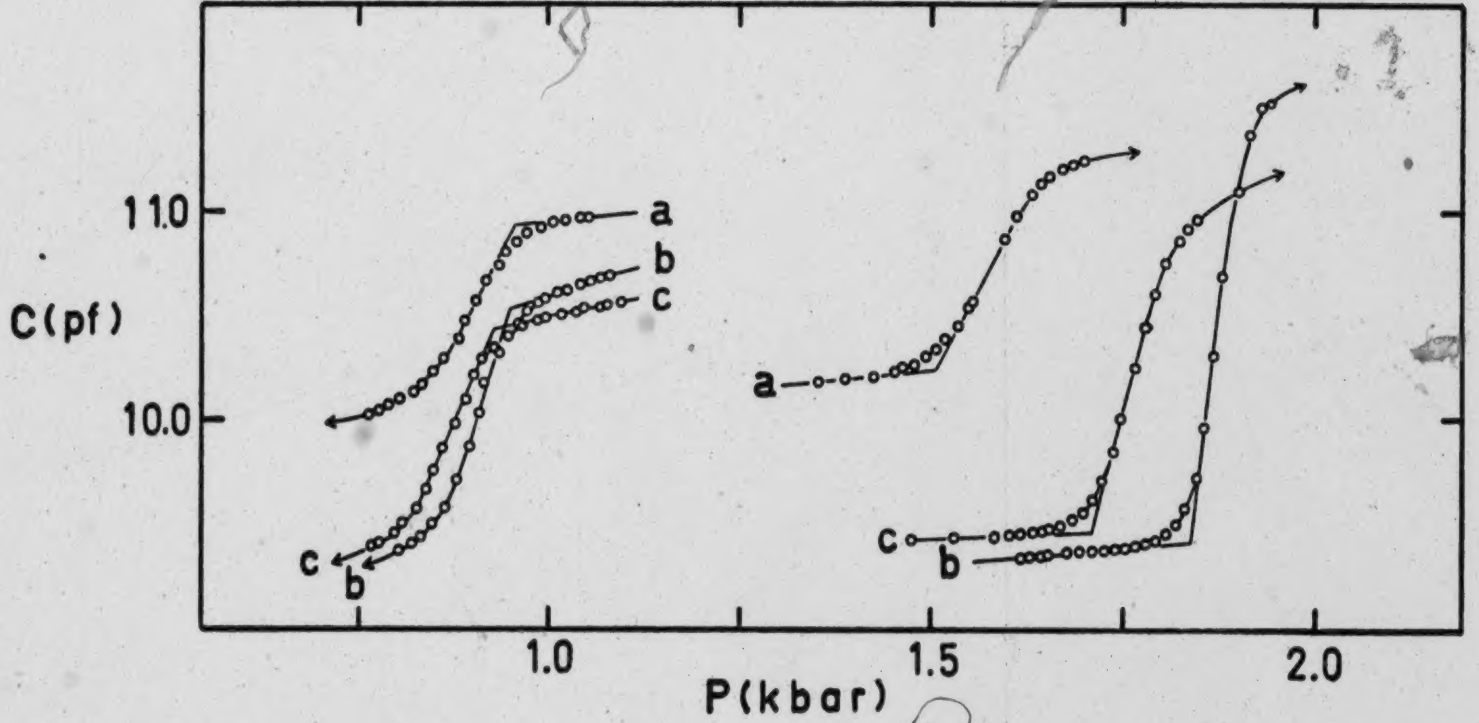

Figure 18. Capacitance vs. pressure plots for pure and impure samples of phenol: a, purified phenol at -10.3°C; b, a sample of impure phenol at -8.9°C; c, the same impure sample at -8.9°C after 48 hours.

compared with 1485 bar for a pure sample. Subsequently, the sample was allowed to sit as phase I for 48 hours and the I → II transition then occurred at 1695 bar. For pure and impure samples, the II → I transformation took place at 947 bar.

These results are consistent with Bridgman's observation (124) that the osmotic pressure of impurities which are soluble in one phase and insoluble in a second will cause the equilibrium line to move toward the region of stability of the second phase. Presumably, in this case, the zone refining did concentrate impurities in the low melting tail of the tube. These impurities were then precipitated out by the first I → II transformation which was shifted to high pressures, while the II → I transformation was unaffected since the impurities were not dissolved in phase II. These impurities clearly had not completely redissolved in phase I in 48 hours. A similar interpretation has been offered to explain certain anomalies in the dielectric relaxation of ice I which occur just after it has been formed from ice II (41).

4.4 The Temperature and Enthalpy Change of the Phenol II to Phenol I Transformation at One Atmosphere

The warming curves of two samples of phenol II and two samples of acetonitrile were obtained by the methods described in Section 2.6. The heating rate of the can was about 0.2°C/min. from -50°C to -40°C.

Plots of log $(T_\infty - T)$ vs. time, shown in Figure 19, showed the warming curve of the can to follow the first order rate law:

$$\frac{dT}{dt} = k\ (T_\infty - T) \qquad [4.1]$$

where T_∞ is the temperature of the bath, T is the temperature of the can, and k is a rate constant. Deviations of the cup temperature from this equation were taken to indicate the onset of a phase transition.

The warming curves of the two samples of phenol II (curves A and B in Figure 19) indicate transformation temperatures of -49.8°C and -47.5°C. The calibration with acetonitrile (curves C and D in Figure 19) suggests that the actual transition temperatures may be as much as 2°C warmer than these, but this still yields fair agreement with the value of -48°C ± 2°C estimated from the phase diagram (Section 4.2).

The molar heat of transformation, $\Delta\bar{H}$, was estimated by assuming heat flow into the cup was proportional to the difference in temperature between the cup and its surroundings. Hence, $\frac{dQ}{dt} = B\Delta T$ where Q is the heat absorbed by the cup, and $\Delta T = T_{cup} - T_{can}$ at time t. Thus,

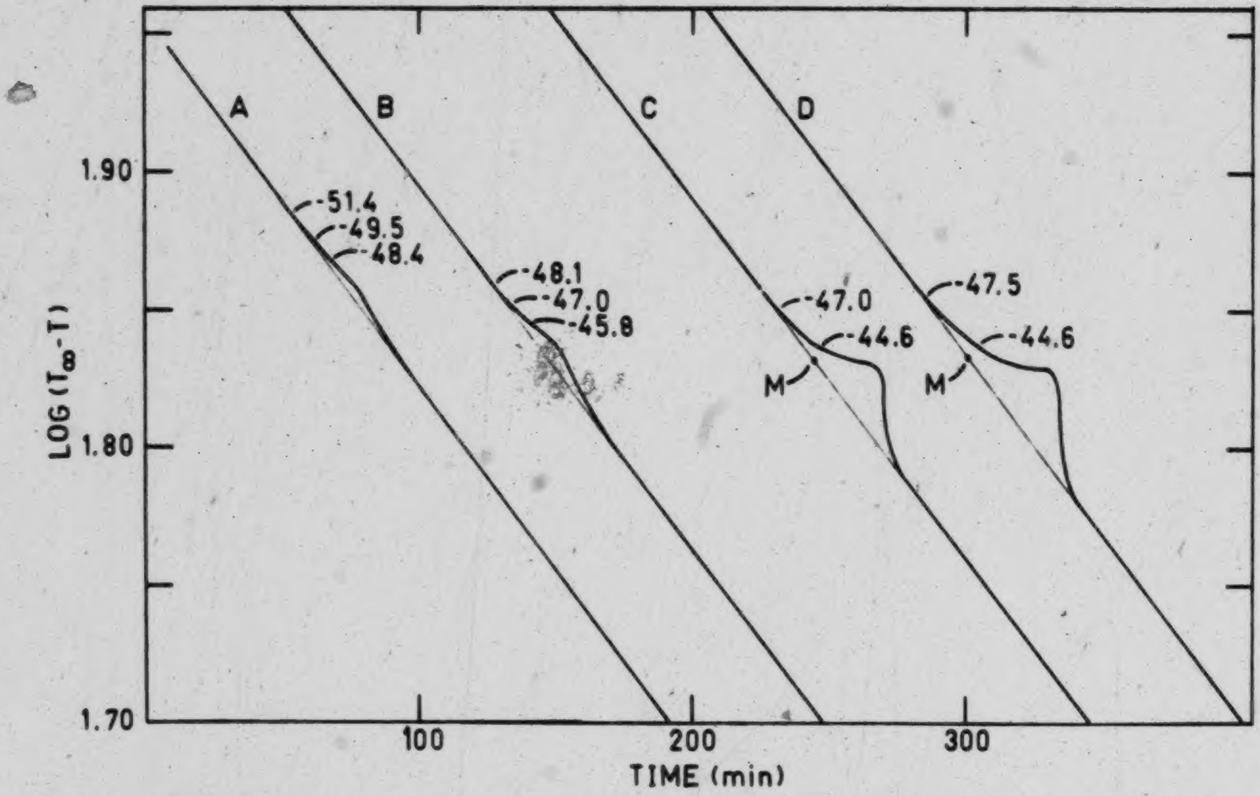

Figure 19. The warming curves for quenched phenol II at one atmosphere. A and B are the warming curves for phenol in the 0.201 cm^3 and the 0.627 cm^3 cups respectively, while C and D are the corresponding calibration curves using acetonitrile. Several temperatures in the regions of transition are indicated. M is the melting point of acetonitrile, -43.9°C (126). T_∞ for each sample was as follows: A, 25.4°C; B, 24.2°C; C, 24.1°C; D, 24.2°C.

$$Q = B\int \Delta T\,dt \qquad [4.2]$$

Q, the total heat which flowed into the cup during the transformation, is equal to the heat of transformation of the sample plus the heat required to raise the temperature of the cup and its contents from T_i to T_f, the initial and final temperatures at which the warming curve of the cup deviates from equation [4.1]. Hence,

$$Q = \left(C_{sample}+C_{cup}\right)\left(T_f-T_i\right) +n\Delta\overline{H} \qquad [4.3]$$

where C refers to the heat capacity of the sample or cup, as labelled and n is the number of moles of sample in the cup. Since the actual densities of phenol II and acetonitrile at -195°C are unknown, and since the uncertainty in the volume of the samples was large (±10%), the room temperature density of phenol II, 1.229 g/cm^3, (Section 3.4) and the density of liquid acetonitrile at its freezing point, 0.8512 g/cm^3 (125) were used to calculate n. For each sample in Figure 19, points on either side of the transition were fitted graphically to a straight line to obtain an expression for the warming curve of the can. This expression was subtracted from points in the area of the transition to give values of ΔT which were then graphically integrated to give $\int\Delta T dt$ and hence B as a function of Q (equation [4.2]). The actual value of B was obtained for each cup from the runs on acetonitrile, for which $\Delta\overline{H}$ is 1.952 kcal/mole (126), using equation [4.3]. C_{cup} was calculated from the weight of the cup and the heat capacity of copper (127), 0.0924 cal/g°C. C_{sample} was calculated from the mass of the sample and the heat capacities of phenol (128) and acetonitrile (129), 0.25 cal/g°C and 0.46 cal/g°C, respectively.

Table 18 lists numerical values for each of the parameters used in equations [4.2] and [4.3] along with the parameters calculated from these equations. Individual values of 0.39 and 0.48 kcal/mole for $\Delta\overline{H}$ of the phenol II - I transformation were obtained using equations [4.2] and [4.3]. These results average to give $\Delta\overline{H} = 0.43 \pm 0.09$ kcal/mole, where the error of ±20% is due to uncertainties in the amount of sample present. This value is slightly higher than the value of 0.31 kcal/mole, obtained by extrapolating Bridgman's isothermal data to -112°C, the temperature at which the I - II equilibrium occurs at one atmosphere. Such a difference is expected because of the irreversible conditions under which the II - I transformation occurs at -47°C to -50°C and one atmosphere.

An accurate knowledge of the weight of sample used would increase the precision of results determined from this apparatus, but the ultimate precision would probably not be better than a few percent. The apparatus is, however, a useful tool for obtaining approximate values of heats and temperatures of transformation, and is well suited to loading at liquid nitrogen temperatures, a prerequisite for measurements on quenched high pressure phases of solids.

Table 18. The enthalpy change of the phenol I → II transformation at one atmosphere. Parameters used in, and determined from, the calculations discussed in Section 4.3 are listed below.

		Run #1	Run #2
	Cup volume	0.201 cm^3	0.627 cm^3
	Cup heat capacity, C_{cup}	0.025 cal/°C	0.041 cal/°C
	B	9.75×10^{-2} cal/sec°C	21.73×10^{-2} cal/sec°C
Acetonitrile	density	0.8512 g/cm^3	0.8512 g/cm^3
	n	3.13×10^{-3} moles	9.76×10^{-3} moles
	$\int \Delta T\,dt$	71.3 sec°C	113.8 sec°C
	$T_f - T_i$	10°C	12°C
	C_{sample}	0.059 cal/°C	0.184 cal/°C
Phenol II	density	1.229 g/cm^3	1.229 g/cm^3
	n	1.97×10^{-3} moles	6.14×10^{-3} moles
	$\int \Delta T\,dt$	14.4 sec°C	24.3 sec°C
	$T_f - T_i$	9°C	9°C
	C_{sample}	0.046 cal/°C	0.144 cal/°C
	$\Delta \bar{H}$	0.386 kcal/mole	0.484 kcal/mole

4.5 Powder X-ray Diffraction Results

A number of x-ray powder diffraction photographs were obtained for phenol I and II at -190°C using a variety of radiation sources. Values for the wavelengths of the radiation from each source were taken from the literature (112) and are listed in Table 19 along with the filter materials. The sample to film distance was 60.0 mm and the measurements were corrected for film shrinkage which varied from 0.00% to 0.18% but was usually less than 0.1%.

For a system such as phenol I, which is orthorhombic (82), the value of each d spacing, d, is given by the expression (129,130)

$$\frac{1}{d^2} = \frac{h^2}{a^2} + \frac{k^2}{b^2} + \frac{l^2}{c^2} \qquad [4.4]$$

where h, k, and l are the Miller indices of the reflection in question and a, b, and c are the sides of the unit cell.

The intensity of each diffracted beam, I_{hkl}, is proportional to the integrated cross-sectional optical density of the ring it produces on the photographic plate (131). For A Debye-Scherrer camera, I_{hkl}, may be calculated (132,133) by the expression

$$I_{hkl} \propto mF^2_{hkl} \frac{1 + \cos^2 2\theta}{\sin^2\theta \cos\theta} \qquad [4.5]$$

Table 19. The wavelength and filter material of each radiation source.[a]

Source	λ (A°)	Filter
Cr	2.2909	Vanadium Pentoxide
Cu	1.5418	Nickel
Mo	0.71069	Zirconium

[a] The wavelengths used here are the intensity weighted mean values of the $K\alpha_0$ lines for each source (112).

where m is multiplicity of the reflecting plane, F_{hkl} is the structure factor of the reflecting plane, and

$$\theta \equiv \sin^{-1} \frac{\lambda}{2d}$$

The sample to film distance of a flat plate camera is not constant as in the Debye-Scherrer camera, but rather increases with θ. This causes an expansion of the diffraction rings as θ increases and hence reduces the cross sectional intensity of each ring. It is easily shown that, for a flat plate camera

$$I_{hkl} \propto mF^2_{hkl}\left[\frac{1 + \cos^2 2\theta}{\sin^2\theta \cos \theta}\right]\left[\frac{\sin 2\theta}{\tan 2\theta}\right] \qquad [4.6]$$

The powder pattern of phenol I at room temperature was calculated from the unit cell and structure factors reported by Gillier-Pandraud (82) (Section 1.5a) using equations [4.4] and [4.6], and is given in Table 20 along with the unit cell parameters. Three photographs of zone refined phenol I, taken with copper Kα radiation using different exposure times, were used to determine the d-spacings at -190°C ± 5°C. The relative intensities of the lines on the best powder photograph were measured to an estimated accuracy of ±10% (Section 2.8) and, by comparing the low temperature relative intensities and d-spacings with those at room temperature, it was possible to index the d-spacings found for phenol I at -190°C. The indexed d-

Table 20. X-ray powder diffraction data for phenol I at room temperature and at -190°C

Phenol I at Room Temperature[a]

a = 6.02 ± 0.02 A°

b = 9.04 ± 0.04 A°

c = 15.18 ± 0.04 A°

α = β = γ = 90°

6 molecules/unit cell

h k l	d(A°)	(I/I_{max})x100
0 1 0	9.040	21
0 0 2	7.590	6
0 1 2	5.813	8
1 0 1	5.595	8
1 1 0	5.010	52
1 1 1	4.758	83
1 0 2	4.717	17
0 1 3	4.415	46
0 2 1	4.332	12
1 1 2	4.182	18

Phenol I at -190°C

a = 6.00 ± 0.03 A°

b = 8.91 ± 0.03 A°

c = 14.59 ± 0.03 A°

α = β = γ = 90°

(I/I_{max})x100	d(A°) (experimental)	d(A°) (calc.)	deviation	no. of photographs
14	8.922 ± 0.003	8.910	-0.012	3
3	7.313 ± 0.034	7.295	-0.018	3
14	5.617 ± 0.008	5.644 5.549	--	3
46	4.974 ± 0.009	4.980	+0.006	3
100	4.683 ± 0.005	4.710 4.634	--	3
51	4.265 ± 0.013	4.268 4.260	+0.003 -0.005	3
19	4.098 ± 0.008	4.111	+0.013	3

Table 20. continued

h k l	d(A°)	(I/I_{max})x100
0 2 2	3.883	44
1 0 3	3.873	38
0 0 4	3.795	18
1 1 3	3.560	19
1 2 1	3.516	12
0 1 4	3.499	12
0 2 3	3.370	11
1 2 2	3.263	33
1 0 4	3.210	13

(I/I_{max})x100	d(A°) (experimental)	d(A°) (calc.)	deviation	no. of photographs
92	3.782 ± 0.007	3.802 3.778	--	3
16	3.637 ± 0.018	3.648	+0.011	3
44	3.477 ± 0.004	3.477 3.474	0.000 -0.003	3
11	3.386	3.376	-0.010	1
8	3.286	3.286	0.000	1
44	3.210 ± 0.003	3.212	+0.002	3
12	3.111 ± 0.008	3.112	+0.001	3

---

[a] Calculated from data in reference 82.

spacings were then used to calculate the unit cell of phenol I at -190°C which was subsequently refined by a least squares procedure using the program DREFINE (134). Table 20 lists the unit cell parameters of phenol I at -190°C along with the d-spacings calculated from the unit cell and the observed powder pattern at -190°C. Each experimental d-spacing is, in most cases, the average of those measured from three photographs and the error limit given is the standard deviation about the mean value. The uncertainties in the cell parameters at -190°C were calculated by the program DREFINE.

From the unit cell parameters listed in Table 20, the volume expansion of phenol I from -190°C to room temperature is 6 ± 2%. This corresponds to a mean thermal expansivity of $3 \pm 1 \times 10^{-4}$/°C. The expansion along the a axis, the direction of the hydrogen bonded spine of the polymeric phenol chain (Section 1.5a), is between 0 and 1%, while the b and c axes expand by 1.5 ± 0.6% and 4.0 ± 0.5%, respectively, indicating that the chains move significantly farther apart as phenol I is heated but change only slightly in length. A similar effect has been observed during x-ray studies on single crystals of acetic acid I (135), a molecular crystal which is also composed of hydrogen bonded polymeric chains. In acetic acid, a volume expansion of 6% between -180°C and 5°C was accomplished solely by increasing the interchain distances, since no change was observed in the length of the hydrogen bonded spine (135). These results are consistent with the expansivities of other molecular crystals since compounds in which Van der Waals interactions represent the only intermolecular forces may expand considerably (an average of 2% in each dimension over 100°C for cyclohexane and neopentane (136)), while ice I, in which the primary intermolecular force is the hydrogen bond, expands by only about 0.5% along each axis between -180°C and -10°C (137,138).

The powder pattern of phenol II at -190°C was determined from photographs of several samples prepared from two lots of zone refined phenol, and is recorded in Table 21. The experimental d-spacings reported are the averages of those measured from photographs taken with chromium, copper and molybdenum Kα radiation. The number of photographs with each radiation which were included in the average is shown in the last column of the table for each line. The error reported for each experimental d-spacing is the standard deviation about the mean. Since d-spacings calculated from small values of θ are less reliable than those calculated from large values of θ (139), the d-spacings calculated from small angle reflections on photographs using copper and molybdenum sources were weighted by one half in calculating the average values of d, as were the d-spacings determined from photographs on which the appropriate line was very weak. The chromium pictures were plagued by fogging which obscured reflections 2, 3 and 4 and which may have hidden weak lines inside reflection 1. The source of this

Table 21. X-ray powder diffraction data for phenol II at -190°C and atmospheric pressure

Unit Cell Parameters for Phenol II

a = 10.59 ± 0.01

b = 16.31 ± 0.02

c = 17.39 ± 0.02

α = β = γ = 90°

24 molecules/unit cell

line	(I/I_{max})x100[a]	d(A°) (experimental)	d(A°) (calc.)	deviation (A°)	h k l	no. of photographs[b]
1	16	11.884 ± 0.030	11.896	+0.012	0 1 1	3 Cr, (3 Cu)
2	<1	10.509	10.590	-0.081	1 0 0	1 Cu
3	2	9.040 ± 0.005	9.045	+0.005	1 0 1	3 Cu
4	1	7.462 ± 0.033	7.383	-0.079	0 2 1	2 Cu
5	21	5.790 ± 0.004	5.797	+0.007	0 0 3	3 Cr, 3 Cu
6	8	4.777 ± 0.006	4.837		1 3 0 2 1 1	3 Cr, 1 Cu
			4.725		0 2 3	
7	89	4.358 ± 0.005	4.358	0.000	2 1 2	3 Cr, 3 Cu

Table 21 continued

line	$(I/I_{max})\times100^a$	d(A°) (experimental)	d(A°) (calc.)	deviation (A°)	h k l	no. of photographs^b
8	8	4.231 ± 0.006	4.227	-0.004	1 3 2	3 Cr
9		4.084 ± 0.005	4.078	-0.006	0 4 0	3 Cr
10	61	3.854 ± 0.007	3.905 3.836		1 1 4 0 2 4	3 Cr, 2 Cu
11	100	3.712 ± 0.004	3.714 3.706		1 3 3 2 3 1	3 Cr, 2 Cu
12	5	3.544	3.530	-0.014	3 0 0	1 Cu
13	14	3.342 ± 0.004	3.335	-0.007	0 4 3	3 Cr, 3 Cu
14	9	3.197 ± 0.005	3.199	+0.002	0 2 5	(3 Cr), 3 Cu
15	67	3.056 ± 0.003	3.054	-0.002	0 5 2	3 Cr, 3 Cu
16	5	2.928 ± 0.001	2.930	+0.002	0 3 5	2 Cu
17	8	2.654 ± 0.002	2.669 2.648		3 4 0 4 0 0	3 Cu, 2 Mo
18	5	2.530 ± 0.004	2.533	+0.003	1 5 4 4 0 2	3 Cu

Table 21 continued

line	$(I/I_{max})\times100^{a}$	$\bar{d}$(A°) (experimental)	d(A°) (calc.)	deviation (A°)	h k l	no. of photographs[b]
19	18	2.445 ± 0.001	2.447	+0.002	3 3 4	3 Cu
20	6	2.339 ± 0.002	2.340	+0.001	2 5 4	3 Cu
21	3	2.243 ± 0.004	2.240	-0.003	4 1 4	3 Cu
22	6	2.180 ± 0.006	2.179	-0.001	4 2 4	3 Cu, 2 Mo
23		2.094 ± 0.003	2.098 2.089		3 5 4 4 1 5	(2 Cu), 2 Mo
24		1.985 ± 0.003	1.989 1.978		5 0 3 4 4 4	(2 Cu), 2 Mo
25		1.867 ± 0.003	1.868	+0.001	5 3 3	2 Mo
26		1.748 ± 0.003	1.746	-0.002	6 1 1	2 Mo
27		1.633 ± 0.003	1.631	-0.002	5 3 6	2 Mo

[a] obtained using Cu Kα radiation

[b] the number of photographs taken with chromium (Cr), copper (Cu) or Molybdenum (Mo) radiation used to calculate the average. Brackets enclose those photographs which were weighted by one half in taking the average.

problem was not located, however possible causes are discussed on page 246 of reference 130.

The presence of phenol I in the phenol II samples would have been indicated by reflections at 4.974 A°, 4.683 A°, 4.265 A° and 3.782 A° (Table 20), all of which were entirely absent. Similarly, the absence of reflections at 3.90 A° and 3.66 A° (140) confirmed that no ice I was present. When samples of phenol II which had been characterized by their powder photographs were warmed to -25°C for 30 minutes, then cooled to -190°C, the resulting diffraction patterns showed that complete transformation to phenol I had occurred.

Although the primary purpose of the x-ray diffraction studies was to unambiguously characterize the two phases of phenol, an attempt was made to index the d-spacings of phenol II on the basis of an orthorhombic unit cell using the Hesse-Lipson method (141,142). This requires the construction of a difference table of values of $1/d^2$ in which one seeks oft-occurring differences which, on the basis of equation [4.4], may indicate values of h^2/a^2, k^2/b^2 or l^2/c^2. Since the difference table revealed values corresponding to $l = 1$, 2 and 3 for a value of $d \simeq 10.6$, line 2 was indexed as 100. Lines 1 and 3 were arbitrarily indexed as 011 and 101 respectively since the volume of the resulting unit cell was consistent with the known density of phenol II as discussed below. The observed d-spacings were indexed on this basis and the unit cell parameters were refined using the program DREFINE. The refined unit cell, the d-spacings calculated from it, and the deviations between the experimental and calculated d-spacings are listed in Table 21. Generally the calculated d-spacings lay within one standard deviation of the experimental ones and all calculated values were within the outer limits of the observed lines on the powder photographs.

From the compression results reported in Section 3.4, the ratio of the molar volume of phenol II to that of phenol I at 10°C and atmospheric pressure, $\bar{V}_{II}(10°C)/\bar{V}_{I}(10°C)$, is 0.921 ± 0.002. If the unit cell defined in Table 21 is assumed to contain 24 molecules, the ratio of molar volumes, $\bar{V}_{II}(-190°C)/\bar{V}_{I}(25°C)$, equals 0.909. Thus, as far as one can determine from available data, the postulated unit cell is consistent with the density of phenol II, and it also rationalizes the powder pattern rather well.

Chapter V. The Dielectric Properties of Phenol I and II

This chapter presents the results of dielectric studies on phenol I and II. Section 5.1 outlines the experimental methods used in the study, while Sections 5.2 to 5.4 present and discuss the results obtained for the two phases. The correction to the dielectric constants for the deformation of the dielectric cell under pressure, and the results of the calculation of the electronic polarization of phenol are used in Sections 5.2 to 5.4, but these topics are not discussed until Sections 5.5 and 5.6, respectively, so as not to interupt the continuity of the presentation.

5.1 Methods for the Determination of the Dielectric Constants of Phenol I and II

The object of this work was to determine dielectric constants of phenol at 10°C as a function of pressure, since such measurements can be used in conjunction with the previously determined compression data (Section 2.3 and 3.4) to calculate molar polarizations. Additional objectives were to determine the dielectric constants of phase I as a function of temperature, in view of the dubious nature of Smyth's data (Section 1.5.a), and to attempt to evaluate the contributions of electronic and atomic polarization to the molar polarization of each phase.

Chan and Chew (22) report that a pressure of 10 bar in a coaxial cell is enough to avoid cracks in the plastic phase of solid cyclohexane. However, measurements on phenol, using the coaxial cell with a constant applied pressure of 1 kbar at temperatures from -70°C to +40°C, showed anomalous behavior which was attributed to the formation of cracks as the sample was cooled. A detailed discussion is presented in Section 5.2. Since it was not practical to attempt to measure the isobaric dielectric constant of phenol as a function of temperature by means of cooling and warming curves, the dielectric constant was instead measured isothermally as a function of pressure in the coaxial cell at a variety of temperatures. The dielectric constant isobars could be readily calculated from such data, and it was assumed that the onset of cracking in the sample would reveal itself by causing the hysteresis curves to become non-reproducible and poorly defined. Evidence obtained from measurements on phenol II which tends to support this assumption is presented in Section 5.3.

In a typical set of measurements the cell constant was determined at room temperature as a function of frequency, as discussed in Section 2.5a. The cell was then loaded in a dry box with a preweighed sample of about 2 g of zone-refined phenol. This was enough to ensure that the central electrode would remain covered with sample when pressure was applied. The sample was annealed overnight at 35°C and a pressure of about 1500 bar before measurements were made. At each temperature the pressure was changed by 125 bar every half-hour and the dielectric readings were taken at several frequencies 25 minutes after each pressure change. At each temperature, readings were taken while increasing and while decreasing the pressure before the temperature was changed. During each set of measurements on phenol I, care was taken not to form any phenol II, lest the volume change at the transition caused the position of the central electrode, and therefore the cell constant to be altered. After all of the data required for phenol I had been obtained from each sample, the sample was taken through the I - II transition at +35°C and was allowed to sit at about 2000 bar at +35°C until the measured capacitance and conductance had stabilized; this required several days. The dielectric measurements on phase II were then made using the procedure described in Section 5.3.

The capacitance and conductance data for each phase were converted to dielectric constants and losses using the cell constant which had been determined before loading the cell. Since the capacitance of the empty cell at 10°C was found to be within 0.05% of its value at 35°C, the cell constant was assumed to be independent of temperature. The cell constant was stable with time because, after measurements on phase I using sample 2 were completed at four temperatures, the measurements at the first temperature were repeated and found to be unchanged. The error introduced by slight variations in the cell constant with temperature was thus estimated to be no greater than 0.10%. Methods for calculating the pressure dependence of the cell constant are discussed in Section 5.5. There was some evidence that the I - II transition in phenol could cause slight changes in the cell constant. This is discussed in Sections 5.2 and 5.3 where the results obtained of phenol I and II are presented.

5.2 The Dielectric Constants of Phenol I as a Function of Temperature and Pressure

Values of the dielectric constants of phenol I at several frequencies, uncorrected for the pressure dependence of the cell constant, were obtained for increasing and decreasing pressures at various constant temperatures, as discussed in Section 5.1, using three zone refined samples of phenol. From the frequency dependence of ε', the dielectric constants measured at 50 kHz were generally found to be free of space charge polarization* (Section 1.3a) and these values are listed in Table 22 for each

---

* See p.159 for a detailed discussion.

Table 22. Dielectric constants of phenol I at 50 kHz, uncorrected for the distortion of the pressure vessel, at various temperatures and apparent pressures.

Sample #1

Temperature=6.5°C

Increasing Pressure			Decreasing Pressure		
P(bar)	ε'(exp)	ε'(smooth)[a]	P(bar)	ε'(exp)	ε'(smooth)
500	-	2.8878	800	-	2.9273
951	2.9021	2.9013	683	2.9214	2.9217
1082	2.9054	2.9053	532	2.9141	2.9141
1218	2.9091	2.9093	418	2.9072	2.9077
1358	2.9132	2.9134	270	2.8990	2.8992
1503	2.9179	2.9179	131	2.8910	2.8909
1640	2.9217	2.9218			
1762	2.9252	2.9254			

Temperature=24.5°C

Increasing Pressure			Decreasing Pressure		
P(bar)	ε'(exp)	ε'(smooth)	P(bar)	ε'(exp)	ε'(smooth)
700	-	2.8900	1100	-	2.9281
945	2.8984	2.8982	976	2.9232	2.9233
1067	2.9021	2.9023	857	2.9184	2.9186
1210	2.9068	2.9070	689	2.9112	2.9113
1344	2.9117	2.9117	564	2.9049	2.9053
1494	2.9168	2.9166	407	2.8966	2.8969
1623	2.9209	2.9209	288	2.8910	2.8907
1768	2.9257	2.9259			

Temperature=35.0°C

Increasing Pressure			Decreasing Pressure		
P(bar)	ε'(exp)	ε'(smooth)	P(bar)	ε'(exp)	ε'(smooth)
820	2.9043*	2.9019	1100	-	2.9327
936	2.9075*	2.9058	965	2.9274	2.9274
1076	2.9110*	2.9103	826	2.9221	2.9220
1230	2.9154	2.9154	703	2.9170	2.9170
1361	2.9196	2.9197	558	2.9120*	2.9118
1500	2.9241	2.9241	381	2.9056*	2.9043
1631	2.9281	2.9282			
1762	2.9325	2.9325			

Temperature=10.0°C[b]

Increasing Pressure			Decreasing Pressure		
P(bar)	ε'(exp)	ε'(smooth)	P(bar)	ε'(exp)	ε'(smooth)
600	-	2.8854	950	-	2.9225
908	2.8941	2.8942	834	2.9179	2.9184
1053	2.8984	2.8982	689	2.9128	2.9129
1181	2.9021	2.9019	547	2.9065	2.9067
1361	2.9071	2.9073	407	2.9002	2.9002
1500	2.9116	2.9115	270	2.8933	2.8934
1628	2.9153	2.9153	137	2.8867	2.8867
1773	2.9199	2.9200			

Sample #2

Temperature=34.9°C

Increasing Pressure			Decreasing Pressure		
P(bar)	ε'(exp)	ε'(smooth)	P(bar)	ε'(exp)	ε'(smooth)
350	-	2.8996	1250	-	2.9414
555	2.9049	2.9050	1139	2.9372	2.9370
703	2.9089	2.9078	1022	2.9320	2.9323
882	2.9140	2.9134	888	2.9271	2.9271
996	2.9167	2.9164	783	2.9226	2.9227
1164	2.9205	2.9208	640	2.9173	2.9170
1329	2.9253	2.9250	495	2.9111	2.9111
1463	2.9275	2.9283	339	2.9051	2.9049
1597	2.9318	2.9318	205	2.9003*	2.8994
1759	2.9362	2.9361			

Temperature=25.0°C

Increasing Pressure

P(bar)	ε'(exp)	ε'(smooth)
300	-	2.8902
535	2.8972	2.8967
655	2.9007	2.9003
806	2.9047	2.9045
954	2.9086	2.9087
1084	2.9124	2.9126
1224	2.9164	2.9166
1369	2.9208	2.9208
1511	2.9249	2.9248
1668	2.9292	2.9293
1799	2.9329	2.9330

Decreasing Pressure

P(bar)	ε'(exp)	ε'(smooth)
1050	-	2.9337
939	2.9291	2.9293
797	2.9229	2.9233
666	2.9173	2.9175
538	2.9114	2.9114
453	2.9058	2.9073
319	2.9004	2.9008
208	2.8952	2.8952

Temperature=10.0°C

Increasing Pressure

P(bar)	ε'(exp)	ε'(smooth)
400	-	2.8896
495	2.8936	2.8922
663	2.8970	2.8966
823	2.9007	2.9008
959	2.9044	2.9043
1096	2.9079	2.9078
1221	2.9109	2.9111
1366	2.9148	2.9149
1506	2.9187	2.9185
1640	2.9221	2.9219
1785	2.9256	2.9256

Decreasing Pressure

P(bar)	ε'(exp)	ε'(smooth)
1000	-	2.9286
831	2.9222	2.9228
695	2.9181	2.9182
552	2.9125	2.9125
399	2.9057	2.9057
270	2.8996	2.8993
151	2.8926	2.8925

Temperature=-0.3°C

Increasing Pressure

P(bar)	ε'(exp)	ε'(smooth)
500	-	2.8942
780	2.9013	2.9004
959	2.9047	2.9044
1110	2.9078	2.9079
1235	2.9108	2.9108
1383	2.9140	2.9141
1500	2.9167	2.9167
1640	2.9195	2.9199
1764	2.9229	2.9227

Decreasing Pressure

P(bar)	ε'(exp)	ε'(smooth)
900	-	2.9260
754	2.9205	2.9215
606	2.9171	2.9166
552	2.9140	2.9146
450	2.9111	2.9105
407	2.9085	2.9088
302	2.9050	2.9044
282	2.9031	2.9035
145	2.8967	2.8972

Sample #3

Temperature=20.2°C

Increasing Pressure

P(bar)	ε'(exp)	ε'(smooth)
300	-	2.8979
470	2.9032	2.9032
629	2.9082	2.9081
786	2.9130	2.9129
917	2.9171	2.9170
1062	2.9212	2.9214
1215	2.9262	2.9262
1375	2.9312	2.9311
1511	2.9352	2.9352
1637	2.9391	2.9391
1759	2.9427	2.9429

Decreasing Pressure

P(bar)	ε'(exp)	ε'(smooth)
979	2.9413	2.9450
854	2.9371	2.9392
714	2.9323	2.9326
566	2.9253	2.9252
455	2.9185	2.9190
305	2.9098	2.9098
139	2.8992	2.8991

Temperature=10.1°C

Increasing Pressure

P(bar)	ε'(exp)	ε'(smooth)
500	-	2.9031
677	2.9096	2.9082
808	2.9130	2.9123
954	2.9166	2.9165
1093	2.9206	2.9206
1235	2.9247	2.9247
1381	2.9290	2.9289
1503	2.9324	2.9325

Decreasing Pressure

P(bar)	ε'(exp)	ε'(smooth)
950	-	2.9435
860	2.9366	2.9400
720	2.9327	2.9343
589	2.9279	2.9286
447	2.9216	2.9214
322	2.9148	2.9146
165	2.9044	2.9044
817	2.9372	2.9382

Temperature=-0.7°C

Increasing Pressure

P(bar)	ε'(exp)	ε'(smooth)
400	-	2.9059
672	2.9123	2.9119
808	2.9150	2.9150
939	2.9180	2.9179
1102	2.9217	2.9216
1233	2.9247	2.9246
1375	2.9280	2.9282
1506	2.9314	2.9314
1640	2.9346	2.9348

Decreasing Pressure

P(bar)	ε'(exp)	ε'(smooth)
800	-	2.9400
680	2.9334	2.9355
552	2.9296	2.9299
404	2.9231	2.9229
276	2.9160	2.9160
134	2.9078	2.9077

Temperature=-10.2°C

Increasing Pressure			Decreasing Pressure		
P(bar)	ε'(exp)	ε'(smooth)	P(bar)	ε'(exp)	ε'(smooth)
500	-	2.9097	700	-	2.9402
791	2.9174	2.9160	555	2.9310	2.9337
948	2.9197	2.9195	396	2.9256	2.9260
1102	2.9229	2.9229	304	2.9213	2.9213
1224	2.9256	2.9256	134	2.9139	2.9139
1369	2.9284	2.9288			
1492	2.9316	2.9313			
1614	2.9341	2.9340			
1745	2.9367	2.9369			

[a] Values of ε' read from the smooth curves drawn through the experimental values of ε'.

[b] These readings were taken after passing the sample through the I-II and II-I transitions. The cell constant is believed to have been slightly altered during the transition.

[*] These values were clearly too high due to electrode polarization.

sample at all the temperatures at which measurements were made. The measurements on sample 1 at 10°C were made after the sample had undergone the I → II and II → I transitions, whereas the measurements at other temperatures were made before any transitions took place. The dielectric constants at 10°C in sample 1 were lower than those at 6.5°C and 24.5°C (Table 22) and, since there was no evidence of electrode polarization in these three results, it was concluded that the cell constant had changed slightly during the phase transitions. On the assumption that the dielectric constants at 750 bar vary linearly with temperature, the values of ε' obtained at 10°C were multiplied by 1.00183 to correct for the change in the cell constant at that temperature. Also, in samples 1 and 2, the frequency dependence of ε' clearly indicated that the 50 kHz values of ε' at high temperatures and low pressures were affected by space-charge polarization. In Table 22, the affected points are marked with asterisks.

To illustrate the results in Table 22, the dielectric constants at 10°C for the three samples are plotted in Figure 20 against the apparent pressure. The results in both the figure and the table are not corrected for the pressure dependence of the cell constant, and points taken immediately after altering the direction of pressure change which were far removed from the compression

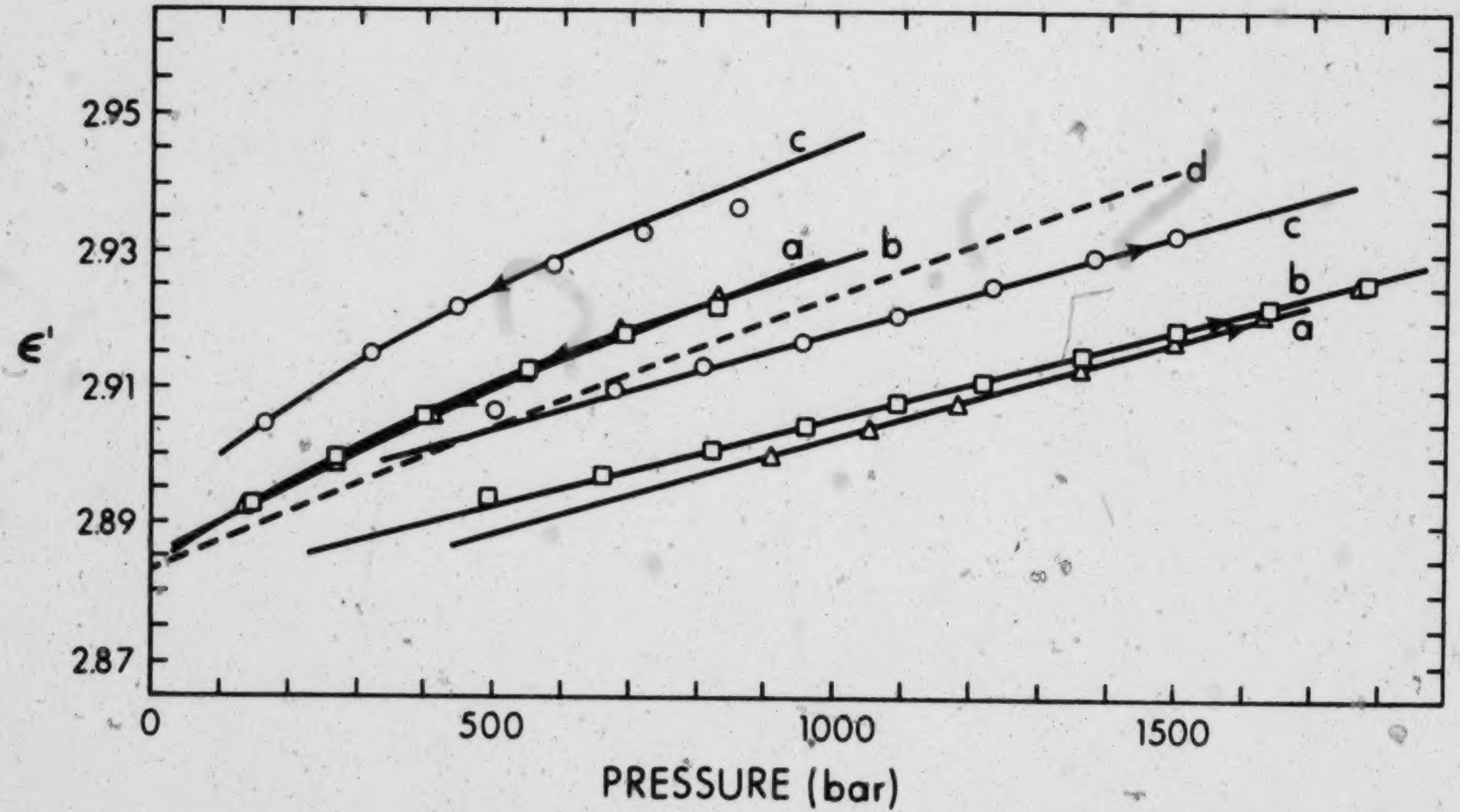

Figure 20. The dielectric constants of phenol I at 50 kHz and 10°C as a function of the apparent pressure. The symbols Δ, □, O denote results obtained from samples 1, 2, and 3. respectively and lines a, b, and c are the smoothed curves drawn through these points. The arrows show the direction of the pressure change. Curve d is the mean for the three samples, equation [5.1], corrected for hysteresis and the pressure dependence of the cell constant.

and decompression curves are not included. Smooth curves, such as a, b, and c in Figure 20, were drawn through the data points that were obviously on the compression and decompression curves, and readings taken from these fitted curves are included in Table 22.

The apparent pressures at which the same value of the uncorrected dielectric constant occurred on the smoothed compression and decompression curves were then averaged to minimize hysteresis effects (Section 1.4b). These dielectric constants were then corrected for the change in the cell constant with pressure by multiplying them by the factor C_p/C_o, the ratio of the cell constant at pressure P to that at ambient pressure, derived and given in Section 5.5. The averaged pressures were corrected for the expansion of the bore of the dielectric cell under pressure using equation [3.1] and assuming a value of 0.75 for the expansion constant, f. The expansion constant was set to 0.75 because the ratio of the sample length to diameter was 2.8 in the coaxial cell, compared to 0.5 in the compression cell for which f=0.38. A deviation of ±0.25 in f would cause errors of only 0.1% and 0.08% in the pressure and cell constant at 3 kbar respectively. The resulting, corrected values of the dielectric constants as a function of pressure were fitted to quadratic equations in pressure by the method of least squares. This reduced the experimental results in Table 22 to twelve quadratic equations, one for each of the four temperatures at which measurements were made on each sample. These equations are listed in Table 23 along with the pressure range over which the data extended, the number of data points used in each least squares fit, and the standard and maximum deviations for each fit. The standard and maximum deviations were all less than 0.0001 and 0.0002, respectively, and the deviations were random, so the fitting procedure introduced no significant error into the results.

The dielectric constants obtained at 10°C can be used with the known compressions of phenol at that temperature (Section 3.4) to determine the molar polarization of phenol I as a function of pressure. Values of ε' at 50 kHz and 10°C, calculated from the equations in Table 23, are listed in Table 24 at several pressures. The mean of the three expressions in Table 23 for ε' at 10 ± 0.1°C is

$$\varepsilon' = 2.8824 + 4.4278 \times 10^{-5} P - 2.9302 \times 10^{-9} P^2 \quad [5.1]$$

where P is the pressure in bar. Values calculated from this expression are included in Table 24 along with the standard deviations of the values of ε' about this mean at each pressure. The standard deviations range from 0.0064 at P = 0 to 0.0088 at P = 1500 and correspond to a precision of about 0.3%. The ratios of the measured values of ε' for each sample in Table 24 to those of the mean

Table 23. The dielectric constant of phenol I at 50 kHz as a function of pressure for various temperatures.

	T(°C)	Dielectric Constant[a], ε'	Highest & lowest pressures used (bar)	No. of points	10⁴ x Deviation Standard	10⁴ x Deviation Maximum
Sample 1	6.5	$2.8758 + 4.5862\text{x}10^{-5}P - 1.7431\text{x}10^{-9}P^2$	344, 1248	8	0.5	0.6
	24.5	$2.8685 + 4.9873\text{x}10^{-5}P - 3.4037\text{x}10^{-9}P^2$	485, 1519	9	1.1	1.3
	35.0	$2.8809 + 4.1352\text{x}10^{-5}P - 6.8752\text{x}10^{-10}P^2$	518, 1498	8	0.5	0.8
	10.0	$2.8773 + 4.2181\text{x}10^{-5}P - 1.2020\text{x}10^{-9}P^2$	346, 1322	8	0.7	0.8
Sample 2	34.9	$2.8909 + 3.5462\text{x}10^{-5}P + 1.7092\text{x}10^{-10}P^2$	290, 1400	8	0.2	0.4
	25.0	$2.8823 + 4.2153\text{x}10^{-5}P - 1.4414\text{x}10^{-9}P^2$	337, 1324	8	0.6	0.6
	10.0	$2.8803 + 4.2720\text{x}10^{-5}P - 3.5512\text{x}10^{-9}P^2$	260, 1324	8	0.4	0.5
	-0.3	$2.8848 + 3.6878\text{x}10^{-5}P - 2.3062\text{x}10^{-9}P^2$	318, 1362	7	0.6	0.9
Sample 3	20.2	$2.8889 + 4.7756\text{x}10^{-5}P - 2.4621\text{x}10^{-9}P^2$	140, 1399	11	1.0	1.7
	10.1	$2.8896 + 4.7935\text{x}10^{-5}P - 4.0375\text{x}10^{-9}P^2$	242, 1312	9	0.3	0.4
	-0.7	$2.8976 + 3.6906\text{x}10^{-5}P - 3.6226\text{x}10^{-10}P^2$	228, 1156	7	0.1	0.2
	-10.2	$2.9002 + 3.6662\text{x}10^{-5}P - 1.1885\text{x}10^{-9}P^2$	306, 1288	7	0.4	0.5

[a] P is the pressure in bar.

Table 24. The Dielectric Constants of Phenol I at 10°C and 50 kHz.

	ε'				
P(bar)	Sample #1	Sample #2	Sample #3	Average	Std. Dev.
0	2.8773	2.8803	2.8896	2.8824	0.0064
250	2.8878	2.8908	2.9013	2.8933	0.0071
500	2.8981	2.9008	2.9126	2.9038	0.0077
750	2.9083	2.9103	2.9233	2.9140	0.0081
1000	2.9183	2.9195	2.9335	2.9238	0.0085
1250	2.9281	2.9282	2.9432	2.9332	0.0087
1500	2.9379	2.9364	2.9524	2.9422	0.0088

are constant to within 0.15%. This suggests that the discrepancy between measurements on different samples is largely due to slight changes in the cell constants caused by the initial compacting of the samples. Equation [5.1] is represented by curve d in Figure 20.

Table 25 lists values of the molar polarization, $\overline{P}$, calculated from the results in Table 24 using the Clausius-Mossotti equation (Section 1.2a). The molecular weight was taken to be 94.11 and the densities were calculated using the volume compressions listed in Table 15 and the relationship

$$d = 1.132/(1 + \frac{\Delta V}{V_o}) \qquad [5.2]$$

where, as in Section 3.1, the density of phenol I at atmospheric pressure and 10°C was assumed to be the same as that at 25°C, 1.132 g/cm^3 (70). At atmospheric pressure and 50 kHz, the molar polarization is 32.05 ± 0.10 cm^3 and is the sum of the electronic and atomic polarizations, i.e. $\overline{P} = \overline{P}_e + \overline{P}_a$ (Section 1.2a), if there is no contribution from dipolar reorientation. $\overline{P}_e$ is calculated in Section 5.6 to be 26.91 ± 0.30 cm^3 and so $\overline{P}_a$, the atomic polarization, is 5.14 ± 0.40 cm^3 at 10°C and one atmosphere, assuming that there is no contribution to the polarization from orientational relaxation.

To investigate whether orientational relaxation was present, the frequency dependence of ϵ' and ϵ'' was

Table 25. The Molar Polarization of Phenol I at 10°C.

		Molar Polarization, $\overline{P}(cm^3)$					
Pressure (bar)	$1 + \frac{\Delta V}{V_o}$	Sample #1	Sample #2	Sample #3	Average	Std. Dev.	Maximum[a] Possible Value
0	1.000	32.00	32.03	32.13	32.05	0.06	32.14
500	0.9888	31.86	31.88	32.02	31.92	0.09	32.03
1000	0.9791	31.75	31.76	31.90	31.80	0.08	31.93
1500	0.9707	31.67	31.66	31.81	31.71	0.08	31.86

[a] Calculated using the error limit in the compression and in the dielectric constant which would tend to minimize the drift of $\overline{P}$ with pressure.

subsequently measured over a range of 100 Hz to 100 kHz at temperatures ranging from -70°C to +40°C, and in no case was there any dispersion or loss which could be attributed to dielectric relaxation. This observation, coupled with the fact that the value 5.14 cm^3 is not abnormally large for $\overline{P}_a$ (143,144), makes it highly unlikely that any dielectric relaxation occurs to high frequency of these measurements. It is possible that dielectric relaxation does occur at frequencies less than 100 Hz at 35°C. Such a relaxation would be slower than that in ice I, extrapolated to 35°C (39), by a factor of 10^4 and, since relaxation in other phases of ice and in the clathrate hydrates is faster than that in ice (145,146), any relaxation involving a significant degree of dynamic migration of Bjerrum defects (3) along the hydrogen bonded chains in phenol is unlikely. Since it is difficult to imagine any other mechanism for dynamic disorder in phenol I, the crystal is very probably orientationally ordered or statically disordered.

It is necessary to determine whether the decrease in molar polarization with pressure in Table 25 is real or whether the error limits are so large that it could be constant. The obvious uncertainties are the ±5% error limits in $-\Delta V/V_o$, an uncertainty of ±0.005 pf in the lead capacitance (Section 2.4a), and the assumption of 75% of ideal expansion of the bore. The last column in Table 25 lists values of the molar polarization, $\overline{P}$, calculated using the limits of these uncertainties which tend to minimize the drift of $\overline{P}$ with pressure. These values clearly show that the decrease of $\overline{P}$ with increasing pressures is real.

The observed decrease in polarization is undoubtedly due to a combination of the effect of pressure on the molecular polarizability, $\alpha_a + \alpha_e$ (20), and density dependent deviations from the Lorentz expression for the local field (Section 1.2a) which are almost certainly present in phenol I and which result from a breakdown in the assumption that the field due to neighbouring molecules is zero. As discussed in Section 1.2a, this assumption is invalid even for cubic solids where the average of such a field is zero. In the case of phenol I, it is very likely that both the average and instantaneous fields are non-zero, and hence an increase in density would almost surely affect the local field (18,147). Decreases in both α_a and α_e with increasing pressure have been reported for solids (20), but it is not possible to determine how much each changes without knowing the pressure dependence of the infinite wavelength refractive index, n_∞ (Section 5.6).

The expressions for the pressure dependence of the dielectric constant at 50 kHz and various temperatures given in Table 23 may be used to determine the isobaric temperature dependence of the dielectric constant of phenol I in the following way. The small differences between the values of the dielectric constants at 10°C were shown earlier to be largely due to slight errors in the value of the cell constant used for each sample. To correct for these errors, adjusted dielectric constant isotherms were determined by multiplying the equations in Table 23 by a factor, constant for all temperatures of a given sample, such that the dielectric constant of phenol I at 10°C and 750 bar equals that of the mean, 2.9140. Such corrections essentially adjust the cell constant of each of the three samples so that they give the same value of the dielectric constant at 10°C and 750 bar. The most accurate value of the dielectric constant was considered to be that at 750 bar since it is near the center of the hysteresis loop. From the dielectric constants in Table 24, the multiplication factors are 1.00196, 1.00127, and 0.99682 for samples 1, 2, and 3 respectively. The adjusted values of dielectric constant at 0, 500, 1000, and 1500 bar are plotted in Figure 21 and listed in Table 26.

The points in Figure 21 and Table 26 which correspond to measurements at 35°C on sample 1 and 25.0°C and 34.9°C on sample 2, deviate significantly from the general trend in a way which is entirely consistent with the onset of electrode polarization as the samples approach the

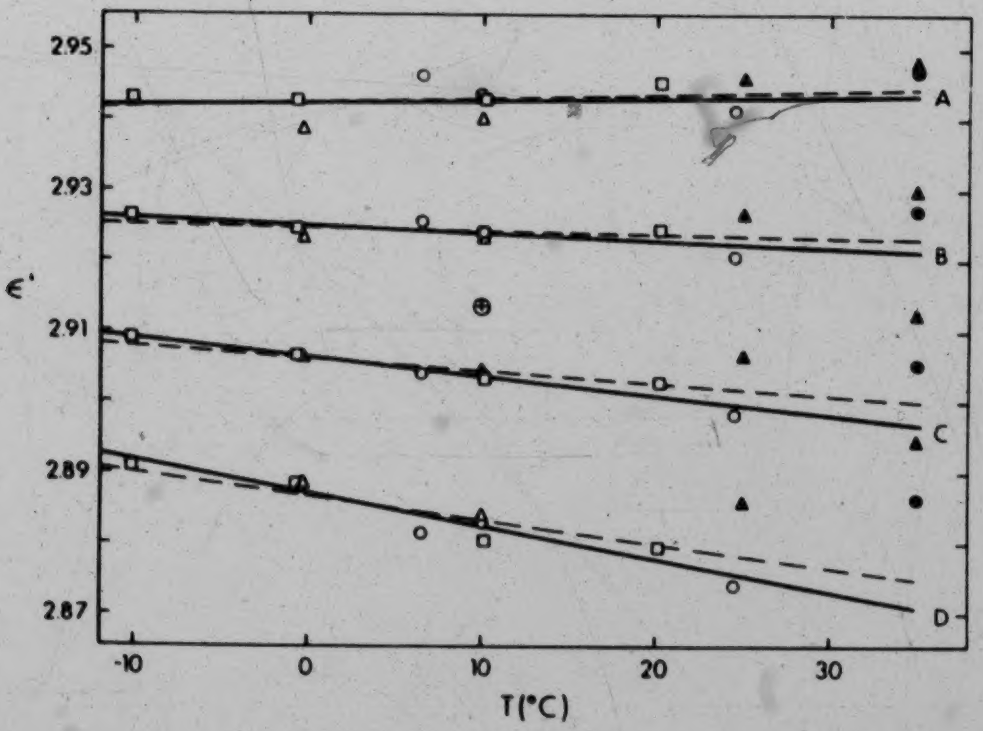

Figure 21. The dielectric constants of phenol I at 50 kHz, after adjusting the cell constants. The symbol ● indicates the value at 10°C and 750 bar at which the results from the three samples were forced to coincide. The symbols O, Δ, ◻ indicate the values obtained from samples 1, 2, and 3 respectively. The solid and dashed lines indicate isobars given in Table 27 as Fit II and Fit I, respectively: A, 1500 bar; B, 1000 bar; C, 500 bar; D, 0 bar.

Table 26. Dielectric constants at 50kHz for phenol I, adjusted for errors in the cell constants for each sample.

	T(°C)	ε'			
		P = 0 bar	P = 500 bar	P = 1000 bar	P = 1500 bar
Sample 1	6.5	2.8814	2.9040	2.9256	2.9465
	24.5	2.8741	2.8983	2.9207	2.9415
	35.0	2.8865	2.9056	2.9273	2.9472
	10.0	2.8831	2.9038	2.9240	2.9437
Sample 2	34.9	2.8945	2.9123	2.9301	2.9482
	25.0	2.8859	2.9066	2.9266	2.9459
	10.0	2.8839	2.9044	2.9231	2.9400
	-0.3	2.8884	2.9063	2.9230	2.9385
Sample 3	20.2	2.8797	2.9029	2.9248	2.9456
	10.1	2.8804	2.9033	2.9241	2.9430
	-0.7	2.8884	2.9067	2.9247	2.9427
	-10.2	2.8910	2.9089	2.9263	2.9431

melting point. Since the presence of electrode polarization is indicated by an increase in ε' with decreasing frequency, it is essential to determine whether the inaccuracy of the bridge at high frequencies (Section 2.4) affects the apparent dielectric constants of materials in which no electrode polarization is present. In fact, the values of ε' obtained from phenol at low temperatures and values obtained for liquid carbon tetrachloride and cyclohexane (Section 2.5a) showed a decrease in ε' of 0.0040± 0.002 as the frequency was raised from 20 kHz to 50 kHz in spite of the fact that no electrode polarization was present in these samples. The absence of electrode polarization was shown by the constant values of ε' between 1 kHz and 10 kHz. The decrease in ε' between 20 kHz and 50 kHz is undoubtedly due to the inaccuracy of the bridge above 10 kHz. It did not have a serious effect on the accuracy of the measurements, but it does suggest that a decrease in ε' of less than 0.0042 between 20 kHz and 50 kHz does not indicate electrode polarization. The 35.0°C and 34.9°C measurements in Table 26 revealed a discrepancy of 0.0080 and 0.0055 between the 50kHz and 20 kHz values of ε' and it must therefore be concluded that electrode polarization was present in both cases. Since the deviation between the 50 kHz and 20 kHz values of ε' from the 25.0°C run was only 0.0042 there is no proof that electrode polarization affected this measurement. Unfortunately no data below 10 kHz was obtained for sample 2 at 25°C.

The data listed in Table 26 for each pressure were fitted to linear equations in temperature by the method of least squares using all the data points below 30°C. These isobars are shown by the broken lines in Figure 21 and are listed as Fit I in Table 27 along with their standard deviations. Because the values of ε' at 25.0°C do deviate significantly from the general trend, the least squares fits of the isobaric data were repeated without using these points. The resulting isobars are listed as Fit II in Table 27 and are shown by the solid lines in Figure 21.

In the original experimental data (Table 22), the width of the hysteresis below 10°C is so great that the values of ε' at 1500 and 1000 bar in Figure 21 are rather uncertain at these temperatures. Further, the standard deviations of the isobaric curve fits for these pressures are of the same order as the difference between ε' at -10°C and +35°C. Therefore the slopes of the 1000 and 1500 bar isobars listed in Table 27 are quite unreliable. The data below 1000 bar is more reliable and shows a greater temperature dependence (Figure 21). The slopes of these isobars are, therefore, better defined, but are subject to the 30% uncertainty arising from the existence of the

Table 27. The dielectric constant of phenol I at 50 kHz as a function of temperature for several pressures.

Fit I[a]

Pressure (bar)	Dielectric Constant[b], ε'	Standard Deviation
0	$2.8868 - 3.276 \times 10^{-4}$ T	0.0035
500	$2.9062 - 1.732 \times 10^{-4}$ T	0.0022
1000	$2.9247 - 4.119 \times 10^{-5}$ T	0.0018
1500	$2.9424 + 7.116 \times 10^{-5}$ T	0.0026

Fit II[c]

Pressure (bar)	Dielectric Constant[a], ε'	Standard Deviation
0	$2.8870 - 4.663 \times 10^{-4}$ T	0.0018
500	$2.9063 - 2.631 \times 10^{-4}$ T	0.0010
1000	$2.9248 - 9.687 \times 10^{-5}$ T	0.0014
1500	$2.9424 + 3.814 \times 10^{-5}$ T	0.0026

[a] Calculated from all of the data below 30°C.

[b] T is the temperature (°C).

[c] Calculated from all of the data below 24.9°C.

two fits.

It is interesting to qualitatively compare the results in Figure 21 to the 0 bar isobar reported by Smyth and Hitchcock (88) and to data obtained in this laboratory by cooling and warming a sample of phenol at a constant pressure of 1 kbar in the coaxial cell. The three sets of results are shown in Figure 22. Curve A in the figure corresponds to Smyth's results, while curves B and D are the 1.0 kbar and 0 bar isobars, respectively, previously depicted in Figure 21. The data obtained by cooling and warming the phenol sample at 1 kbar is depicted by curve XYZ. This sample had been taken through the I → II and II → I transitions prior to taking these measurements, so the cell constant may have changed somewhat during the transition. On the assumption that the cell constant had changed, the original data were multiplied by the factor 0.9856 to bring the point at 10°C into agreement with curve B.

The increase in dielectric constant with decreasing temperature shown by lines B and D is the behavior expected, except in the rare cases where the temperature dependence of the polarization is unusually large and positive. The exponential decrease in Smyth's values of ϵ' with temperature undoubtedly arises from cracks in his samples, a problem inherent in the technique he used

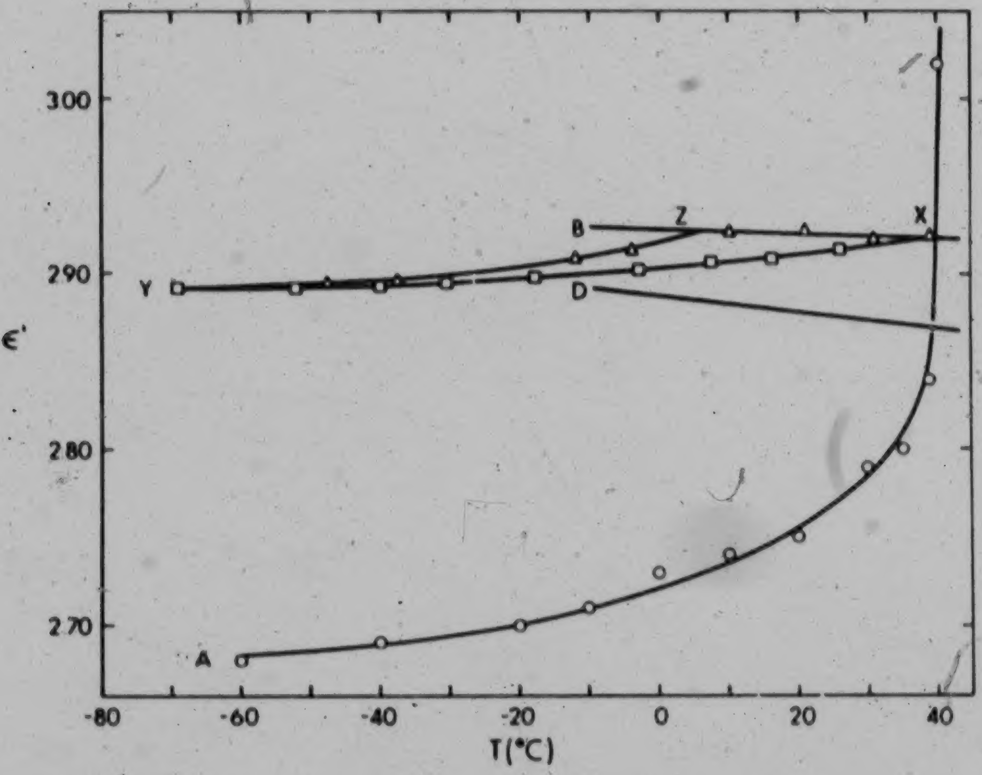

Figure 22. Dielectric constant isobars for phenol I obtained by different methods. Curve A represents the cooling curve of Smyth and Hitchcock at 0 bar. Curves XY and YZX represent cooling and warming curves, respectively, obtained in the coaxial cell at 1 kbar. Lines B and D are the 1.0 kbar and 0 kbar isobars taken from Figure 21.

(88), and from the influence of electrode polarization. In support of this latter point, his values of ε' increase rapidly with decreasing frequency above 35°C. With reference to the 1.0 kbar cooling curve of phenol (XYZ in Figure 22), cracks appear to have formed as the sample was cooled from X to Y because ε' decreased. The sample must have compacted to some degree at the lower temperatures however since, after reaching point Z, the warming curve follows the 1.0 kbar isobar rather closely. The appearance of cracks under an applied pressure as high as 1 kbar is particularly noteworthy because phenol I is usually regarded as a relatively plastic phase.

It is clear from the above results, that the technique of determining the temperature dependence of the isobaric dielectric constant of a solid in a coaxial cell by cooling and warming the sample at constant pressure is an unreliable one. Chan and Chew (22,136) have had some success using this technique on cyclohexane and neopentane, but, because shearing of the sample is necessary to convert the uniaxial stress generated at the piston face to hydrostatic pressure, pressure gradients will be present in all but the most plastic substances. Because of these pressure gradients, the practice of simultaneous measurement of dielectric constant and sample volume in the same coaxial vessel (136) is particularly suspect. This technique does yield mean values of ε' at given values of mean sample density so long as no cracks are present but such values would scarcely be the isobaric ones in any sample of appreciable rigidity, since the pressure gradients must become much more severe at low temperatures. For this reason the method of determining the isothermal dielectric constant of a solid as a function of the average pressure between the compression and decompression curves at several temperatures, as discussed previously in this chapter, is preferred. Although it is more time consuming, the dielectric constant isobars obtained using this method are certainly more reliable, since failure to observe well defined compression and decompression curves clearly indicates the temperatures at which the pressure gradients are so severe as to render further measurements meaningless.

The temperature coefficients of the dielectric constant, $\left(\frac{\partial \varepsilon'}{\partial T}\right)_P$, at atmospheric pressure and 500 bar, are defined by the equations in Table 27. An uncertainty of about 30% in each coefficient is evident from the existence of two possible fits. Further evidence of their reliability can be obtained by using the Clausius-Mossotti equation (Section 1.2a) to calculate the isobaric thermal expansivity of phenol I at atmospheric pressure and at 500 bar. The thermal expansivity at pressure P is defined as

$$\alpha_P = \frac{1}{V_o}\left(\frac{\partial V}{\partial T}\right)_P \qquad [5.3]$$

where, in this case, V_o is the molar volume at atmospheric pressure and 10°C. α_P can readily be related to the dielectric constant, ε', using the Clausius-Mossotti equation, so that

$$\alpha_P = \frac{V_P}{V_o} \cdot \frac{-3}{(\varepsilon-1)(\varepsilon+2)}\left(\frac{\partial \varepsilon}{\partial T}\right)_P \qquad [5.4]$$

where V_P, ε, and $(\partial\varepsilon/\partial T)_P$ are the molar volume, dielectric constant and temperature coefficient of the dielectric constant at pressure P and, in this case, 10°C. This equation assumes that the molar polarization, $\bar{P}$, is independent of temperature. If this assumption is replaced by the more plausible one that the molar polarization, $\bar{P}$, is a function of density only, so that

$$\left(\frac{\partial \bar{P}}{\partial V}\right)_P = \left(\frac{\partial \bar{P}}{\partial V}\right)_T = \frac{1}{V_o}\left(\frac{\partial \bar{P}}{\partial (V/V_o)}\right)_T \qquad [5.5]$$

then the thermal expansivity at pressure P is given by

$$\alpha_P = \frac{\dfrac{V_P}{V_o} \cdot \dfrac{-3}{(\varepsilon-1)(\varepsilon+2)}\left(\dfrac{\partial \varepsilon}{\partial T}\right)_P}{1 - \dfrac{V_P}{V_o} \cdot \dfrac{1}{\bar{P}_P} \cdot \left(\dfrac{\partial \bar{P}}{\partial (V/V_o)}\right)_T} \qquad [5.6]$$

where $\bar{P}_P$ is the molar polarization at pressure P. The term $(\partial\bar{P}/\partial(V/V_o))_T$ was determined by fitting the average values of $\overline{P}$ in Table 25 to a linear function of V/V_o using the least squares method. The data was found to fit the expression

$$\overline{P}(\mathrm{cm}^3) = 20.30 + 11.75 \frac{V}{V_o} \qquad [5.7]$$

with a maximum deviation of 0.01 cm^3. Hence $(\partial P/\partial(V/V_o))$ at 10°C equals 11.75 cm^3 and is independent of pressure to within the precision of the data in Table 26. Values of α_P at 10°C, calculated using equations [5.4] and [5.6] are listed in Table 28. Values of $\overline{P}_p$ and V_p/V_o for the calculation were taken from Table 25, and values of ε' and $(\partial\varepsilon'/\partial T)_p$ were calculated from the expressions in Table 27.

The only known value of α_P for phenol I is the average value between -190°C and +20°C at atmospheric pressure deduced from the x-ray data in Section 4.5 to be $3 \pm 1 \times 10^{-4}$ $°C^{-1}$. The values in Table 28, calculated from equations [5.6] are consistent with this value and the values using Fit II are in better agreement with the x-ray results than those using Fit I. It should be pointed out that the mean expansivity from -190°C to +20°C probably underestimates the expansivity at 10°C since α_P usually increases with temperature (148).

The ratio of the expansivity at atmospheric pressure to that at 500 bar in Table 30 is 1.9 ± 0.1 no matter which fit or which method of calculating the expansivity

Table 28. Isobaric thermal expansivities of phenol I at 10°C.

	Thermal expansivity[a], α_P		
	Atmospheric Pressure	500 bar	α_o/α_{500}
Equation [5.4]			
Fit I[b]	$1.17\text{x}10^{-4}$	$5.6\text{x}10^{-5}$	2.0
Fit II[b]	$1.52\text{x}10^{-4}$	$8.4\text{x}10^{-5}$	1.8
Equation [5.6]			
Fit I[b]	$1.71\text{x}10^{-4}$	8.9x1-$^{-5}$	1.9
Fit II[b]	$2.43\text{x}10^{-4}$	$1.33\text{x}10^{-4}$	1.8

[a] Units are $(\text{deg.C})^{-1}$

[b] Refers to the two sets of expressions given in Table 27.

was used. The only data for molecular crystals in the literature with which to compare this result is the ratio 1.2 found by Chan and Chew (136) for cyclohexane I at 0°C. For solid xenon at about -150°C, Swenson (149) has found that the ratio of the expansivities at 0 and 1000 bars is about 1.4 and this ratio is about 1.5 to 1.8 for several organic liquids (150,151,152). The ratio for phenol I is larger than those found for these compounds. This may be because the thermal expansivities calculated here are based on rather poorly defined values of $(\partial\varepsilon'/\partial T)_P$ or it may be simply because the cited systems are very dissimilar to phenol I in structure. Considering the uncertainties involved, the expansivities listed in Table 28 using Fit II should probably only be regarded as being accurate to ±50%.

To summarize this section, a dielectric study of phenol I was carried out at temperatures from -70°C to +40°C over a pressure range of 0 to 1500 bar at frequencies from 100 Hz to 100 kHz. No dielectric relaxation was observed over this temperature and frequency range and it was concluded that dynamic orientational disorder is probably not present in phenol I. The dielectric constants and molar polarization were measured at 10°C and the polarization was observed to be a linear function of density to within the precision of the measurements. The atomic polarization at 10°C and atmospheric pressure was calculated. Dielectric constant isotherms were measured as a function of pressure from -10°C to +35°C and these were used to calculate the isobaric temperature dependence of the dielectric constant. This data, in turn, was used to calculate the thermal expansivities of phenol at 500 bars and atmospheric pressure to a rather low accuracy.

5.3 The Dielectric Constant and Molar Polarization of Phenol II at 10°C

Each of the three samples used to obtain the dielectric constants of phenol I in the coaxial cell (Section 5.2) was subsequently used to determine the dielectric constants of phenol II. As discussed in Section 5.4, the I → II transformation was invariably accompanied by a broad dispersion which, at 10°C, extended to frequencies higher than the range of the bridge, and whose magnitude decreased with time. This dispersion is apparently not an intrinsic property of phenol II (Section 5.4) and it was necessary to ensure that it was not present before the experimental dielectric constant at 50 kHz could be considered to be the intrinsic dielectric constant of phenol II. Since carrying out the I → II transformation slowly at warm temperatures had been found to minimize the magnitude of the dispersion (Section 5.4), the samples were taken through the transition over a period of several hours at temperatures near 38°C. The samples were then left at 38°C and 2000 bar until the dispersion had largely disappeared. This required three days for samples 1 and 3, and ten days for sample 2. The temperature was then lowered to 10°C and the dielectric constant and loss were measured as a function of frequency for increasing and decreasing pressures, changing the pressure by about 300 bar every 30 minutes and making the measurements 25 minutes later. The resulting values of ε' at 50 kHz are plotted in Figure 23 as a function of the applied pressure, with neitner ε' nor pressure corrected for deformation of the pressure vessel. If conditions were ideal, these values, after correction for deformation of the dielectric cell, would represent the static dielectric constants of phenol II, ε_o, however there are a number of complicating factors which are discussed below.

In spite of the precautions taken, some residual dispersion was present in each sample and it increased in magnitude as the run progressed. The magnitude of ε'' was, of course, frequency dependent but at 20 kHz ε'' increased from about 0.005 to 0.12 over the course of each run. The Cole-Cole plots of the dispersion region were similar to those shown in Section 5.4 except that there was evidence of slight D.C. conductance in samples 1 and 3. The difference in ε' between 50 kHz and 1 kHz was initially 0.025, 0.020, and 0.010 in samples 1, 2, and 3 respectively.

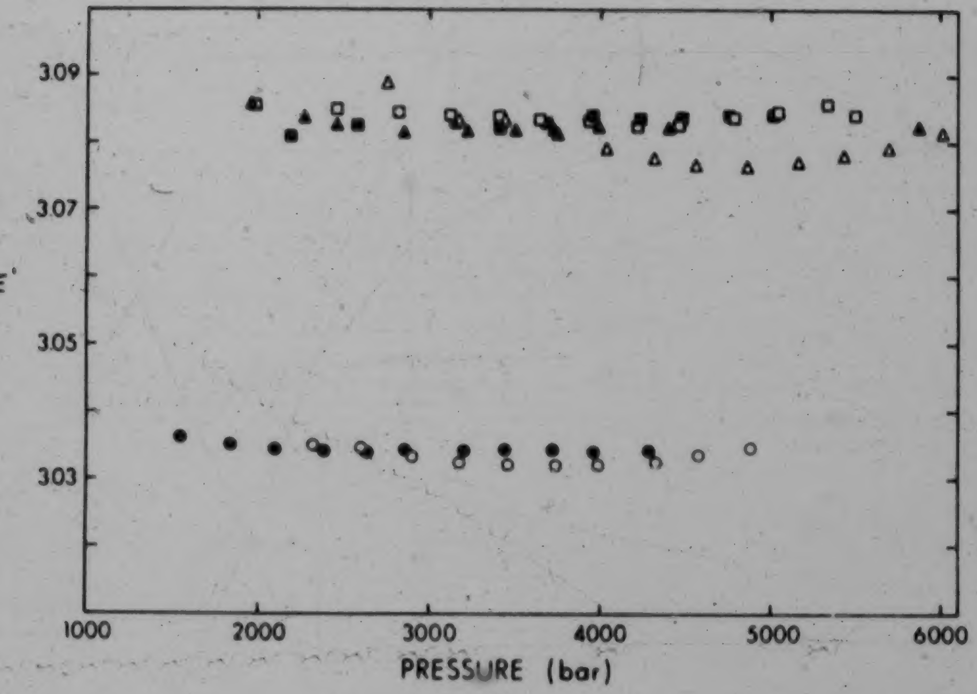

Figure 23. The apparent dielectric constants of phenol II at 10°C, measured in the coaxial cell at 50 kHz and plotted against the applied pressure. The circles, triangles and squares indicate measurements on samples 1, 2, and 3, respectively, and the open and solid symbols indicate measurements made while increasing and decreasing the pressure, respectively.

These values approximately doubled over the course of the run but did not vary consistently with either pressure or time. The dispersion effects did not show any consistent behavior and are not well understood (Section 5.4). They probably caused the observed values of ε' at 50 kHz to exceed the true static dielectric constant by about 0.01 to 0.05, excluding the effects of pressure gradients in the cell.

The lack of a pronounced pressure dependence of ε' in Figure 23 could indicate that the increase in ε' with pressure is just large enough to cancel the decrease in the cell constant caused by the pressure deformation of the dielectric cell compounds. The effect might also be caused by large pressure gradients in the cell and/or the formation of cracks in the samples. Since the data in Figure 23 do not show well defined hysteresis, it is impossible to calculate the internal pressure in the cell by averaging the apparent pressures at which given values of ε' occur and, hence, the data cannot be corrected for the pressure dependence of the cell constant. Whichever of the above effects is the cause of the pressure independence of the apparent dielectric constant, the most reliable data points are those at low pressures. If the values of ε' at 2000 bar in Figure 23 are assumed to be correct for that pressure, they may be corrected for the pressure dependence of the cell constant, using the methods given in Section 5.5 with the expansion coefficient set to 0.75 as in Section 5.2, to yield the values 3.044, 3.094 and 3.095 for the 50 kHz dielectric constants of samples 1, 2, and 3, respectively. Because of the uncertainty in the true pressure, and the evidence that the phase transition may have caused small changes in the cell constant (Section 5.2), it was necessary to determine the 2 kbar dielectric constants in a completely different apparatus to check the reliability of these results.

The parallel plate dielectric cell, shown in Figure 11b (Section 2.5b) can be used to measure absolute dielectric constants, provided that the distance between the plates is known. Pressure gradients in this type of cell should be minimal since only a small amount of shear is required to convert the uniaxial pressure at the face of the piston to hydrostatic pressure (Section 2.5). The capacitance of such a cell is given by the expression (153)

$$C' = \bar{\varepsilon}_o \, \varepsilon' \, \frac{A}{s} \qquad [5.8]$$

where s is the vertical distance between the plates (cm), ε' is the real dielectric constant of the sample, $\bar{\varepsilon}_o$ is the permittivity of free space (8.854×10^{-2} pf/cm), A is the area of the guarded plate (cm^2), and C' is the real capacitance (pf). To measure the static dielectric constant of phenol II, the parallel plate cell was loaded with about

5 g of sample. C' at 50kHz was then determined as a function of increasing and decreasing pressure for each phase at 10°C. The effects of hysteresis were minimized by the methods described later in this section to yield values of the capacitance at various averaged pressures.

The capacitance values were converted to dielectric constants in the following way. The plate area, A, was determined from its diameter to be 3.661 ± 0.003 cm^2 and was assumed to be independent of pressure. The sample volume at pressure P, V_P, is given by the expression

$$V_P = \pi r_P^2 s + k \qquad [5.9]$$

where r_P is the radius of the bore of the dielectric cell and s is the distance between the plates at pressure P, and k is the 'dead space' in the dielectric cell. The 'dead space' is the volume of the cell when the faces of the pistons are touching one another, i.e. when $s = 0$. k was assumed to be independent of pressure, and was determined from the dimensions of the cell to be 0.11068 ± 0.00010 cm^3. The radius of the bore at pressure P, r_P, was calculated from its value at atmospheric pressure using equation [3.1] with the expansion constant, f, set equal to the value used for the compression cell, 0.38, because the relative sample and cell dimensions were comparable in both cases. The amount of sample in the cell was determined by using the dielectric constant of phenol I at 10°C and 750 bar, ε'_{750}, which is 2.9140 (Table 24), to calculate s at that pressure through equation [5.8], and hence the volume at 750 bar, V_{750}, from equation [5.9]. The sample volume at any other pressure, V_P, can be calculated from the compression results in Section 3.4. The dielectric constant at pressure P, ε'_P, was then determined by manipulating equations [5.8] and [5.9] to yield

$$\varepsilon'_P = \varepsilon'_{750} \left(\frac{C'_P}{C'_{750}}\right)\left(\frac{V_P - k}{V_{750} - k}\right)\left(\frac{r^2_{750}}{r^2_P}\right) \qquad [5.10]$$

where C'_P is the capacitance at pressure P.

Two runs on zone refined phenol were made in the parallel plate cell at 10°C. Both samples were taken through the I → II transition over a period of several hours at 38°C, then left at 38°C and 2 kbar for several days to minimize the dispersion in phase II. Measurements on the first sample, hereafter designated sample 4 to avoid confusion with the three samples used in the coaxial cell, were made first on phase I, then on phase II, then again on phase I. The resulting capacitance values are plotted in Figure 24 against the applied pressure. The two sets of results for phase I in the figure agree to within 0.01 pf. The difference between them is believed to be caused by the extrusion of a small amount of sample, either into

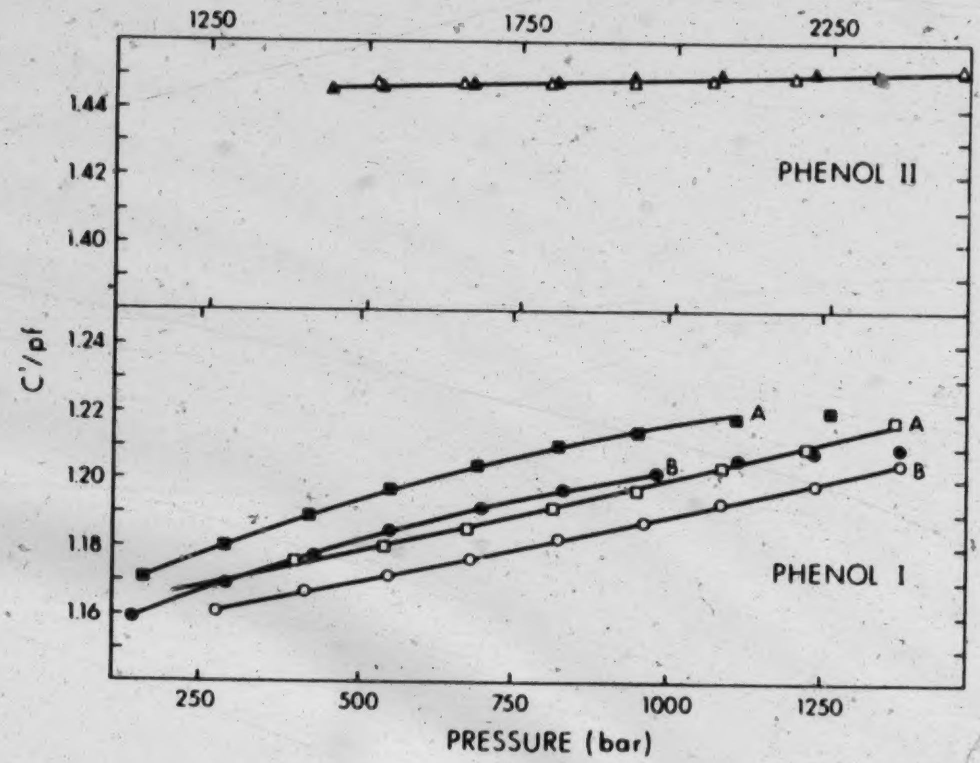

Figure 24. The capacitance at 50 kHz of the parallel plate dielectric cell containing sample 4 at 10°C, plotted against the applied pressure. The open and solid symbols indicate measurements made while increasing and decreasing the pressure, respectively. For phenol I the circles and squares, and the smoothed curves, B and A, drawn through them, indicate measurements made before and after, respectively, the measurements on phase II.

the interstices in the pistons, or past the triangular sealing rings. The extrusion most probably occurred during or after the I → II transition at 38° C, since the II→I transition was carried out at 10°C, where the sample would be less plastic. For this reason the second set of data on phase I, taken after the II → I transition, were used to calculate the dielectric constants of phenol II. Measurements on the second sample, sample 5, were made first on phase II, then on phase I, then again on phase II and are shown in Figure 25. In this case, the first set of results for phase II is considered to be the most compatible with those of phenol I, both because the high temperature of the I → II transition favoured extrusion and because significant dispersion was observed during the second run on phase II.

The magnitude of the dispersion in phase II was greater in sample 4 than in the first set of measurements on sample 5 and in both cases it did not vary by more than a few percent with either pressure or time over the course of the run. The value of C" at 20 kHz was about 0.002 pf for sample 4 and about 0.0007 pf for sample 5. From the values of ε' calculated later in this section, these values correspond to values of 0.0045 and 0.0016 respectively for ε'' at 20 kHz and, hence, the dispersion in samples 4 and 5 was lower than that observed in samples 1-3, for each of which ε'' varied from 0.005 to 0.012.

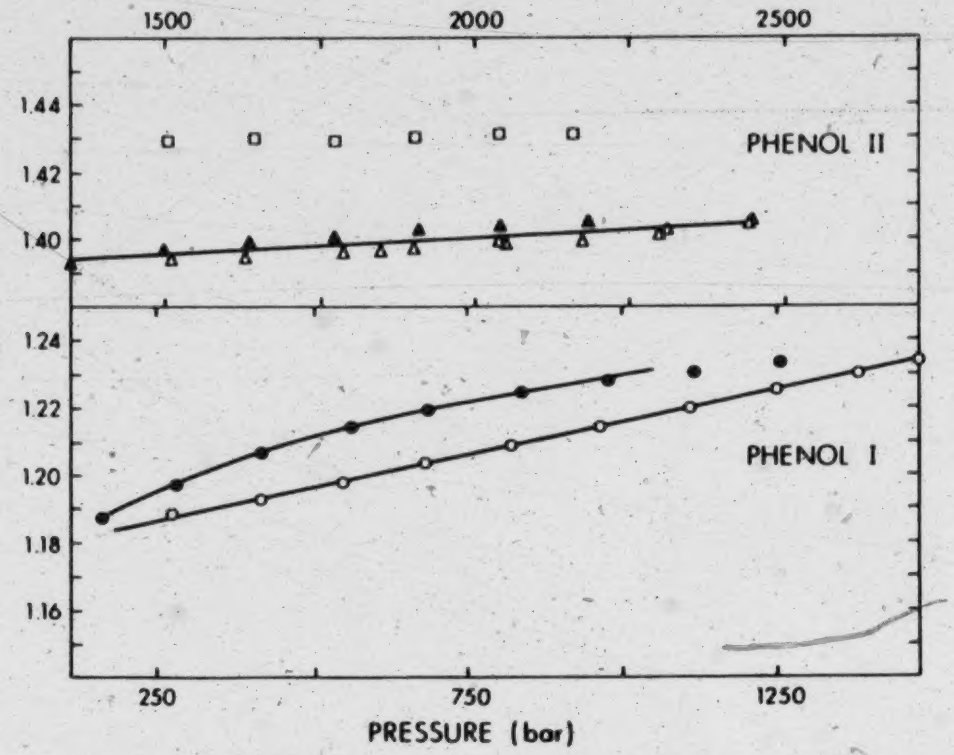

Figure 25. The capacitance at 50 kHz of the parallel plate dielectric cell containing sample 5 at 10°C, plotted against the applied pressure. The open and solid symbols denote measurements made while increasing and decreasing the pressure, respectively. For phenol II, the triangles and squares indicate measurements made before and after, respectively, those made on phenol I.

This observation is confirmed by the increase in C' between 50 kHz and 1 kHz, which was 0.0050 pf and 0.0033 pf respectively for samples 4 and 5. The corresponding increases in ϵ' are about 0.011 and 0.007 respectively, compared with 0.05 to 0.02 observed for samples 1 to 3.

The values of the capacitance which were clearly on the compression and decompression curves for phenol I in Figures 24 and 25 were fitted graphically to smooth curves, as described in Section 5.4 for runs using the coaxial cell. Table 29 lists the experimental values and the values read from the smoothed curves. The capacitance of phenol I was then calculated as a function of the averaged pressure, and was converted to the dielectric constant using the methods and equations described above. Values of the capacitance and dielectric constant are given in Table 30 for several average pressures, together with the squared ratio of the radius of the cell bore at pressure P to that at one atmosphere, $(r_P/r_O)^2$, and the volume, V_P, of the sample at pressure P, which were used in equations [5.8] to [5.10].

The results from sample 4 (Figure 24) do not show any clearly defined hysteresis in phase II and this is almost certainly because the pressure range was not great enough to take the sample from the true compression curve to the true decompression curve or vice versa (Section 1.4b). The results from sample 5 tend to support this hypothesis

Table 29. The capacitance at 50 kHz of the parallel plate dielectric cell containing samples 4 and 5 as phenol I at 10°C.

SAMPLE 4

Increasing Pressure			Decreasing Pressure		
Pressure (bar)	Capacitance (pf)		Pressure (bar)	Capacitance (pf)	
	Experimental	Fitted[a]		Experimental	Fitted[a]
392	1.1758	1.1750	1250	1.2206	-
535	1.1807	1.1807	1099	1.2185	1.2193
669	1.1860	1.1860	943	1.2143	1.2144
807	1.1915	1.1914	816	1.2100	1.2100
941	1.1969	1.1970	682	1.2046	1.2045
1078	1.2036	1.2036	545	1.1974	1.1976
1214	1.2100	1.2100	413	1.1894	1.1898
1358	1.2167	1.2168	278	1.1807	1.1807
1479	1.2221	1.2221	148	1.1703	1.1703

Table 29 (Continued)

SAMPLE 5

Increasing Pressure			Decreasing Pressure		
Pressure (bar)	Capacitance (pf)		Pressure (bar)	Capacitance (pf)	
	Experimental	Fitted[a]		Experimental	Fitted[a]
262	1.1885	1.1842	1245	1.2320	-
407	1.1923	1.1923	1104	1.2305	-
540	1.1977	1.1979	969	1.2283	1.2290
670	1.2033	1.2033	829	1.2248	1.2248
813	1.2088	1.2090	677	1.2192	1.2195
955	1.2145	1.2145	553	1.2142	1.2142
1099	1.2199	1.2200	407	1.2067	1.2064
1239	1.2253	1.2253	272	1.1972	1.1972
1372	1.2300	1.2301	138	1.1867	1.1868
1473	1.2339	1.2339			

[a] Values read from smooth curves drawn through the experimental points.

Table 30. The dielectric constants of phenol I and II at 10°C, measured in the parallel plate cell, and related data.

SAMPLE 4

	Pressure (bar)	Capacitance C' (pf)	r_P^2/r_o^2 [a]	Sample Volume V_P (cm^3)	ε'
Phase I	0	-	1.00000	5.22076	-
	250	1.1725	1.00013	5.19068	2.884
	500	1.1854	1.00025	5.16229	2.900
	750	1.1977	1.00038	5.13605	2.914
	1000	1.2093	1.00050	5.11165	2.928
Phase II	2000	1.4489	1.00101	4.66826	3.209

SAMPLE 5

	Pressure (bar)	Capacitance C' (pf)	$r_P/r_o\ ^2$	Sample Volume V_P (cm^3)	ε'
Phase I	0	-	1.00000	5.15135	-
	250	1.1892	1.00013	5.12147	2.886
	500	1.2025	1.00025	5.09369	2.901
	750	1.2142	1.00038	5.06776	2.914
	1000	1.2237	1.00050	5.0469	2.922
Phase II	2000	1.3998	1.00101	4.62592	3.058

[a] r and r_o are the radii of the cell bore at pressure P and at one atmosphere, respectively; r_o = 0.5605 in.

since, in this case, the pressure range used was 200 bar greater than that used for sample 4, and a slight hysteresis can be seen in Figure 25. The pressure range could not be extended further because the high pressure limit of the press had been reached. Because the hysteresis was not properly defined, it was impossible to calculate the pressure dependence of ε', but, since the pressure range was great enough to cause slight hysteresis effects to appear, the values of the pressure and average capacitance near the centre of the pressure range are probably reliable. Accordingly, the observed capacitance at 2000 bar was used to calculate the dielectric constant of phenol II for samples 4 and 5 using equations [5.8] to [5.10]. The experimental values of the capacitance are listed in Table 30, along with the parameters used, and the results.

The values of ε' for phase I, which are listed in Table 30, are plotted against pressure in Figure 26, together with the function describing the results obtained from the coaxial cell, equation [5.1]. The value at 750 bar was of course used as the origin for the parallel plate calculations, as described previously. The remaining values agree to better than 0.25% and, although the deviations are not random, the agreement was as good as could be expected from the possible errors.

The values of ε' for phenol II at 2 kbar determined from samples 1 to 5 are collected in Table 31. The values

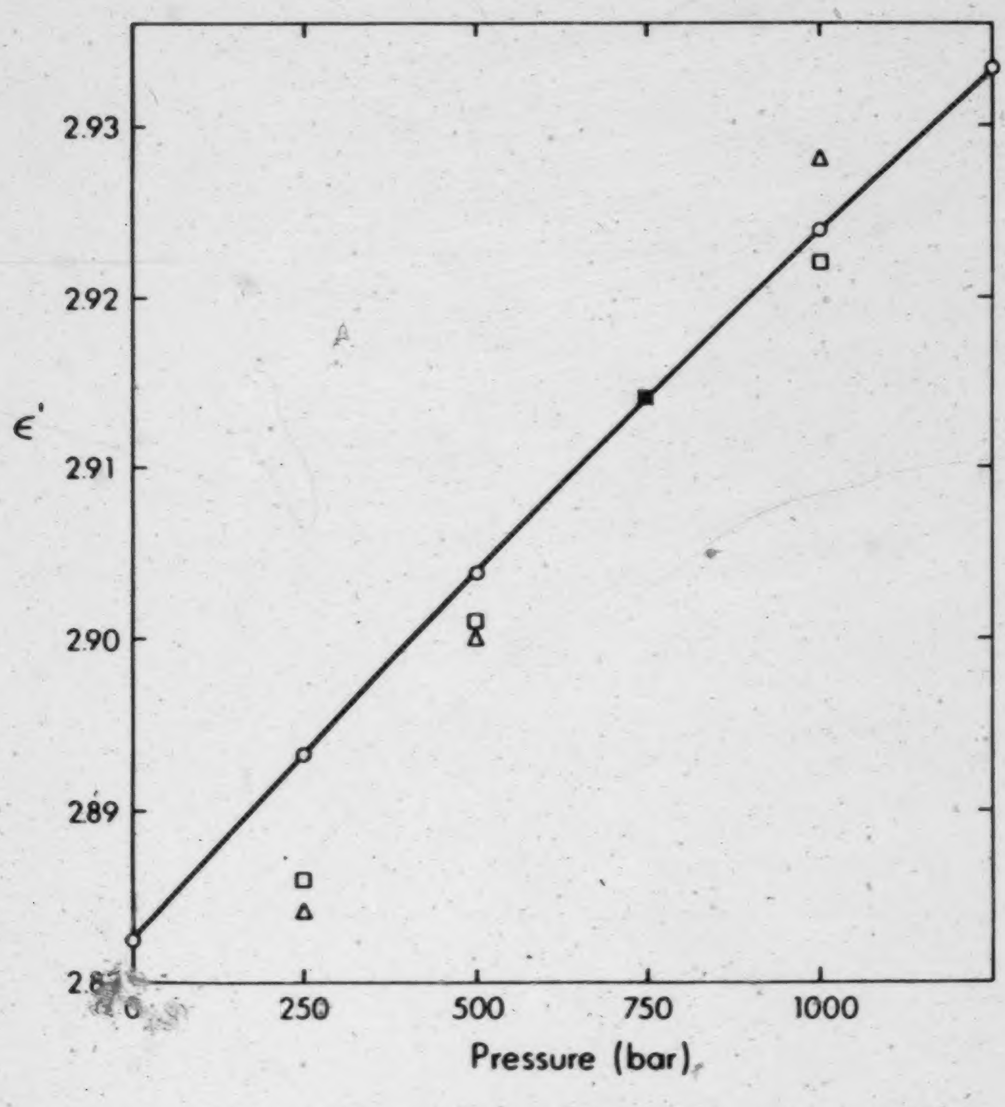

Figure 26. The dielectric constant of phenol I at 10°C and 50 kHz plotted against pressure. The curve represents the results obtained from the coaxial cell, equation [5.1], and the triangles and squares indicate the results from samples 4 and 5, respectively, from Table 30. ⊕ marks the point at which the results from the two cells were forced to agree.

Table 31. The dielectric constant and molar polarization of phenol II at 2 kbar and 10°C[a].

Sample	ϵ'	Molar Polarization $\bar{P}$ (cm^3)
1	3.044	30.27
2	3.094	30.70
3	3.095	30.71
4	3.209	31.67
5	3.058	30.39

[a] The density of phenol II at 2 kbar is 1.260 g/cm^3.

from the coaxial and parallel plate cells are consistent with one another, although the result from sample 4 may be somewhat too high due to its dispersion. In samples 1 to 3 the effects of the high dispersion may be offset by the presence of pressure gradients in the coaxial cell. The mean value of the 50 kHz dielectric constant of phenol II at 2 kbar and 10°C is 3.10 ± 0.06 where the error limit is the standard deviation about the mean. The molar polarization of each sample was obtained using the density calculated from the compressions given in Chapter III, and a molecular weight of 94.11. The results, which are listed in Table 31, show the mean molar polarization of phenol II at 2 kbar and 10°C to be 30.75 cm^3 with a standard deviation of 0.50 cm^3.

The molar polarizations of phenol I and II are plotted against (V/V_o) in Figure 27. The experimental uncertainties are too great to permit one to conclude that, in spite of the phase transition, the polarization of phenol II lies on the line defined by the density dependence of the molar polarization of phenol I. The variation of the molar polarization of phase II with pressure is, of course, unknown because it was not possible to determine the pressure dependence of the dielectric constant of this phase using the available apparatus.

Since no studies on dispersion free samples were

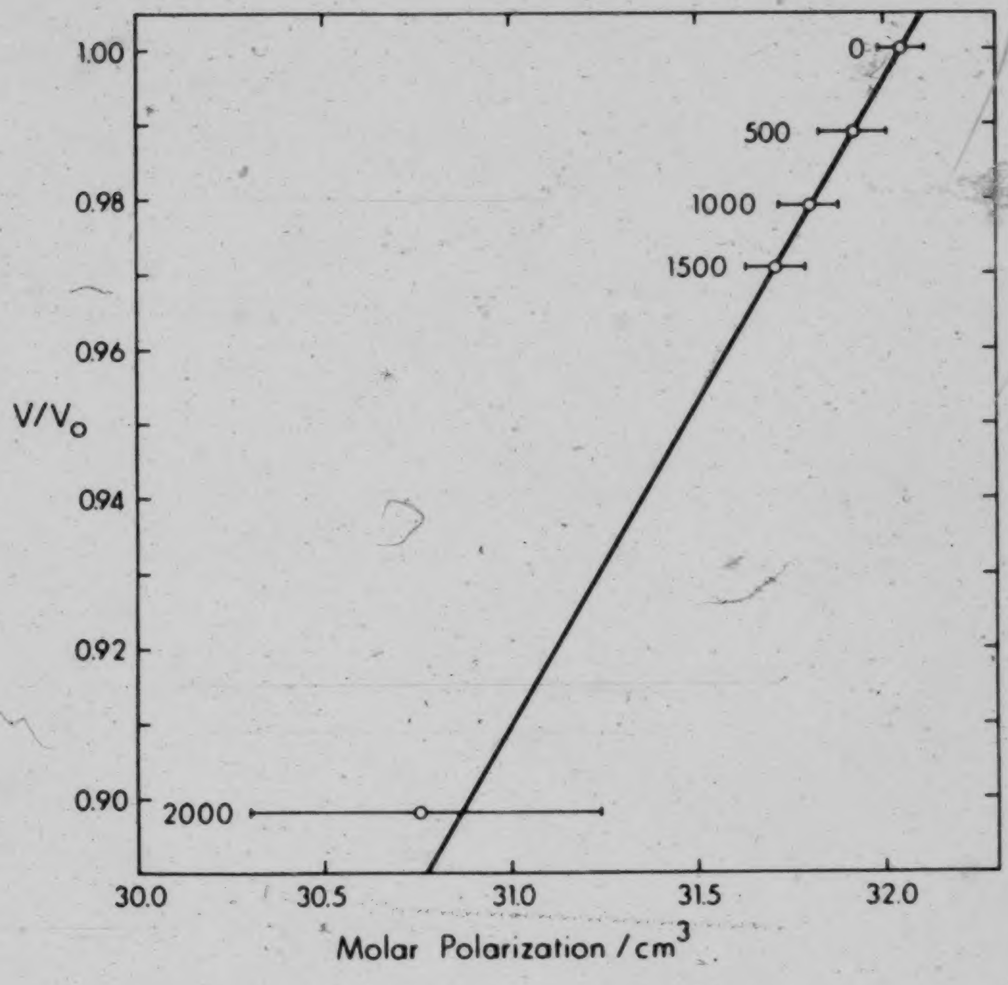

Figure 27. The molar polarization of phenol I and II at 10°C as a function of (V/V_o). The horizontal bars show the standard deviations of the results. The number beside each point is the pressure in bar. The line is the least squares fit of the phenol I data points, $P = 20.30 + 11.75 (V/V_o)$.

carried out as a function of temperature, there is no direct evidence that relaxation processes to high frequency of 100 kHz at 10°C do not exist, however the low value of the molar polarization tends to support this hypothesis. For this reason, using the arguments given in Section 5.2 for phenol I, dynamic disorder is probably not present in phenol II.

5.4 The Transient Dispersion in Phenol II

The transformation of a sample of phenol I into phenol II in both the coaxial and parallel-plate dielectric cells was invariably accompanied by the appearance of dielectric dispersion. The dispersion decayed with time, but often did not disappear completely. The loss showed two maxima, one at about 9 kHz at 10°C, the other to high frequency of 100 kHz at 10°C, but the two Cole-Cole arcs were not fully separated (Section 1.2b). Since the object of the dielectric studies was to obtain the static dielectric constants of phenol II, and since the transitory nature of the dispersion suggested it was not an intrinsic property of the phase, only a few runs were devoted to study of the dispersion itself. The experiments which were carried out are described below, along with a discussion of the analysis of the data and the interpretation of the results.

Figure 28 shows Cole-Cole plots depicting the time-

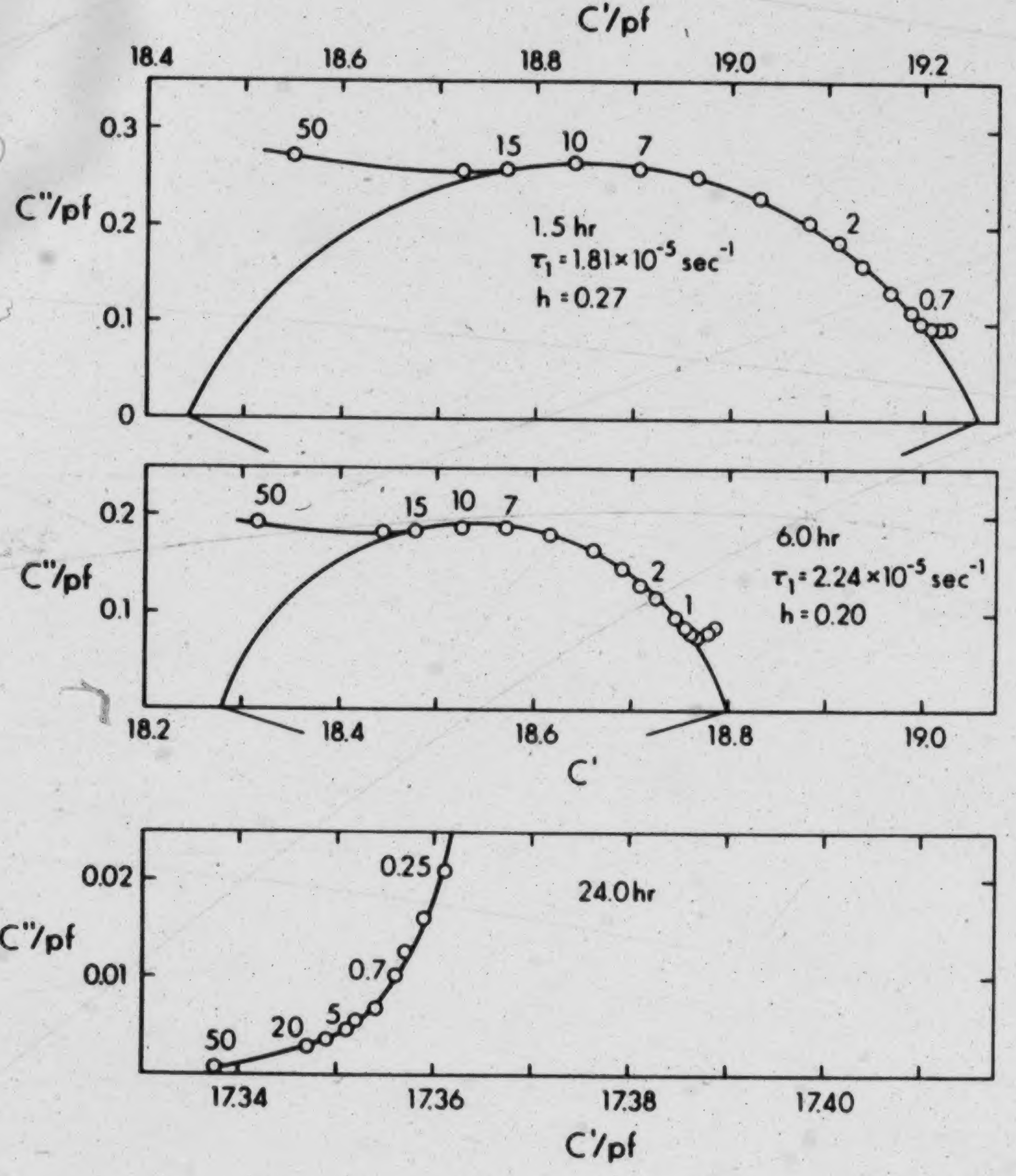

Figure 28. Cole-Cole plots showing the decay in the magnitude of the dispersion in a sample of newly formed phenol II in the parallel plate dielectric cell at 11.5°C and 2 kbar. The elapsed time since the I → II transformation, the relaxation time, and the Cole-Cole distribution parameter obtained for each arc are also shown.

dependent decrease in the magnitude of the dispersion in a sample of newly formed phenol II in the parallel plate cell (Figure 11a) at 2 kbar and about 11.5°C. Within 24 hours of the I → II transition, the dispersion had decayed to the point where no dielectric relaxation was detected. Figure 29 shows similar plots for a sample of zone refined phenol in the coaxial cell at about 3375 bar and 25°C. In this case the dispersion had not disappeared after 25 hours and the rate of decay had become very slow. In neither case did the relaxation time of the low frequency relaxation change substantially as the decay progressed. From a limited number of observations, the dispersion in the parallel plate cell seemed to disappear more rapidly in thin samples than in thick ones and, in general, the rate of decay in the parallel plate cell was faster than in the coaxial cell. The magnitude of the dispersion in newly formed phenol II was qualitatively observed to decrease as the temperature of the transition was raised. The rate of decay also increased as the temperature was raised and appeared to be more rapid at low pressures. The data obtained in this work do not indicate whether the magnitude of the high frequency dispersion is the same, relative to the low frequency dispersion, for different samples. Although no experiments were carried out to determine if the high frequency loss was proportional to the low frequency loss as the dispersion decayed, the low

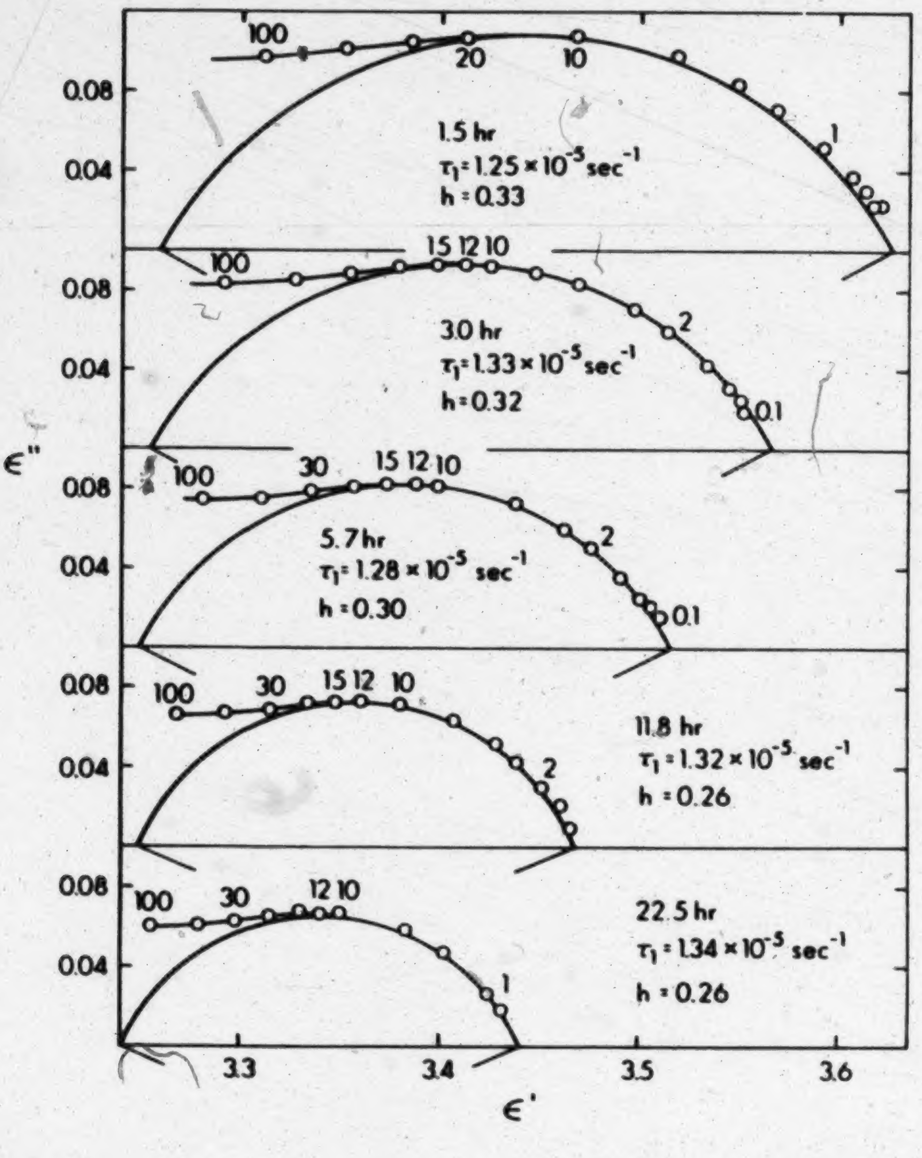

Figure 29. Cole-Cole plots showing the decay in the magnitude of the dispersion in a sample of newly formed phenol II in the coaxial dielectric cell at 25°C and 3375 bar. The elapsed time since the I → II transition, the relaxation time, and the Cole-Cole distribution parameter obtained for each arc are also shown.

value for the capacitance at 50 kHz after the low frequency dispersion had disappeared (Figure 28), suggests that the high frequency dispersion had also disappeared by the time the measurements were taken.

To determine the temperature dependence of the dispersion, the frequency dependence of C' and C" was measured in the parallel plate cell at a constant pressure of 2 kbar and a variety of temperatures, using two samples of zone refined phenol, hereafter designated samples 6 and 7. Cole-Cole plots of some of the resultant data are presented in Figures 30 and 31. Since the frequency range of the bridge did not permit capacitance measurements over the complete range of the dispersion, no attempt was made to resolve the two relaxation processes using equations such as equation [1.20]. Instead, the data points on the high or low frequency end of the overall dispersion were fitted to a semicircular arc using the method outlined in Section 1.2b. If the value of C' at the centre of the arc correspond very closely to a data point, τ_o was calculated from the frequency of that point, otherwise the parameters of the semicircle were used in equation [1.17] to determine values of τ_o. The values of τ_o so obtained correspond to the maxima of the observed loss with an estimated accuracy of ±10% but, as such, they do not necessarily represent the macroscopic relaxation times of the two processes which combine to produce the observed dispersion. It can

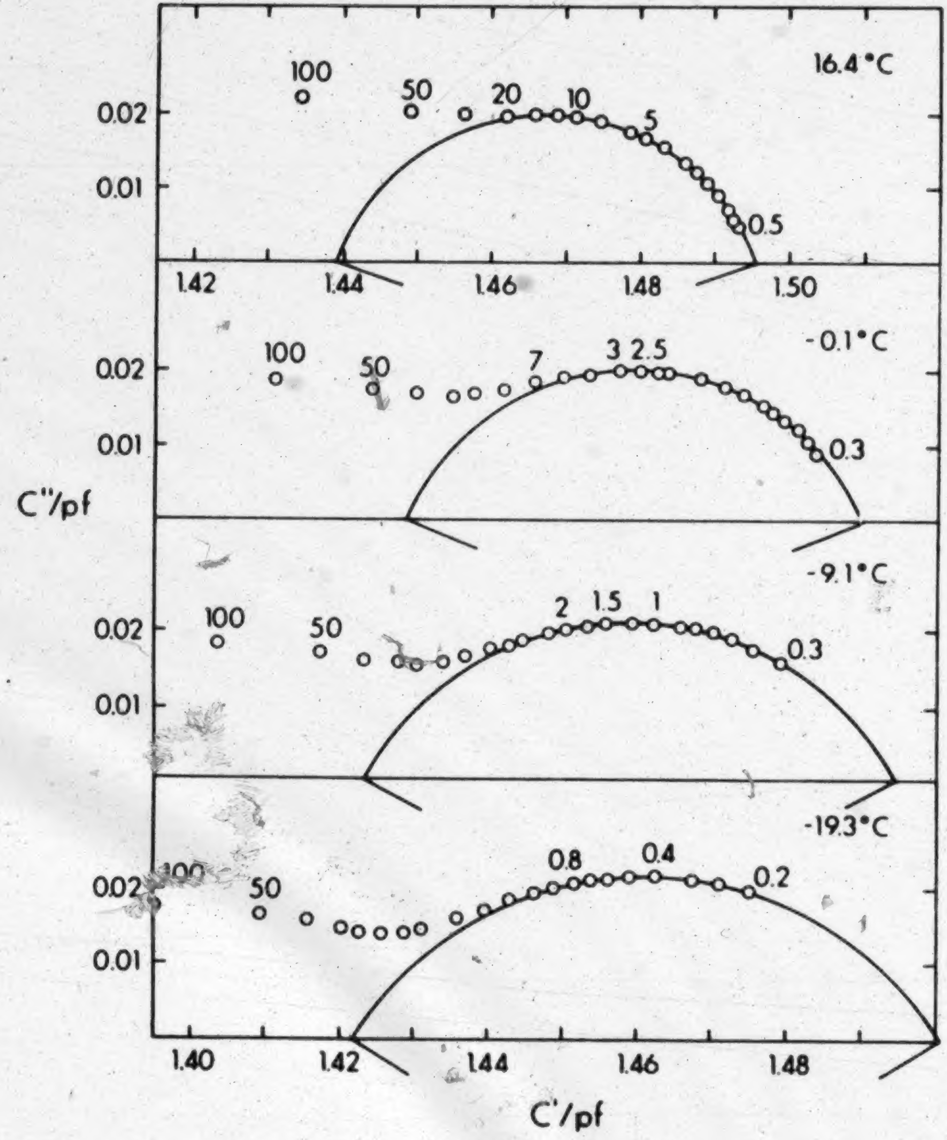

Figure 30. Cole-Cole plots of the transient dispersion in sample 7 at several temperatures, and the arc to which each plot was fitted.

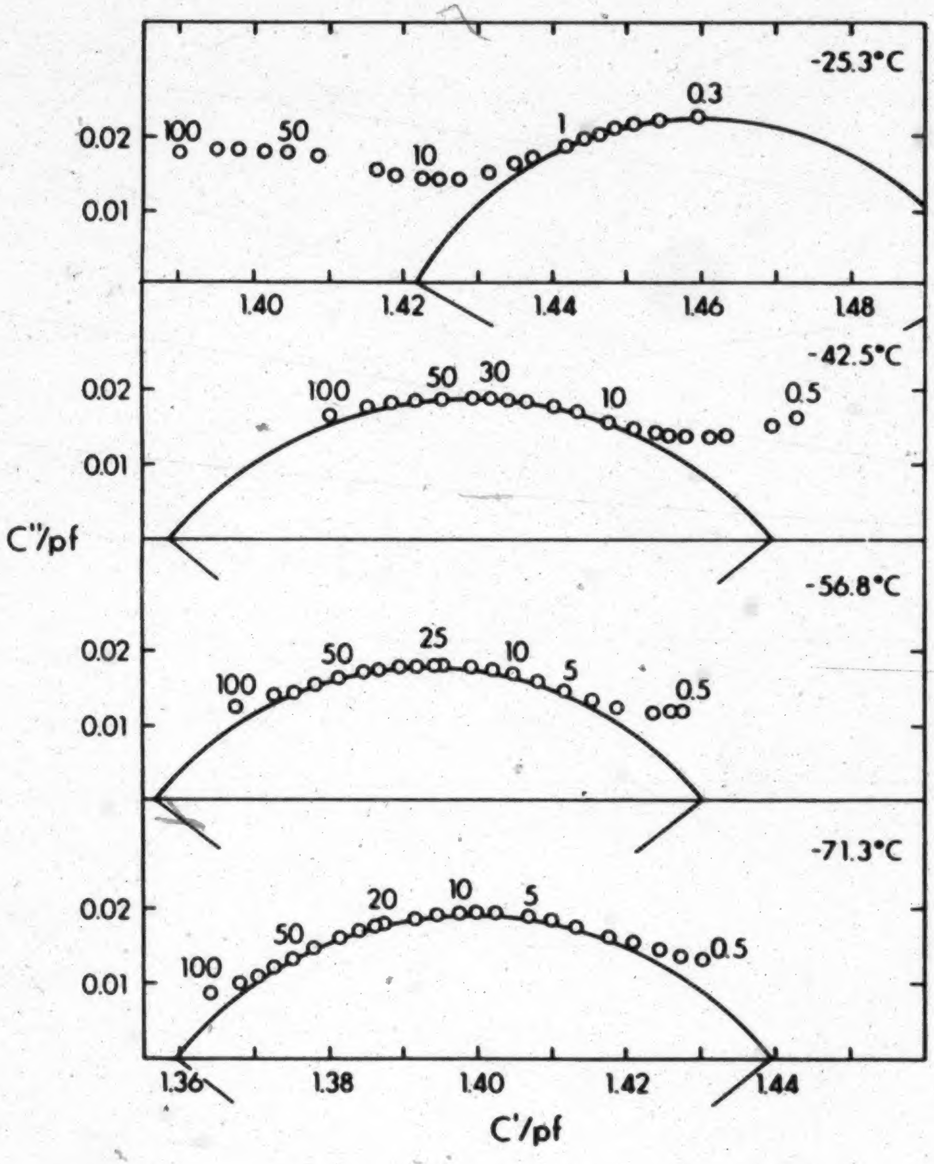

Figure 31. Cole-Cole plots of the transient dispersion in sample 7 at several temperatures, and the arc to which each plot was fitted.

be seen from Figure 3, that this procedure underestimated the value of τ_o for the low frequency process, τ_1, and overestimated the value of τ_o for the high frequency process, τ_2. This error increases as τ_1 and τ_2 approach one another. It can also be seen from Figure 3 that the value of C_∞ for the low frequency arc was underestimated by this procedure and the value of C_o for the high frequency arc was overestimated. Obviously then, the values obtained for the distribution parameter, h, are only meaningful in a very qualitative sense.

The values of τ_o for the two relaxation processes are listed in Tables 32 and 33 for samples 6 and 7 respectively, along with the values of C_o, C_∞ and h which characterize each fitted semicircle. The values of τ_o which were obtained from each fit were used to construct the plot of log τ_o against 1/T, shown in Figure 32. If the enthalpy of activation of the relaxation processes, ΔH_A^*, is constant over the temperature range, such a plot will be linear since, from the Arrhenius equation (154)

$$\frac{d \log \tau_o}{d\,(1/T)} = 0.2186 \ \Delta H_A^* \ \text{(cal/mole)} \qquad [5.11]$$

Accordingly, the data in Figure 32 for each relaxation process were fitted to a straight line using the least squares technique. The standard deviations for the low and high frequency dispersions were 0.086 and 0.076

Table 32. Relaxation parameters obtained from sample 6 at several temperatures and 2 kbar.

T(°C)	C_o(pf)	C_∞(pf)	h	τ_o(sec)	log τ_o	$10^3/T(^oK)$
10.0	1.5390	1.4602	0.20	$2.64\text{x}10^{-5}$	- 4.579	3.532
0.6	1.5188	1.4457	0.21	$5.30\text{x}10^{-5}$	- 4.275	3.653
-3.3	1.4665	1.4243	0.13	$7.23\text{x}10^{-5}$	- 4.141	3.706
-26.6	1.4593	1.4072	0.28	$4.82\text{x}10^{-5}$	- 3.317	4.056
-48.9	1.4158	1.3478	0.46	$3.54\text{x}10^{-6}$	- 5.451	4.459
-67.5	1.4190	1.3560	0.39	$1.04\text{x}10^{-5}$	- 4.981	4.862
-7.9	1.4300	1.3940	0.25	$9.44\text{x}10^{-5}$	- 4.025	3.770

Table 33. Relaxation parameters obtained from sample 7 at several temperatures and 2 kbar.

T(°C)	C_o(pf)	C_∞(pf)	h	τ_o(sec)	log τ_o	$10^3/T(^\circ K)$
+2.6	1.4812	1.4288	0.20	3.17×10^{-5}	- 4.498	3.626
-8.6	1.4704	1.4157	0.24	9.95×10^{-5}	- 4.002	3.780
-18.5	1.4746	1.4100	0.33	2.45×10^{-4}	- 3.611	3.927
-27.4	1.4713	1.4155	0.22	5.68×10^{-4}	- 3.245	4.069
-48.5	1.4280	1.3547	0.43	4.90×10^{-6}	- 5.309	4.451
-56.8	1.4306	1.3517	0.42	7.23×10^{-6}	- 5.141	4.622
-65.5	1.4370	1.3578	0.43	1.22×10^{-6}	- 4.912	4.816
-71.3	1.4397	1.3595	0.42	1.99×10^{-5}	- 4.701	4.954
-61.5	1.4405	1.3595	0.43	7.94×10^{-6}	- 5.100	4.725
-50.1	1.4369	1.3592	0.42	5.27×10^{-6}	- 5.278	4.483
-42.5	1.4391	1.3389	0.44	3.94×10^{-6}	- 5.404	4.336
-25.3	1.4980	1.4220	0.33	7.98×10^{-6}	- 3.098	4.035
-19.3	1.5010	1.4220	0.36	3.72×10^{-4}	- 3.429	3.939
-9.1	1.4943	1.4232	0.32	1.33×10^{-4}	- 3.877	3.787
-0.1	1.4900	1.4292	0.26	6.12×10^{-5}	- 4.213	3.662
+16.4	1.4394	1.4957	0.22	1.30×10^{-5}	- 4.885	3.454

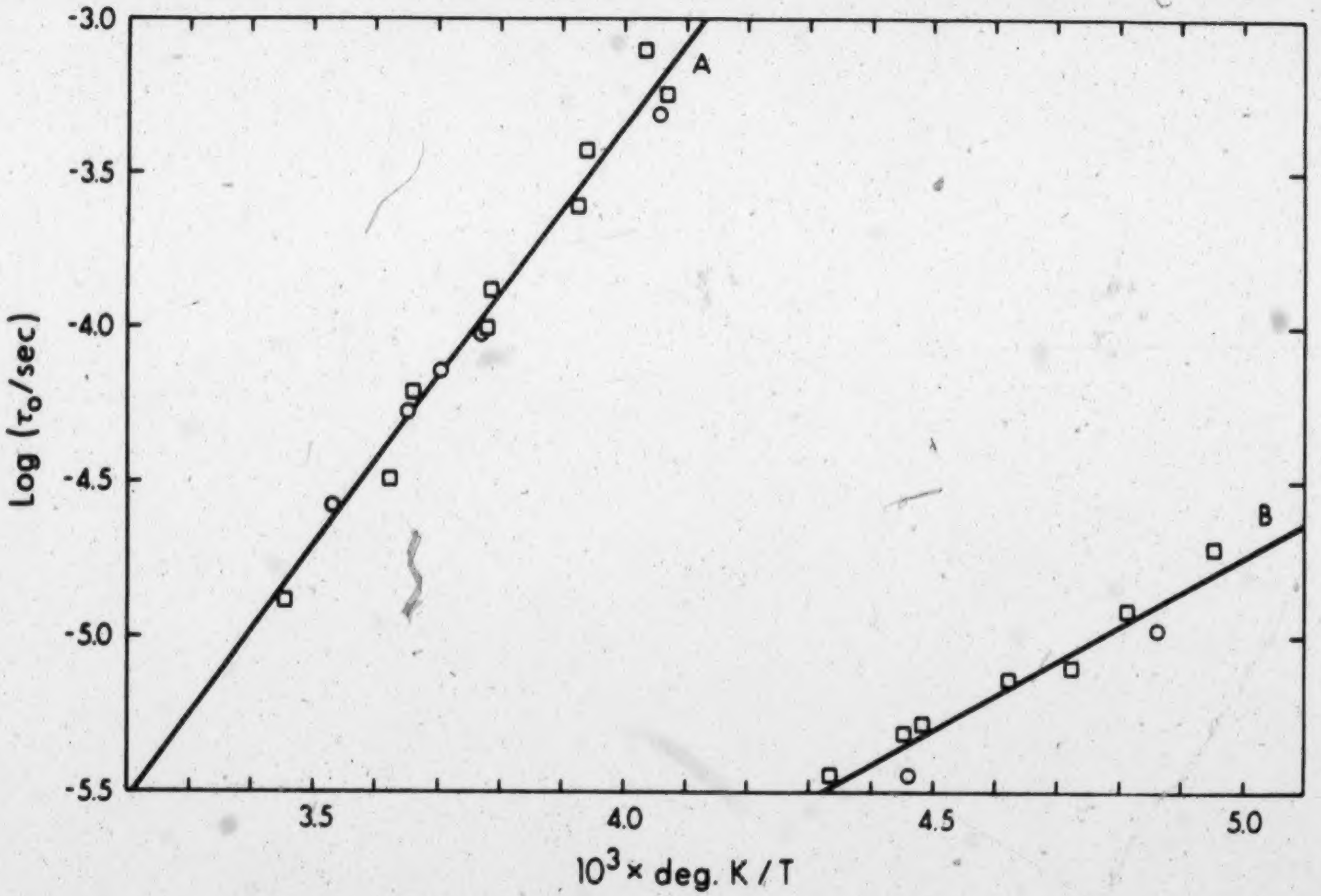

Figure 32. The temperature dependence of the apparent relaxation times for the low and high frequency dispersions. The straight lines, A and B, are the least squares fits of the data from the low and high frequency dispersions, respectively.

respectively. The expression obtained for the low frequency dispersion was

$$\log \tau_1 = 2.730 \times \frac{10^3}{T} - 14.278 \qquad [5.12]$$

and, for the high frequency dispersion,

$$\log \tau_2 = 1.094 \times \frac{10^3}{T} - 10.213 \qquad [5.13]$$

The Arrhenius enthalpy of activation for each process were calculated from equation [5.11] to be 12.5 ± 0.6 kcal/mole for the low frequency dispersion, and 5.0 ± 0.5 kcal/mole for the high frequency dispersion. The error limits were calculated from the effect the standard deviation of each fit could have on the slope of that line. These limits do not include the error introduced by the fact that the Cole-Cole plots were not properly resolved.

Since both dispersion processes are transient, and since no such effect is observed in phase I, the relaxation is probably not the intrinsic relaxation of some impurity (for instance ice). One possible explanation of the low frequency dispersion, is that it results from Maxwell-Wagner effects which are caused by the precipitation of thin layers of conducting impurity as the sample is taken through the transition (Section 4.3). Since the transition is thought to begin at the face of the piston, the impurities would be laid down in parallel sheets ahead of the propagating transition. From Section 1.3b, the relaxation time resulting from such impurities may be calculated assuming that $d_1 >> d_2$ and $\sigma_2 \geq \sigma_1$ in equation [1.26] to yield

$$\tau_o = \bar{\varepsilon}_o \frac{\varepsilon_2}{\sigma_2} \qquad [5.14]$$

where components 1 and 2 are the pure sample and impurity, and d, σ and ε are the thickness, conductivity, and dielectric constant, respectively. The decay of the dispersion could well result from the impurities slowly redissolving in phase II. This would cause a decrease in the magnitude of the dispersion which would have little effect on the relaxation time since equation [5.14] is approximately independent of the thickness of the impurity. The amount of impurity required to produce such an effect may be as little as 0.1%, depending on the values of the conductivity and dielectric constant of the impurity (44). The decay could also be caused by a gradual conglomeration of the impurities into spheroids without changing τ_o by more than a factor of two (45). If this low frequency dispersion is in fact due to Maxwell-Wagner effects, the temperature dependence of the relaxation time is simply due to the change in the conductivity, σ_2, with temperature. The high frequency dispersion may result from Maxwell-Wagner effects due to a separate impurity, or it may be due to a molecular reorientation process at the interface between the phenol II and the impurity which causes the low frequency dispersion. If the latter hypothesis is correct, the mean enthalpy of activation is 5 kcal/mole with a rather broad distribution of relaxation times. The reorientation might well result from the rotation of the phenol hydroxyl groups at the phenol-impurity interface since the enthalpy of activation is about that required to break a hydrogen bond.

5.5 Corrections to Dielectric Constants Obtained in the Coaxial Cell for Cell Deformation under Pressure

In Sections 5.2 and 5.3, the dielectric data obtained in the coaxial cell were corrected for the variation of the cell constant with pressure. This section describes the arguments and equations used to make the corrections.

The cell constant of the coaxial dielectric cell changes under hydrostatic pressure both because of the expansion of the cylinder bore and because of the contraction of the length and radius of the central electrode. The expansion, Δb, of the bore radius, b, of the coaxial cell may be calculated using equation [3.1]. The contraction of the length, L, and radius, a, of a cylindrical inner electrode may be calculated in the following way. If the changes in length and radius under a pressure P are defined as ΔL and Δa respectively, then at pressure P, $L = L_o+\Delta L$, $a = a_o+\Delta a$, and $b = b_o+\Delta b$ where L_o, a_o, and

b_o are, respectively, the length and radius of the inner electrode, and the radius of the bore, all at ambient pressure. Furthermore, the volume of the cylindrical inner electrode, V, is $\pi a^2 L$. In the pressure range used here, one may assume that $L_o >> \Delta L$ and $a_o >> \Delta a$. Since

$$\left(\frac{\partial V}{\partial P}\right)_T = \left(\frac{\partial V}{\partial L}\right)_T \left(\frac{dL}{\partial P}\right)_T + \left(\frac{\partial V}{\partial a}\right)_T \left(\frac{da}{\partial P}\right)_T ,$$

L and a may be related to the compressibility, β, of the steel used to construct the cell, by the expression

$$\beta = \frac{-1}{V_o}\left(\frac{\partial V}{\partial P}\right)_T \simeq \frac{-1}{L_o}\left(\frac{\partial L}{\partial P}\right)_T - \frac{2}{a_o}\left(\frac{\partial a}{\partial P}\right)_T \qquad [5.15]$$

where V_o is the volume of the inner electrode at ambient pressure. If the changes in the length and the radius of the inner electrode are proportional to their magnitude (i.e. if $(\Delta L/L_o) = (\Delta a/a_o)$), then from equation [5.15],

$$\frac{1}{L_o}\left(\frac{\partial L}{\partial P}\right)_T = \frac{1}{a_o}\left(\frac{\partial a}{\partial P}\right)_T = \frac{-1}{3}\beta \qquad [5.16]$$

Thus the values of L and a at pressure P are calculated by multiplying their values at ambient pressure by $(1 - \beta P/3)$. The compressibility of the steel β, can be calculated from Poisson's ratio, ν, and Young's modulus, E, using the expression (155)

$$\beta = (3 - 6\nu)/E \qquad [5.17]$$

For Vascomax 350, 18% nickel maraging steel, $\nu = 0.26$ and

$E = 29.1 \times 10^6$ psi. (118), so that $\beta = 7.17 \times 10^{-7}$ bar^{-1}.

For a coaxial cell with a cylindrical inner electrode, the ratio of the cell constant at one atmosphere, C_o, to that at pressure P, C_p, is given by the expression (144):

$$\frac{C_o}{C_P} = \frac{L_o}{L} \frac{\log(b/a)}{\log(b_o/a_o)}$$

If the inner cylinder is tapered, C_o/C_p may be calculated by approximating the inner electrode by 'n' cylindrical electrodes whose radii vary from a(1), the maximum radius, to a(n), the minimum radius. a(1) and a(n) at pressure P are obtained by multiplying their values at ambient pressure by $(1 - \beta P/3)$. Thus

$$\frac{C_o}{C_P} = \sum_{i=1}^{n} \frac{L_o}{nL} \cdot \frac{\log(b/a(i))}{\log(b_o/a_o(i))} \qquad [5.18]$$

where $a(i) = a(1) + i\,[a(n) - a(1)]\,/n$ [5.19]

and $a_o(i)$ is the value of a(i) at ambient pressure.

The values of C_o/C_p listed in the last column of Table 34 for several pressures were calculated from equation [5.18], using equation [3.1] to calculate b, and equation [5.16] to calculate L and a(i). The cell parameters at ambient pressure are $a_o(1) = 0.1461$ in., $a_o(n) = 0.1150$ in., and $b_o = 0.246$ in. The outer radius of the cell, c, which is required in equation [3.1], was 1.00 in.

Table 34. The effect of pressure on the cell constant of the coaxial dielectric cell.

	True pressure (bar)	Apparant pressure (bar)	Bore radius (in.)	$(C_o/C_p)^a$	$(C_o/C_p)^{b,c}$
f = 1.00	0	0	0.24600	1.00000	1.00000
	1000	1001.4	0.24617	1.00109	1.00172
	2000	2005.5	0.24634	1.00218	1.00343
	3000	3012.3	0.24651	1.00328	1.00514
	4000	4021.9	0.24667	1.00437	1.00686
f = 0.75	0	0	0.24600	1.00000	1.00000
	1000	1001.0	0.24612	1.00082	1.00144
	2000	2004.1	0.24625	1.00164	1.00288
	3000	3009.2	0.24638	1.00246	1.00433
	4000	4016.4	0.24650	1.00328	1.00577

[a] Calculated from the bore expansion only.

[b] Calculated from the bore expansion and the electrode compression.

[c] The corrected dielectric constants used in this chapter were calculated from values in this column with f = 0.75.

It was found that setting n equal to 10 gave sufficient precision in the values of C_o/C_p. Values of C_o/C_p calculated from equation [5.18] by considering the expansion of the bore only, i.e. by setting $a(i) = a_o(i)$ and $L = L_o$, are listed in the second last column of Table 34 to illustrate the relative contributions of the bore expansion and the electrode contraction. Values of C_o/C_p are listed in Table 34 for two values of the expansion constant, f (equation [3.1]). The correction to the apparent dielectric constants was applied by multiplying them by the appropriate value of C_o/C_p calculated considering both the bore expansion and the electrode deformation with f = 0.75.

5.6 The Electronic Polarization of Phenol

The values for the static dielectric constants of phenol I (Section 5.2) yielded the sum of the atomic and electronic polarization. In order to calculate the atomic polarization, it is necessary to determine the electronic polarization of phenol I.

The electronic polarization can be calculated from the Lorenz-Lorentz equation (Section 1.2a) using a value of the refractive index measured at a wavelength long enough to be free of dispersion effects due to electronic absorptions. The refractive indices can rarely be determined experimentally at sufficiently long wavelengths, but the value needed can be obtained from measurements at shorter wavelengths through relationships which describe the frequency dependence of the refractive index in regions removed from the electronic absorptions. Such an equation is the Sellmeier equation (156), which describes the behavior of the refractive index, n, as a function of its wavelength, λ, by assuming that the low frequency dispersion is due to 'm' electronic transitions, so that

$$n^2 = n_\infty^2 + \sum_{k=1}^{m} \frac{B_k}{\lambda^2 - \lambda_{ok}^2} \qquad [5.20]$$

B_k and λ_{ok} may be treated as arbitrary constants, while n_∞ represents the infinite wavelength refractive index, that is the refractive index that would exist to infinitely low frequency of the electronic transitions if no other transitions were present. If m = 1, the constants B and λ_o may be calculated by manipulating equation [5.20] to yield,

$$\lambda_o^4 - (\lambda_j^2 + \lambda_i^2)\, \lambda_o^2 + \lambda_i^2\, \lambda_j^2 - \frac{B(\lambda_j^2 - \lambda_i^2)}{n_i^2 - n_j^2} = 0 \qquad [5.21]$$

where n_i and n_j are the refractive indices at λ_i and λ_j, then solving for λ_o^2, B and n_∞ using the refractive indices at three wavelengths in equations [5.20] and [5.21].

Timmermans (67) has reported the refractive index of liquid phenol at 45°C and several wavelengths. His values are consistent with the earlier results of Eisenlohr

(157). Since the electronic polarization is often, to a first approximation, independent of density (Section 1.2a), the value of $\bar{P}_e$ calculated from the liquid is useful in the interpretation of polarization data for solid phases of phenol.

Table 35 presents Timmermans' data for liquid phenol. The parameters of the Sellmeier equation were calculated to be $n_\infty = 1.51500$, $B = 2.4132 \times 10^4$ nm^2, and $\lambda_o = 184.43$ nm, using the values of refractive index indicated by asterisks in Table 35. The other values of the refractive index calculated from these parameters agree with the experimental ones to within 0.0002, so the value of n_∞ deduced from the data should be accurate to at least 0.001 (156). Timmermans' has reported the density of liquid phenol at 45.0°C as 1.05446g/cm^3 (67), in agreement with the more recent data of Fried and Pick (158). If these values of n_∞ and density are used in the Lorenz-Lorentz equation (Section 1.2a), the electronic polarization of liquid phenol at 45.0°C is calculated to be $\bar{P}_e = 26.91 \pm 0.02$ cm^3. This value is in good agreement with the value of 27.0 cm^3 calculated by Donle and Gehrekens (159) from Eisenlohr's data. The value of 27.5 cm^3 calculated by Smyth (73) from the same data probably arose from faulty extrapolation, perhaps from the use of the 2-term Cauchy formulation (156).

The 'sodium D' refractive indices of phenol crystals

Table 35. The refractive index of liquid phenol at 45° and several wavelengths.

Radiation Source	Wavelength (nm)	$\frac{dn}{dT} \times 10^4$ °C	n (experimental)	n (calculated)	deviation
He(r)	667.82	4.9	1.53421	1.53421*	0
H (α)	656.29	5.0	1.53480	1.53494	0.00014
Na(D)	589.32	-	1.54027	1.54021	-0.00006
He(y)	587.56	5.0	1.54053	1.54037	-0.00016
He(g)	501.57	5.1	1.55117	1.55117*	0
H (β)	486.14	5.2	1.55381	1.55390	0.00009
He(v)	447.15	5.2	1.56225	1.56225*	0

* Points used to calculate the Sellmeier parameters.

and their melt at 41°C have been reported (160) with values of 1.5400 and 1.5930 being assigned to the liquid and crystal respectively. Since the liquid value is somewhat lower than Timmermans' figure of 1.54227 at that temperature, the refractive index of the crystals should probably only be considered accurate to ±0.0025. Assuming that the density of solid phenol is unchanged from its value of 1.132 taken at 25°C, (70) the sodium D molar polarization of the solid is 28.17 ± 0.10 cm^3, while that of liquid phenol, from Timmermans' data, is 28.01 cm^3. Thus, the values of the molar polarization at the sodium D line agree to within 0.5% and, therefore, it seems likely that the value of $\overline{P}_e$ for solid phenol, which should be determined using n_∞, lies within about 1% of the liquid value , i.e. $\overline{P}_e = 26.9 \pm 0.3$ cm^3 for solid phenol.

Chapter VI. The Static Dielectric Constants of the Liquefied Fluoromethanes

Although the dielectric constants of many halomethane liquids have been studied extensively (107), the dielectric properties of the liquid fluoromethanes have not been reported. The dielectric constants of many chloro, bromo, and iodo methanes have been satisfactorily rationalized by Buckley and Maryott (23) using a modification of the Onsager equation which allows for the nonspherical shape of the molecules. Their treatment ignored the atomic polarization and the anisotropy of the polarizability of the molecules. These assumptions should be less valid for the fluoromethanes, because the electronic polarizations of the fluoromethanes are smaller and more anisotropic (177) than those of the other halomethanes. It is therefore of interest to attempt to account for the static dielectric constants of the fluoromethanes by an Onsager treatment. This chapter describes the measurement and analysis of the static dielectric constants of the liquid fluoromethanes. Section 6.1 introduces the Onsager equation, along with Buckley and Maryott's modification of it. The experimental methods are described in Sections 6.2 and 6.3, and the results are presented and discussed in Sections 6.4 and 6.5.

6.1 The Onsager Equation and Other Related Equations

The Onsager equation (161-163) attempts to explain the behavior of the static dielectric constants of polar liquids by assuming the liquids to be composed of spherical, non-associated, dipolar molecules which possess isotropic polarizabilities. The molecule is represented as a polarizable point dipole, located in the centre of an otherwise empty, spherical cavity which is embedded in a homogeneous medium having the static dielectric constant of the bulk liquid. Following the terminology used by Wilson (162) and Hill (163), the internal field acting on the molecule is represented as the sum of two fields, the reaction field, $\overline{R}$, and the cavity field, $\overline{G}$. The reaction field is caused by the polarization of the surrounding medium by the instantaneous dipole and exists in part even in the absence of an applied field. The dipole moment of the molecule is thus enhanced, relative to its gas phase dipole moment, μ_o , by the reaction field and by the cavity field. The cavity field is caused by the applied electric field, and acts parallel to that field. It should be noted that Böttcher (164) defines the reaction field in a different way.

The Onsager equation essentially describes the contribution of molecular reorientation to the total dielectric constant, that is, it relates the static dielectric constant, ε_o, and the limiting high frequency dielectric constant, ε_∞, which would be obtained from a Cole-Cole plot of the relaxation, to the gas phase molecular dipole moment. It may be written in the form (163)

$$\frac{(\varepsilon_o - \varepsilon_\infty)(2\varepsilon_o + \varepsilon_\infty)}{\varepsilon_o(\varepsilon_\infty + 2)^2} = \frac{4\pi N_o \mu_o^2}{9kT\overline{V}} \qquad [6.1]$$

where N_o is Avogadro's number, $\overline{V}$ is the molar volume, μ_o is the gas phase dipole moment, k is Boltzmann's constant, and T is the absolute temperature. ε_∞ may be related to the isotropic molecular polarizability, α, by the Clausius-Mossotti equation (Section 1.2a) and making this substitution in equation [6.1] yields a second form of the Onsager equation (163)

$$\frac{(\varepsilon_o - 1)(2\varepsilon_o + 1)}{9\varepsilon_o}\overline{V} = \frac{4}{3}\pi N_o \left[\frac{\alpha}{1 - \frac{\alpha}{v}g} + \frac{\mu_o^2}{3kT(1 - \frac{\alpha}{v}g)^2}\right] \qquad [6.2]$$

where v is the volume of the cavity surrounding each dipole and equals $\overline{V}/N_o$, and

$$g = \frac{4\pi}{3}\left(\frac{2\varepsilon_o - 2}{2\varepsilon_o + 1}\right) .$$

The isotropic polarizability, α, in equation [6.2] is, by definition, the sum of the electronic and atomic polarizabilities of the molecule in the liquid state. Although the only polarizability data usually available is that of the gas phase, the liquid polarizabilities may be approximated by the sum of the gas phase atomic and electronic polarizabilities plus the additional contribution to the atomic polarizability caused by the inter-molecular lattice vibrations of the liquid state. This latter quantity is referred to as the 'lattice mode' polarizability, α_{lm}, in this work, and it is associated with a resonant absorption band in the far infra-red whose intensity is roughly proportional to μ_o^2/I, where I is the average of the moments of inertia of the molecule about the axis perpendicular to the dipolar axis (165,166). This suggests that α_{lm} arises from rotational oscillations of the molecule about its equilibrium position in the liquid (165). If this is so, the dipole moment derivative of this absorption is perpendicular to the molecular dipole, and thus the anisotropic lattice mode polarizability parallel to the dipole must be zero, while the lattice mode polarizability perpendicular to the dipole may be rather large (166).

The effect of the anisotropy of the molecular polarizability was not considered in equations [6.1] and [6.2] and this obviously imposes a serious restraint on their reliability. A consideration of this anisotropy (162) leads to an equation which differentiates between the polarizability in the direction of the cavity field, and that in the direction of the dipolar axis of the molecule in calculating the reaction field. The former may be approximated by the isotropic polarizability of the molecule, while the latter is simply the polarizability along the dipolar axis. This more general form of the Onsager equation is

$$\frac{(\varepsilon_o - 1)(2\varepsilon_o + 1)}{9\varepsilon_o}\bar{V} = \frac{4}{3}\pi N_o \left[\frac{\alpha}{1 - \frac{\alpha}{v}g} + \frac{\mu_o^2}{3kT(1 - \frac{\alpha_d}{v}g\ )^2}\right] \quad [6.3]$$

where α is the isotropic polarizability, and α_d is the polarizability along the dipolar axis. The dipolar polarizability, α_d, may be approximated by the gas phase atomic plus electronic dipolar polarizations since the lattice mode polarizability along this axis was shown previously to be small. Obviously, however, the lattice mode polarizability can have a large effect on the isotropic polarizability, particularly if the term μ_o^2/I is large for the molecule in question.

Another limitation of equations [6.1] and [6.2] is that they were derived for spherical molecules. Buckley and Maryott (23) have extended equation [6.2] to include both oblate and prolate spheroidal molecules in which the permanent dipole is aligned along the axis of symmetry. Their equation, which assumes the polarizability to be isotropic, takes the form

$$\frac{(\varepsilon_o - 1)(2\varepsilon_o + 1)}{9\varepsilon_o}\overline{V} = \frac{4}{3}\pi N_o \left[\frac{\alpha k_\alpha}{1 - \frac{\alpha}{v} g k_R} + \frac{\mu_o^2}{3kT(1 - \frac{\alpha}{v} g k_R)^2}\right] k_c \quad [6.4]$$

k_α, k_R, and k_c are constants which are calculated from the eccentricity, e, of the molecule. For a prolate spheroid,

$$e = \sqrt{1 - (\tfrac{b}{a})^2}$$

and, for an oblate spheroid

$$e = \sqrt{1 - (\tfrac{a}{b})^2}$$

where a and b are the axes of the spheroid, with a being the dipolar axis. In practice, a and b are determined by measuring the diameter required to rotate the molecule about the axis in question using Fisher-Hirschfelder-Taylor models.

For a prolate spheroid:

$$k_R = \frac{3}{2}\left(\frac{2\varepsilon_o + 1}{\varepsilon_o}\right)\left(\frac{1 - e^2}{e^3}\right) \frac{\left[-1 + \frac{1}{2e}\ln\frac{1 + e}{1 - e}\right]\left[\frac{-e}{1 - e^2} + \frac{1}{2}\ln\frac{1 + e}{1 - e}\right]}{\frac{-e^2}{1 - e^2} + \frac{\varepsilon_o - 1}{\varepsilon_o}\left(-1 + \frac{1}{2e}\ln\frac{1 + e}{1 - e}\right)}$$

$$k_c = \frac{k_R}{\beta}$$

$$\beta = \frac{9}{2}\left(\frac{1 - e^2}{e^2}\right)^2 \left[-1 + \frac{1}{2e}\ln\frac{1 + e}{1 - e}\right]\left[\frac{1}{1 - e^2} - \frac{1}{2e}\ln\frac{1 + e}{1 - e}\right]$$

$$k_\alpha = 1/k_c$$

For an oblate spheroid:

$$k_R = \frac{3}{2}\left(\frac{2\varepsilon_o + 1}{\varepsilon_o}\right)\left(\frac{\sqrt{1 - e^2}}{e^3}\right) \frac{\left[-1 + \frac{\sqrt{1 - e^2}}{e}\mathrm{Tan}^{-1}\frac{e}{\sqrt{1 - e^2}}\right]\left[e\sqrt{1 - e^2} - \mathrm{Tan}^{-1}\frac{e}{\sqrt{1 - e^2}}\right]}{\left[e^2 + \frac{\varepsilon_o - 1}{\varepsilon_o}\left(-1 + \frac{\sqrt{1 - e^3}}{e}\mathrm{Tan}^{-1}\frac{e}{\sqrt{1 - e^2}}\right)\right]}$$

$$k_c = \beta k_R$$

$$\frac{1}{\beta} = \frac{9}{2}\left(\frac{1}{e^4}\right)\left[-1 + \frac{\sqrt{1 - e^2}}{e}\mathrm{Tan}^{-1}\frac{e}{\sqrt{1 - e^2}}\right]\left[\left(1 - e^2\right) - \frac{\sqrt{1 - e^2}}{e}\mathrm{Tan}^{-1}\frac{e}{\sqrt{1 - e^2}}\right]$$

$$k_\alpha = 1/k_c$$

The calculations of reference 23 could only be reproduced if, in the prolate case, $k_c = \frac{k_R}{\beta}$ with β defined as in reference 23, and not $k_c = \beta k_R$ as stated in that reference. For a spherical molecule $k_\alpha = k_c = k_R = 1$ and equation [6.4] reduces to equation [6.2].

The success of equations [6.2], [6.3], or [6.4] in describing the static dielectric constants of a liquid is evaluated by calculating G, where $G = \mu_o^2$ (calculated)/ μ_o^2 (gas phase). If G equals unity at many temperatures, then the fit is perfect. Using equation [6.4], Buckley and Maryott were able to treat many systems successfully (23) in spite of the fact that they used the isotropic sodium D polarizabilities and thus ignored the contributions of the atomic and liquid lattice polarizations to those polarizabilities. They also found, empirically, that G values which drifted with temperature became constant if the cavity volume, v, was fixed at some arbitrary value, rather than being allowed to vary with density as in the original Onsager equation. In their work, Buckley and Maryott forced G to be unity by treating the eccentricity as a variable parameter. A more physically meaningful approach is to set the eccentricity to the value expected from the molecular shape, and to vary the polarizability within the physically meaningful limits in an attempt to obtain a value of G equal to unity. If no reasonable value of the polarizability yields a value of G equal to one, then an interpretation using the ideas presented in the following paragraph is justified.

Kirkwood and Frohlich (167) have considered the case of associated molecules, and have derived an equation identical with equation [6.2] except that the term μ_o^2 is replaced with the term $G\mu_o^2$, where G, the 'Correlation Function', can be calculated from statistical mechanical models of liquid structure and is identical to the G defined above. Kirkwood considers values of G greater than unity to be the result of molecular association which favours parallel alignment of the dipoles in the liquid, while values of G less than unity imply antiparallel alignment. It should be stressed that such interpretations of values of G which differ from unity are only valid after the effects of molecular shape and the anisotropy of the molecular polarizabilities in the phase in question have been considered.

6.2 Purification of Materials

Matheson reagent grade carbon tetrafluoride and fluoroform, and reagent grade methyl fluoride and difluoromethane from the Columbia Organic Chemicals Co. were introduced into a high vacuum system through a 25 x 2 cm column containing sodium hydroxide pellets and then passed through an 80 x 1.5 cm column of high-activity silica gel at room temperature. The silica gel was supplied by the Burrell Corporation and was previously activated by heating at 220°C for several hours under a pumping vacuum of less than 10^{-5} torr. The gas was then condensed into a trap at -196°C. After about 25 ml of the solidified gas had been collected, it was distilled into a flask containing sodium hydroxide pellets, allowed to warm up, and held at -90°C for one hour (-130°C for CF_4). It was then distilled into a cell and electrolyzed at ~1 kv/cm and -90°C (-130°C for CF_4) for one hour. After this purification stage, the sample was distilled into the previously cooled and evacuated capacitance cell.

To avoid contamination of the samples, the vacuum system was thoroughly evacuated overnight, and the silica gel reactivated between runs. Carbon tetrafluoride was introduced into the system first, followed by fluoroform difluoromethane, and lastly, methyl fluoride. This was the order of increasing sample conductance, and should have minimized the accumulation of ionic impurities in the cell. Sample conductances ranged from <1 x 10^{-13} mho/cm for CF_4 to 8.2 x 10^{-11} mho/cm for CH_3F, as measured at 5 kHz and the warmest temperature to which each sample was taken.

6.3 Dielectric Constant Measurements on Liquefied Gases

Capacitance measurements were carried out in a guarded, 3-terminal dielectric cell which had stainless steel plates set 3 mm apart. The cell constant was determined to be 2.4870 ± 0.0080 pf from room-temperature measurements on air, and on Eastman spectro-grade cyclohexane, and Matheson Coleman and Bell spectro-grade carbon tetrachloride and carbon disulfide, all of which were taken from freshly opened bottles. The dielectric constants at the exact temperature used were taken from reference 107. The capacitance of the evacuated cell was used to determine the temperature dependence of the cell constant, assuming that the lead capacitance did not change from its room temperature value of 0.020 pf. This calibration was carried out before introducing the first sample of each fluoromethane, and the resulting calibration curves are shown in Figure 33. Capacitance was measured using the GR 1615A bridge, calibrated as described in Section 2.4.

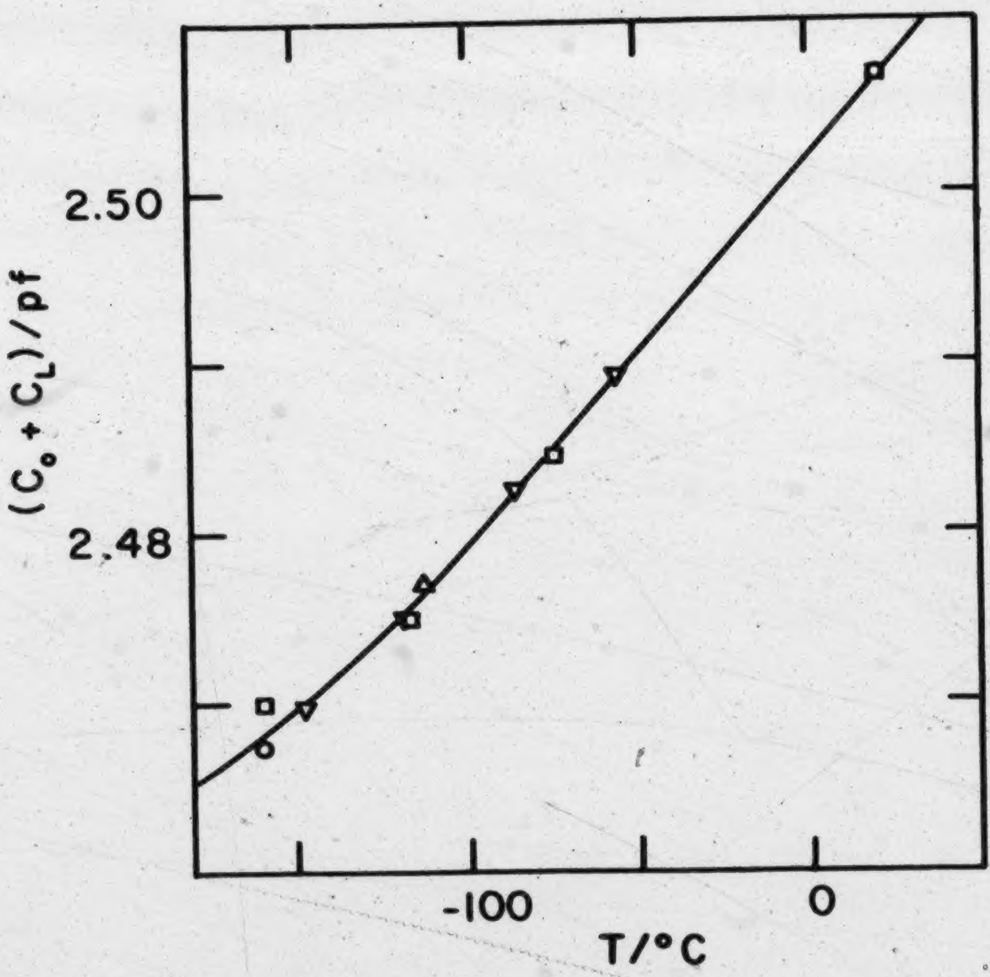

Figure 33. The capacitance of the evacuated dielectric cell as a function of temperature. Different symbols refer to values obtained before runs on each compound: ○ , CF_4; □ , CHF_3; △ , CH_2F_2; ∇ , CH_3F.

Temperature control was achieved by surrounding the cell with an insulated box which was cooled by a controlled stream of cold nitrogen gas. Regulation of the gas stream was effected by feedback from an iron-constantan thermocouple which was placed inside a 25 ml bulb of isopentane inside the cold box. A calibrated copper-constantan thermocouple, surrounded by indium for good thermal contact, was glued to the outside of the cell to monitor its temperature. To ensure that this thermocouple did, in fact, indicate the sample temperature, i.e., that were no effects due to temperature gradients along the sample, the dielectric constant of a sample of carbon disulfide was measured in the dielectric cell at -78°C, using both this method of temperature control and a constant temperature bath. The results were identical and, hence, the accuracy of these temperature measurements is believed to be the same as the accuracy of the thermocouple calibration, which was ± 0.3°C at -160°C and ± 0.1°C at -80°C (Section 2.2). The details of the cell and box are shown in Figure 34.

Runs were carried out on two samples of each compound. Each sample was distilled into the cell in situ and was allowed to reach thermal equilibrium. Capacitance readings were then taken at 5, 10, 20, and 50 kHz before changing the temperature. Although some electrode polarization was observed for CH_3F, the 50 kHz value of the

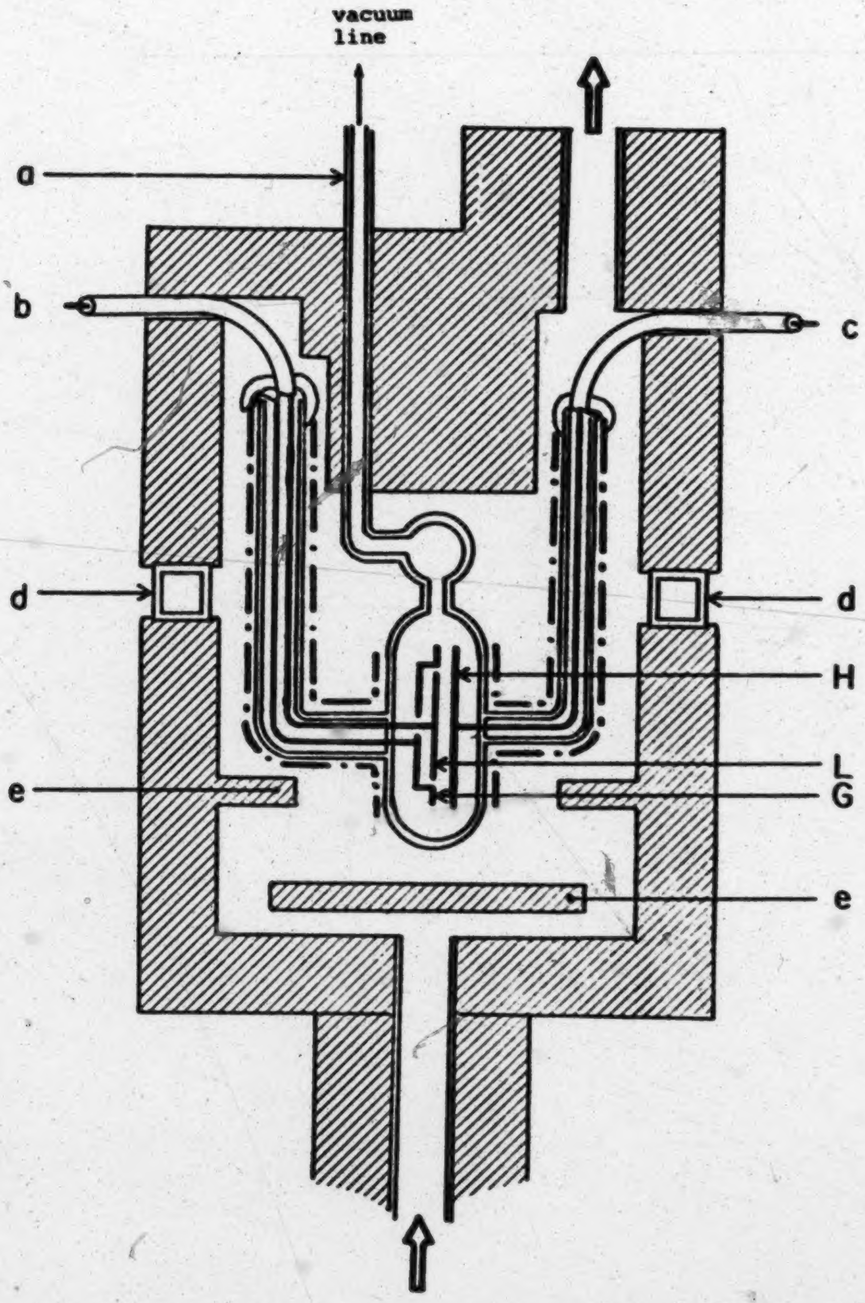

Figure 34. The dielectric cell for measurements on liquefied gases in its insulated box. The high, low, and guard electrodes are designated H, L, and G; a, the connection to the vacuum line; b, coaxial cable to low and guard electrodes; c, coaxial cable to high electrode; d, evacuated quartz observation window; e, baffle. The entrance and exit ports for the cold nitrogen gas are shown by the large arrows. The broken line represents copper braid shielding which was set at the guard potential.

dielectric constant was taken to be correct since it agreed with the values at 20 kHz and 10 kHz to within 0.025% and 0.045% respectively in the worst case. The results obtained for each compound are listed in the first two columns of Table 36 and are illustrated in Figure 35.

6.4 The Molar Polarization of Carbon Tetrafluoride

The dielectric constants for carbon tetrafluoride given in Table 36 were fitted to a linear equation in temperature, as shown in Figure 35, using the least squares technique. The expression so obtained was

$$\varepsilon = -\ 2.673 \times 10^{-3}\ T(^{\circ}K) + 1.2936 \qquad [6.5]$$

so that, at -132.2°C, the value of the static dielectric constant is 1.647 ± 0.005. The error estimate is based on uncertainties in the cell constant and differences in the results of the two runs. The value of ε at that temperature is important because the only recorded density for liquid carbon tetrafluoride is 1.624 g/cm^3 at -132.2°C (168). Using these numbers, the molar polarization, $\overline{P} = \overline{P}_e + \overline{P}_a$, was calculated from the Clausius-Mossotti equation (Section 1.2a) to be 9.61 ± 0.06 cm^3, assuming a value of 88.00 for the molecular weight. This result compares with a value of P = 9.73 cm^3 and a maximum error of ± 0.08 cm^3, reported for carbon tetrafluoride in the gas

Table 36. The dielectric results for the fluoromethanes in the liquid state.

(a) CH_3F

T(°C)	ε_0	Density (g/cm³)	G Column 1 $P=P_e=6.56$ cm³ $e=0$	Column 2 $P=P_a+P_e=7.49$ cm³ $e=0$	Column 3 $P=P_a+P_e=7.49$ cm³ $e=0.436$	Column 4 $P=P_a+P_e$(an)$=9.00$ cm³ $e=0.436$	Column 5 $P=12.2$ $e=0.436$
−140.4	47.62	1.002	1.46	1.36	1.48	1.33	1.04
−138.4	46.40	0.9982	1.45	1.35	1.47	1.32	1.03
−121.6	38.45	0.9669	1.41	1.32	1.43	1.29	1.02
−120.7	37.98	0.9652	1.41	1.32	1.43	1.29	1.01
−100.9	30.95	0.9269	1.37	1.28	1.38	1.25	1.00
−97.7	29.93	0.9206	1.36	1.27	1.38	1.25	0.99
−82.4	25.77	0.8897	1.33	1.25	1.35	1.22	0.98
−79.5	25.06	0.8837	1.32	1.24	1.34	1.22	0.98

(b) CH_2F_2

T(°C)	ε_0	Density (g/cm³)	G Column 1 $P=P_e=6.68$ cm³ $e=0$	Column 2* $P=P_a+P_e$ $e=0$	Column 3 $P=P_e=6.68$ cm³ $e=0.553$	Column 4 $P=P_e$(an)$=6.73$ cm³ $e=0.553$	Column 5 $P=12.3$ $e=0.553$
−121.0	53.74	1.376	1.94	—	1.69	1.68	1.04
−110.2	47.82	1.350	1.90	—	1.65	1.65	1.03
−100.5	43.00	1.327	1.85	—	1.61	1.61	1.01
−90.2	38.77	1.301	1.81	—	1.59	1.58	1.01
−78.4	34.50	1.270	1.77	—	1.55	1.55	1.00
−72.9	32.65	1.257	1.74	—	1.53	1.53	0.99
−57.4	28.19	1.219	1.68	—	1.49	1.48	0.98
−49.2	26.11	1.199	1.65	—	1.46	1.46	0.97

*P_a not known.

Table 36 continued.

(*c*) CHF_3

T(°C)	ε_0	Density (g/cm³)	G Column 1 $P = P_e = 7.80\ cm^3$ $r = 0$	 Column 2 $P = P_e + P_a = 9.01\ cm^3$ $r = 0$	 Column 3 $P = P_e + P_a = 9.01\ cm^3$ $r = 0.417$	 Column 4 $P = P_e + P_a(an) = 8.55\ cm^3$ $r = 0.417$	 Column 5 $P = 14.8$ $r = 0.417$
−148.0	40.70	1.679	1.84	1.71	1.58	1.63	1.02
−143.9	38.74	1.665	1.83	1.70	1.57	1.62	1.02
−127.4	32.04	1.609	1.79	1.66	1.54	1.59	1.01
−120.8	29.76	1.587	1.77	1.65	1.53	1.57	1.01
−110.7	26.69	1.553	1.74	1.62	1.51	1.55	1.01
−101.2	24.07	1.521	1.70	1.59	1.48	1.52	1.00
−85.0	20.24	1.466	1.64	1.53	1.43	1.47	0.98
−82.9	19.78	1.459	1.63	1.52	1.42	1.46	0.98

(*d*) CF_4

T(°C)	ε_0
−146.9	1.685
−144.5	1.681
−131.7	1.644
−131.6	1.647

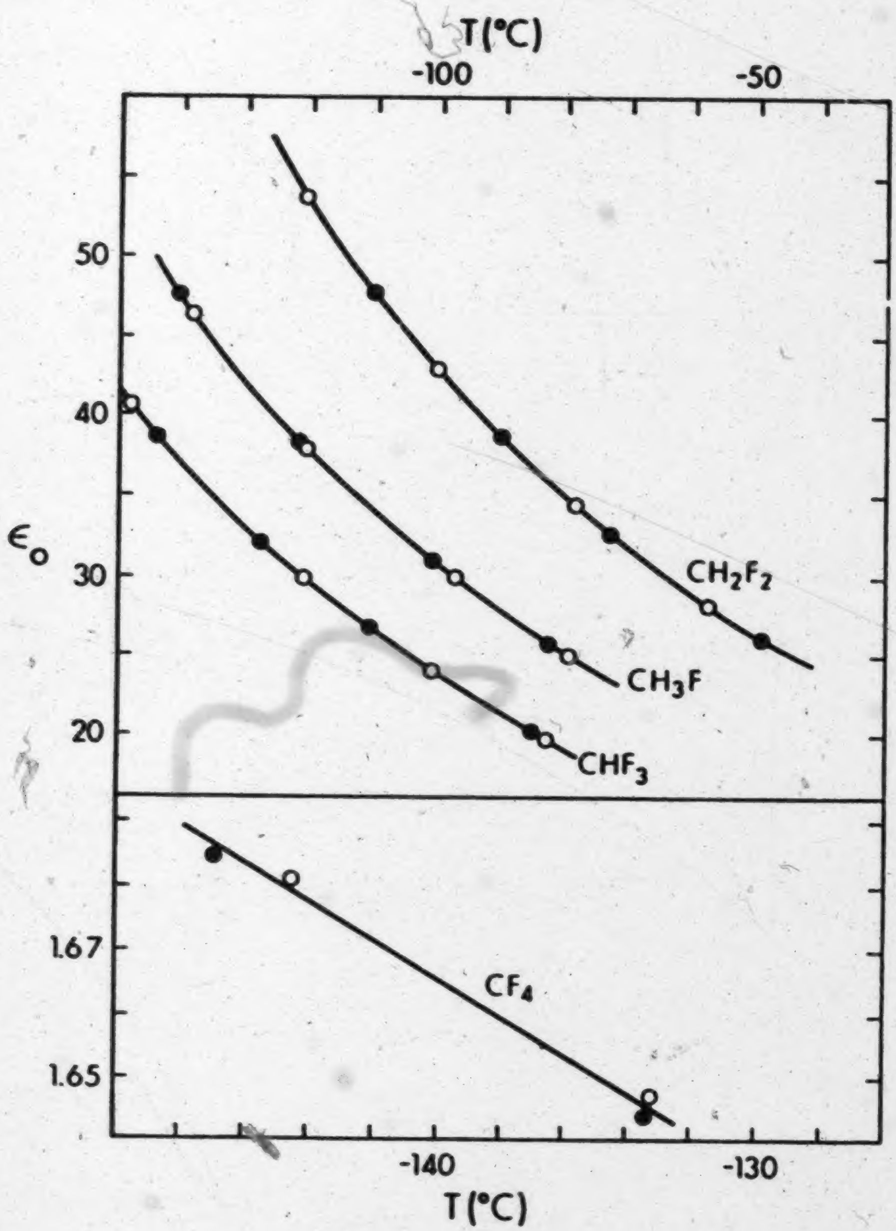

Figure 35. The static dielectric constants of the liquid fluoromethanes as a function of temperature. The open and closed circles represent measurements on different samples of each compound.

phase by A. Baugh Tipton _et_ _al_. (169) in the range 20°C to 350°C. Clearly the difference between the two values is only marginally significant.

The thermal expansivity of carbon tetrafluoride at -132.2°C was calculated to be 3.40 ± 0.03 x 10^{-3}/°C, by using the value of $\left(\frac{\partial \varepsilon}{\partial T}\right)_P$ obtained from equation [6.5] in equation [5.4].

6.5 The Static Dielectric Constants of Fluoroform, Difluoromethane, and Methyl Fluoride

The dielectric constants of the polar fluoromethanes are listed in the first two columns of Table 36. From the uncertainty in cell constant, and from the reproducibility of duplicate runs, the absolute error is estimated to be ± 0.8% for all values, with a precision of ± 0.3% between two samples of the same compound.

The values of G listed in Table 36 were calculated from the spheroidal Onsager equation, equation [6.4], at various levels of sophistication, as outlined below. The gas phase dipole moments were taken to be 1.851 for methyl fluoride (170), 1.97 for difluoromethane (171), and 1.649 for fluoroform (170). All molecular weights were taken from reference 99. The remaining data for all of these calculations is listed in Table 36. The densities of methyl fluoride (172), difluoromethane (173) and fluoroform (174) were taken from the data of other workers. The densities listed for methyl fluoride and fluoroform agree with those of Shinsaka and Freeman (173) to within 0.18%. The polarizations, $\bar{P}$, were considered to be interchangeable with the polarizabilities, α, through the Clausius-Mossotti equation (Section 1.2a). The values of the gas-phase atomic plus electronic polarizations, $\bar{P}_a + \bar{P}_e$, were obtained from reference 170 except for CH_2F_2 for which $\bar{P}_a$ is unknown. Values of the electronic polarizations, $\bar{P}_e$, were obtained for methyl fluoride and difluoromethane from the bond polarizabilities (175), and the value for fluoroform was that measured by Bridge and Buckingham for the gas (176).

Columns 1 and 2 of Table 36 show that the spherical Onsager equation, equation [6.2], cannot describe these systems well, although the G values are closer to unity when atomic polarization is included. The data for the prolate spheroid, methyl fluoride, is particularly interesting, since its shape should cause the Onsager value of G to be less than unity (23). The axial ratios, b/a, were determined from Fisher-Hirschfelder-Taylor atomic models to be 0.9 for CH_3F, 1.2 for CH_2F_2 and 1.1 for CHF_3. The values of G listed in column 3 of Table I were calculated using these axial ratios and the spheroidal modification to Onsager's equation, equation [6.4]. These results show that the large values of G in columns 1 and 2 cannot be explained by molecular shape alone. In no case was the drift in G with temperature reduced by assuming a constant arbitrary cavity volume.

An Onsager equation which considers both molecular shape, and the anisotropy of molecular polarizability has not yet been derived, however a comparison of the spherical Onsager equations, [6.2] and [6.3], does yield some useful generalizations about the spheroidal equation, [6.4]. From equation [6.3], it is apparent that the dipolar polarizability will affect the resulting values of G much more strongly than will the cavity field, or isotropic, polarizability, particularly if ε_o is large (20). Hence, if the liquid polarizabilities do not differ significantly from the gas phase values, the value of the polarizability parallel to the dipole should be used in place of the isotropic polarizability of the gas in equation [6.4] to give the best Onsager fit. If the polarization parallel to the cavity field in the liquid is very much larger than the polarization in the gas phase, because the contribution of the lattice mode polarization is large, then the cavity field term could have a significant effect on the G values. If this is the case, since the lattice mode polarization does not affect the polarizability in the direction of the dipole (166), a value intermediate between the isotropic polarizability of the liquid and polarizability in the direction of the dipole in the gas will give the best fit. The ensuing discussion assumes that these generalizations are also valid for the spheroidal Onsager equation.

Following the arguments presented in Section 6.1, an attempt was made to find a plausible value of the molar polarization which would yield values of G near unity, when used in conjunction with the measured values of eccentricity in equation [6.4]. The polarization along the dipolar axis can be crudely estimated for methyl fluoride and fluoroform by adding the component of the anisotropic electronic polarization (176,177) along that axis, to the isotropic value of $\bar{P}_a$. The values so obtained are shown in Table 36. Column 4 of Table 36 lists values of G for methyl fluoride and fluoroform calculated from these crude anisotropic polarizabilities. The values of G for difluoromethane in column 4 were calculated using the anisotropic value of $\bar{P}_e$ alone because the atomic polarization is not known. Use of these anisotropic polarizations does not significantly improve the values of G. Column 5 lists values of G which were forced to approach unity by using the rather large values of the polarization shown above the column. The large discrepancy between the estimated anisotropic polarization and that required to set G near unity must indicate either that the lattice vibrations of the liquid make a very large contribution to the cavity field polarization, or that the presence of inter-molecular forces favours parallel alignment of the dipoles in the liquid and, hence, values of G greater than unity.

In Section 6.1, it was pointed out that the intensity of the far infrared absorption which is attributed to the lattice vibrations of the liquid is approximately proportional to μ_o^2/I. From the Kramers-Kronig relationship (178), the contribution of this band to the polarization will be highly dependent on its position and shape, but a very rough correlation between μ_o^2/I and the magnitude of the lattice mode polarization would be expected. Table 37 lists values of μ_o^2/I for several halomethanes calculated from the values of μ_o listed in this work and in reference 23, and the moments of inertia, I, determined from microwave spectra (179). Because the far infrared absorption associated with the lattice vibrations merges with the absorption from relaxation (180), it is not possible to calculate the lattice mode contribution to the isotropic polarization from the far infrared spectrum with certainty. A Kramers-Kronig treatment of the far infrared spectrum of CH_3I (165) indicates, however, that the total absorbance from 20 cm^{-1} to 70 cm^{-1} would increase the isotropic polarization from the "sodium D" value of 19.3 to 24, and so the contribution of the lattice modes might well be significant. From the relative values of μ_o^2/I, for the fluoromethanes, the effect of lattice vibrations on the cavity field polarization would follow the order $CH_3F > CH_2F_2 > CHF_3$. Hence, although this effect might account for the high values of the molar polarization required to

Table 37. Values of μ_o^2/I for several halomethanes[a].

	$\frac{\mu_o^2}{I}$ $(D^2/g\ cm^2) \times 10^{44}$
CH_3F	1040
CH_3Cl	554
CH_3Br	370
CH_3I	249
CH_2F_2	457
CH_2Cl_2	92
CHF_3	335
$CHCl_3$	38

---

[a] $I = \frac{I_x + I_y}{2}$, where z is the dipolar axis.

set G = 1 for CH_3F, and possibly for CH_2F_2, the high value required for CHF_3 cannot be entirely accounted for by the contribution of the liquid lattice modes. The high values of G listed in columns 3 and 4 of Table 36 for fluoroform must thus indicate, at least in part, that the molecular dipoles tend to align parallel, perhaps due to hydrogen bonding (181-184).

If the lattice vibrations do significantly influence the isotropic polarizations of the fluoromethanes, they might also be expected to influence those of the methyl halides. Table 38 lists the values of molar polarization which are required to set the values of G for the methyl halides equal to unity. The calculations were made using the measured eccentricities and the dipole moments listed by Buckley and Maryott (23) in equation [6.4]. In Table 38, the molar polarizations obtained for methyl chloride and methyl bromide are in close agreement with the 'sodium D' values of the molar polarizations which were used by Buckley and Maryott and which underestimate the sum of the isotropic atomic and electronic polarizations to some degree. Methyl iodide, however, requires a polarization which is 22% smaller than this lower limit. These results can be rationalized using arguments similar to those used above, if the tendency for antiparallel dipole alignment increases in the order $CH_3F < CH_3Cl < CH_3Br < CH_3I$ because, as can be seen in Table 37, the contribution of the lattice

Table 38. The discrepancies between the gas phase molar polarizations and those required to fit the methyl halides to the spheroidal Onsager equation using molecular eccentricities.

	$\overline{P}$, the gas phase molar polarization (cm^3)	$\overline{P}'$, the polarization required to set G = 1 in equation 6.4 (cm^3)	$\frac{\overline{P}' - \overline{P}}{P}$
CH_3F	9.00[a]	12.2	+0.36
CH_3Cl	11.7[b]	12.5	+0.05
CH_3Br	14.6[b]	14.6	0.00
CH_3I	19.3[b]	14.9	-0.22

[a] The sum of the anisotropic electronic polarization along the dipolar axis, and the isotropic atomic polarization.

[b] The isotropic 'sodium D' value of the molar polarization.

vibrations is expected to increase in the reverse order. These two effects may roughly cancel each other for CH_3Cl and CH_3Br, so that their static dielectric constants can be fitted to equation [6.4] using the measured eccentricities and the sodium D values of the molar polarization.

6.6 Conclusion

In the absence of an exact knowledge of the polarization parallel to the dipolar axis and the cavity field polarization , deviations of G from unity do not necessarily imply liquid structure. The static dielectric constants of the fluoromethanes can be rationalized either by assuming significant parallel dipole correlation in all members of the series or, by assuming a significant lattice mode polarization which follows the order $CH_3F > CH_2F_2 > CHF_3$, and that a degree of parallel dipole correlation is present in CHF_3. An increasing tendency for antiparallel alignment of the methyl halides, with increasing size of the halogen, is consistent with both arguments.

References

1. C. P. Smyth, Dielectric Behavior and Structure (McGraw-Hill, Toronto, 1955), Chapter 5.

2. P. W. Bridgman, Collected Experimental Papers (Harvard University Press, Cambridge, 1964).

3. D. Eisenberg and W. Kauzmann, The Structure and Properties of Water (Oxford University Press, 1969), Chapter 3.

4. E. Whalley, D. W. Davidson and J. B. R. Heath, J. Chem. Phys., 48, 2362 (1968).

5. E. Whalley, D. W. Davidson and J. B. R. Heath, J. Chem. Phys., 45, 3976 (1966).

6. G. J. Wilson, R. K. Chan, D. W. Davidson and E. Whalley, J. Chem. Phys., 43, 2384 (1965).

7. J. E. Bertie and D. A. Othen, Can. J. Chem., 50, 3443 (1972).

8. D. A. Othen, Ph.D. Thesis, The University of Alberta, 1972.

9. Marco Solinas, Ph.D. Thesis, The University of Alberta, 1973.

10. J. E. Bertie and E. Whalley, J. Chem. Phys., 40, 1646 (1964).

11. J. E. Bertie, L. D. Calvert and E. Whalley, J. Chem. Phys., 38, 840 (1963).

12. J. J. Brophy, Basic Electronics for Scientists (McGraw-Hill, Toronto, 1966), p. 89.

13. H. V. Malmstadt, C. G. Enke and E. C. Toren, Electronics for Scientists (Benjamin, New York, 1962), p. 577.

14. Reference 1, p. 54.

15. C. F. Johnson and R. H. Cole, J. Amer. Chem. Soc., 73, 4536 (1951).

16. N. E. Hill, W. E. Vaughan, A. H. Price and M. Davies, Dielectric Properties and Molecular Behavior (Van Nostrand Reinhold, London, 1969), p. 15.

17. C. J. F. Böttcher, The Theory of Electric Polarisation (Elsevier, New York, 1952), p. 177.

18. Reference 16, p. 191.

19. Reference 17, p. 261.

20. E. Whalley, Adv. in High Press. Res. 1, 143 (1966).

21. J. E. Bertie, H. J. Labbe and E. Whalley, J. Chem. Phys., 50, 4501 (1969).

22. R. K. Chan and H. A. Chew, Can. J. Chem., 47, 2249 (1969).

23. F. Buckley and A. A. Maryott, J. Research Nat. Bur. Stand., 53, 229 (1954).

24. Reference 16, p. 197.

25. J. Yvon, Actual. Scient. Ind., 203 (1935).

26. J. G. Kirkwood, J. Chem. Phys., 4, 592 (1936).

27. W. F. Brown, J. Chem. Phys., 18, 1193 (1950).

28. A. D. Buckingham and J. A. Pople, Trans Far. Soc., 51, 1029 (1955).

29. K. S. Cole and R. H. Cole, J. Chem. Phys., 9, 341 (1941).

30. Reference 16, p. 297.

31. Reference 16, p. 48, 287.

32. Reference 16, p. 69, 316.

33. Reference 16, p. 316.

34. Reference 16, p. 290.

35. Reference 16, p. 84.

36. R. H. Cole, J. Chem. Phys., 23, 493 (1955).

37. G. Williams, J. Phys. Chem., 63, 537 (1959).

38. W. Dannhauser, J. Chem. Phys., 55, 629 (1971).

39. R. P. Auty and R. H. Cole, J. Chem. Phys., 20, 1309 (1952).

40. D. W. Davidson, Can. J. Chem., 46, 1024 (1968).

41. S. R. Gough and D. W. Davidson, J. Chem. Phys., 52, 5442 (1970).

42. W. Dannhauser and R. H. Cole, J. Amer. Chem. Soc., 74, 6105 (1952).

43. P. Dansas, P. Sixou and R. Arnoult, Colloque Ampère 14, 647 (1967).

44. Reference 16, p. 58.

45. L. K. H. van Beek, Prog. in Dielectrics, 7, 69 (1967).

46. Reference 16, p. 282.

47. R. W. Crowe and C. P. Smyth, J. Amer. Chem. Soc., 73, 5406 (1951).

48. W. J. Moore, Physical Chemistry (Prentice Hall, New Jersey, 1962), 3rd ed, p. 109.

49. S. D. Hamann, Physico-Chemical Effects of Pressure (Butterworths, London, 1957), p. 61.

50. P. W. Bridgman, The Physics of High Pressure (G. Bell & Sons, London, 1931), p. 253.

51. See, for example, I. Klotz, Chemical Thermodynamics (Benjamin, New York, 1964), p. 173; or Reference 48, p. 103.

52. L. A. K. Stavely, Quart. Rev. 3, 65 (1949).

53. E. Whalley and J. E. Bertie, J. Chem. Phys., 46, 1264 (1967).

54. Reference 3, p. 121.

55. Reference 8, pp. 44-63.

56. S. Sunder, Ph.D. Thesis, The University of Alberta, 1972.

57. D. G. Thomas and L. A. K. Stavely, J. Chem. Soc., 2572 (1951).

58. G. Tammann, Z. Physik. Chem., A75, 75 (1911).

59. E. B. Smith, Phys. Chem. Solids, 9, 182 (1958).

60. A. R. Ubbelohde, Nature, Lond., 169, 832 (1952).

61. D. H. Everett and W. I. Whitton, Trans. Far. Soc., 48, 749 (1952).

62. D. H. Everett and F. W. Smith, Trans. Far. Soc., 50, 187 (1954).

63. D. H. Everett, Trans. Far. Soc., 50, 1077 (1954).

64. J. A. Enderby, Trans. Far. Soc., 51, 835 (1955).

65. D. H. Everett, Trans. Far. Soc., 51, 1551 (1955).

66. P. W. Bridgman, Proc. Am. Acad. Sci., 52, 57 (1916).

67. J. Timmermans and Mme. Hennaut-Roland, J. Chim. Phys., 34, 693 (1937).

68. J. Timmermans, Physico-Chemical Constants of Pure Organic Compounds (Elsevier, New York, 1950), Vol. I, p. 459.

69. Reference 68, Vol. 2, p. 297.

70. R. J. L. Andon, D. P. Biddiscombe, J. D. Cox, R. Handley, D. Harrop, E. F. G. Herington and J. F. Martin, J. Chem. Soc. (London) 1960, 5246.

71. R. Handley, Analyt. Chim. Acta, 17, 115 (1957).

72. N. Schoorl (1903), cited in reference 67, but no reference listed.

73. S. E. Kamerling and C. P. Smyth, J. Amer. Chem. Soc., 55, 462 (1933).

74. F. H. Rhodes and A. L. Markley, J. Phys. Chem., 25, 528 (1921).

75. J. Kendall and J. J. Beaver, J. Amer. Chem. Soc., 43, 1853 (1921).

76. C. F. Cross, E. J. Beven and Th. Hieberg, Ber. 33, 2017 (1900).

77. Martignon, Bull. Soc. Chim., 43, 155 (1885).

78. H. D. Gibbs, Philipp. J. Sci., 3, 361 (1908).

79. von B. Meuthen and M. v. Stackelberg, Z. Elektrochem., 64, 387 (1960).

80. C. Scheringer. O. J. Wehrhahn and M. v. Stackelberg, Z. Elektrochem., 64, 387 (1960).

81. C. Scheringer, Z. Krist., 119, 273 (1963).

82. H. Gillier-Pandraud, Bull. Soc. Chem. France 1967, 1988.

83. J. C. Evans, Spectrochim. Acta, 16, 1382 (1960).

84. W. Maier and K. R. Fröhner, Spectrochim. Acta, 11, 977 (1959).

85. A. V. Korshanov, Ref. Zh. Fiz., 1963, Abstr. No. 9 D 321, cited in Chem. Abstr., 61, 195e (1964).

86. J. W. Brasch, R. J. Jakobsen, W. G. Fateley and N. T. McDevitt, Spectrochim. Acta., 24A, 203 (1968).

87. R. J. Jakobsen and J. W. Brasch, Spectrochim. Acta., 21, 1753 (1965).

88. C. P. Smyth and C. S. Hitchcock, J. Amer. Chem. Soc., 54, 4631 (1932).

89. V. A. Tolkachev and V. J. Kovalevski, Zh. Fiz. Khim., 44, 1365 (1970).

90. P. W. Bridgman, Proc. Am. Acad. Sci., 51, 55 (1915).

91. W. Kofler, A. Kofler and L. Kofler, Microchemie ver Mikrochim. Acta., 38, 218 (1951).

92. J. Naveau, Bull. Soc. Chim. Belges, 70, 662 (1961).

93. M. St. Flett, Proc. Intern, Meeting Mol. Spectry. 4th Bologna, 1959, 2, 703.

94. S. E. Babb, in High Pressure Measurement, ed. Gardini and Lloyd (Butterworths, Washington, 1962), p. 115.

95. R. S. Dodson and R. G. P. Greig, Brit. J. Appl. Phys., 16, 1711 (1965).

96. P. W. Bridgman, Proc. Am. Acad. Arts Sci., 72, 227 (1938).

97. N. A. Pushin and J. V. Grebenschtschikow, Z. Physik. Chem., 113, 75 (1924).

98. A. Defrain and N. Trang Linh, Comptes Rendues Acad. Sci. Paris 263, 1337 (1966).

99. The Handbook of Physics and Chemistry, 48th ed., edited by R. C. Weast (Chemical Rubber Co., Cleveland, 1967), p. D 16.

100. E. F. G. Herington, Zone Melting of Organic Compounds (Blackwell, Oxford, 1963), pp. 3-24.

101. J. Mitchell and D. M. Smith, Aquametry (Interscience, New York, 1948), pp. 107, 115.

102. H. Yeager and B. Kratochvil, J. Phys. Chem. 73, 1963 (1969).

103. H. Snecker, J. I. Lauritzen, R. J. Corruccini and S. T. Lonberger, Reference Tables for Thermocouples. Nat. Bur. Standards (U.S.), Circ. 561 (Apr. 27, 1955).

104. G. S. Kell and E. Whalley, J. Chem. Phys., 48, 2359 (1968).

105. Instruction Manual, Type 1615A Capacitance Bridge. (General Radio, West Concord, Mass., 1963).

106. P. W. Bridgman, Proc. Am. Acad. Arts Sci. 49, 627 (1914).

107. A. A. Maryott and E. R. Smith, Tables of Dielectric Constants of Pure Liquids, NBS Circ. 514 (1951).

108. J. E. Bertie and E. Whalley, Spectrochim. Acta., 20, 1349 (1964).

109. Reference 8, p. 70.

110. Reference 56, p. 82.

111. B. Post, R. J. Schwartz and I. Fankuchen, Rev. Sci. Inst., 22, 218 (1951).

112. G. H. Stout and L. H. Jensen, X-ray Structure Determination (Macmillan, New York, 1968), p. 12.

113. I. Waller and R. W. James, Proc. Royal Soc. (London) 117A, 214 (1927).

114. R. J. Roark, Formulas for Stress and Strain (McGraw-Hill, Toronto, 1965), p. 308.

115. J. C. Slater, Phys. Rev., 23, 488 (1924).

116. P. W. Bridgman, Proc. Am. Acad. Arts Sci., 64, 19 (1929).

117. P. W. Bridgman, Proc. Am. Acad. Arts Sci., 71, 387 (1937).

118. Preliminary Data, 18% Nickel 350 Maraging Steel (International Nickel Co. of Canada, Toronto, 1968).

119. Reference 98, pp. B208, B223.

120. S. N. Vaidya and G. C. Kennedy, J. Phys. Chem. Solids, 31, 2329 (1970).

121. M. Born and K. Huang, Dynamical Theory of Crystal Lattices (Oxford University Press, 1954), p. 111.

122. P. W. Bridgman, J. Appl. Phys. 17, 225 (1946).

123. P. W. Bridgman, Proc. Am. Acad. Arts Sci. 47, 441 (1911), see p. 533.

124. Reference 89, p. 59.

125. Reference 68, p. 527.

126. W. E. Putnam, D. M. McEachern Jr., and J. K. Kilpatrick, J. Chem. Phys. 42, 749 (1965).

127. Reference 98, p. D96.

128. G. S. Parks, H. M. Huffman and Mark Barmore, J. Am. Chem. Soc. 55, 2733 (1933).

129. N. F. M. Henry, H. Lipson, W. A. Wooster, The Interpretation of X-ray Powder Diffraction Photographs (Macmillan, London, 1960), p. 178.

130. L. V. Azaroff and M. J. Buerger, The Powder Method (McGraw-Hill, New York, 1958), p. 48.

131. Reference 130, p. 184.

132. Reference 130, p. 201.

133. M. J. Buerger, Crystal Structure Analysis (Wiley, New York, 1960), p. 173.

134. K. Simpson, Ph.D. Thesis, The University of Alberta (1973).

135. I. Nahringbauer, Acta Chem. Scand. 24, 453 (1970).

136. H. A. Chew and R. K. Chan, Can. J. Chem. 51, 2141 (1973).

137. Von R. Brille and A. Tippe, Acta Cryst. 23, 343 (1967).

138. S. Laplaca and B. Post, Acta Cryst. 13, 503 (1960).

139. Reference 129, p. 179.

140. J. E. Bertie, L. D. Calvert, and E. Whalley, J. Chem. Phys. 38, 840 (1963).

141. Reference 129, p. 181.

142. Reference 130, p. 84.

143. Reference 16, pp. 241-245.

144. Reference 1, p. 420.

145. Reference 3, p. 113.

146. D. W. Davidson, in Water: A Comprehensive Treatise, edited by F. Franks (Plenum Press, New York, 1972), Vol. II, Chapter 3.

147. Reference 17, p. 199.

148. Reference 50, p. 136.

149. C. Swenson, The Physics and Chemistry of High Pressure (Soc. Chem. Ind., 1963), p. 41.

150. G. Jenner and M. Millet, J. Chim. Phys. 68, 677 (1971).

151. Reference 50, pp. 128-133.

152. G. Jenner and M. Millet, High Temperature-High Press. 2, 205 (1970).

153. F. W. Sears, Electricity and Magnetism (Addison-Wesley, Reading, Mass., 1951), p. 205.

154. Reference 16, p. 316.

155. Reference 114, p. 91.

156. Reference 17, p. 253.

157. F. Eisenlohr, Ber. 44, 3188 (1911).

158. V. Fried and J. Pick, Collection Czech. Chem. Commun., 26, 954 (1961).

159. H. L. Donle and K. A. Gehrekens, Z. Phys. Chem. B18, 316 (1932).

160. F. Nechai, Soviet Phys. Tech. Phys., 1, 423 (1956).

161. L. Onsager, J. Amer. Chem. Soc., 58, 1486 (1936).

162. J. Norton Wilson, Chem. Rev., 25, 377 (1939).

163. Reference 16, p. 18.

164. Reference 17, p. 63.

165. S. R. Jain and S. Walker, J. Phys. Chem., 75, 2942 (1971).

166. B. Morris and D. W. Davidson, Can. J. Chem., 49, 1243 (1971).

167. Reference 16, pp. 23-31.

168. O. Ruff and R. Keim, Z. Anorg. Chem. 201, 225 (1931).

169. A. Tipton, A. P. Deam, and J. E. Boggs, J. Chem. Phys., 40, 1144 (1964).

170. H. Sutter and R. H. Cole, J. Chem. Phys., 52, 132 (1970).

171. D. R. Lide Jr., J. Amer. Chem. Soc., 74, 3548 (1952).

172. A. V. Grosse, R. C. Wackher and C. B. Linn, J. Phys. Chem., 44, 278 (1940).

173. K. Shinsaka and G. R. Freeman, unpublished work.

174. O. Ruff, Berichte, 69, 302 (1936).

175. J. A. Beran and L. Kevan, J. Phys. Chem., 73, 3860 (1969).

176. N. J. Bridge and A. D. Buckingham, Proc. Royal Soc. (London), A295, 334 (1966).

177. R. J. W. LeFevre, Rev. Pure Appl. Chem., 20, 67 (1970).

178. See, for example, F. Stern, Solid State Phys., 15, 331 (1963); S. Maeda and P. N. Schatz, J. Chem. Phys., 36, 571 (1962).

179. C. H. Townes and A. L. Schawlow, Microwave Spectroscopy (McGraw-Hill, New York, 1955), p. 618.

180. G. Birnbaum and E. R. Cohen, J. Chem. Phys., 53, 2885 (1970).

181. C. J. Creswell and A. L. Allred, J. Amer. Chem. Soc., 85, 1723 (1963).

182. A. Allerhand and P. von Rague Schleyer, J. Amer. Chem. Soc., 85, 1715 (1963).

183. N. Thorp and R. L. Scott, J. Phys. Chem., 60, 1441 (1956).

184. R. J. W. LeFevre, G. L. D. Ritchie, and P. J. Stiles, Chem. Commun., 253, 326 (1966).